ornl

ORNL/TM-13052

OAK RIDGE NATIONAL LABORATORY

LOCKHEED MARTIN

Some Investigations of the Reaction of Activated Charcoal with Fluorine and Uranium Hexafluoride

G. D. Del Cul
L. D. Trowbridge
D. W. Simmons
J. N. Fiedor
L. M. Toth
D. F. Williams

MANAGED AND OPERATED BY
LOCKHEED MARTIN ENERGY RESEARCH CORPORATION
FOR THE UNITED STATES
DEPARTMENT OF ENERGY

DISCLAIMER

ORNL/TM-13052

Chemical Technology Division

Some Investigations of the Reaction of Activated Charcoal with Fluorine and Uranium Hexafluoride

G. D. Del Cul
L. D. Trowbridge
D. W. Simmons
J. N. Fiedor
L. M. Toth
D. F. Williams

Date Published: September 1998

Prepared by the
Oak Ridge National Laboratory
Oak Ridge, Tennessee 37831-6181
managed by
LOCKHEED MARTIN ENERGY RESEARCH CORP.
for
U.S. DEPARTMENT OF ENERGY
under contract DE-AC05-96OR22464

CONTENTS

LIST OF TABLES

LIST OF FIGURES

ABSTRACT

The Molten Salt Reactor Experiment (MSRE) at Oak Ridge National Laboratory has been shut down since 1969, when the fuel salt was drained from the core into two Hastelloy N drain tanks at the reactor site. Over time, fluorine (F_2) and uranium hexafluoride (UF_6) moved from the salt through the gas piping to a charcoal bed, where they reacted with the activated charcoal. Some of the immediate concerns related to the migration of F_2 and UF_6 to the charcoal bed were the possibility of explosive reactions between the charcoal and F_2, the existence of conditions that could induce a criticality accident, and the removal and recovery of the fissile uranium from the charcoal.

This report addresses the reactions and reactivity of species produced by the reaction of fluorine and activated charcoal and between charcoal and F_2–UF_6 gas mixtures in order to support remediation of the MSRE auxiliary charcoal bed (ACB) and the recovery of the fissile uranium. The chemical identity, stoichiometry, thermochemistry, and potential for explosive decomposition of the primary reaction product, "fluorinated charcoal," was determined.

Well-defined carbon-fluoride solids (C_xF) result from the fluorination of charcoal, and their properties are uniquely dependent upon the temperature of fluorination. The reaction of a gas mixture of UF_6 and F_2 with an excess of carbon in a fixed bed results in two distinct reaction zones: an initial zone that contains all the uranium as intercalated uranium fluorides and oxyfluorides, followed by a fluorinated charcoal zone.

The top 12 in. of the ACB is known by gamma scan and thermal analysis to contain about 2.6 kg of ^{233}U. According to our laboratory tests, a few feet of fluorinated charcoal extends beyond the uranium front. The remainder of the ACB, about 80 ft, should consist of unreacted charcoal.

The uranium-bearing zone has less bound fluorine than fluorinated charcoal and cannot be made to decompose explosively (i.e., deflagrate). Fluorinated charcoal can be made to deflagrate by rapid heating to temperatures above that at which they formed, and the intensity of this decomposition depends on the temperature of fluorination. The sudden exothermic decomposition with formation of gaseous products (CF_4, C_2F_6, etc.) can produce high temperatures and pressures of near explosive characteristics.

1. INTRODUCTION

The Molten Salt Reactor Experiment (MSRE) was operated at the Oak Ridge National Laboratory (ORNL) from 1965 to 1969 to test the concept of a high-temperature, homogeneous fluid–fueled reactor. It was fueled with a molten salt mixture of LiF-BeF_2-ZrF_4-UF_4 (64.5-30.3-5.0-0.13 mol %), which was melted at 450°C and which served as both the fuel and the coolant. This fluid was circulated by a large impeller pump that circulated the fluid between the reactor core and the primary heat exchanger. A secondary coolant of LiF-BeF_2 (66-34 mol %), which was driven by a similar impeller pump, transferred the heat from the primary heat exchanger to an air- cooled radiator. About 4000 kg (~2 m^3) of fuel salt constituted the fuel charge circulating in the fuel salt circuit. Originally, the MSRE was fueled with ^{235}U, but after successful operation with this isotope, the ^{235}U was removed by fluorinating the salt. Afterward, the salt was reconstituted with $^{233}UF_4$ (containing 220 ppm ^{232}U) to demonstrate that the system could function equally well on this product of a ^{232}Th thermal breeding cycle. After the successful completion of this campaign, the MSRE was terminated by draining the fuel salt from the reactor circuit into two drain tanks on a lower level of the MSRE facility. At the end of the experiment in December of 1969, the fuel salt was allowed to solidify in the tanks and has remained there for the past 29 years.[1]

At the time of the MSRE operation, radiolytic effects on the fuel salt were recognized as a probable occurrence if the salt were stored below 100°C, with the net effect that fluorine gas could be liberated from the frozen salt mixture and cause corrosion and/or overpressurization of the drain tank containment system. To prevent the accumulation of this reactive gas, the frozen salt (which was usually at ~40°C because of the self-heating generated during fission product decay) was heated to 200°C on an annual basis to recombine the fluorine generated with the "reduced" sites left in the salt.

In the late 1980s, an increase in radioactivity in one of the gas lines in the North Electrical Services Area (NESA) was found, and it was suggested that mobile UF_6 could be responsible for this increase. Uranium could plausibly migrate only as UF_6, which, in turn, could only be formed directly or indirectly from radiolytic fluorine and UF_4 in the fuel salt. Because the annual annealing operation would serve to drive this condensable gas from the drain tanks to cooler surfaces, such as the gasline protrusion into the NESA, the annual annealing operation was postponed until a better understanding of the fuel salt behavior was obtained.

In early 1994, two 1000-mL gas samples were withdrawn from a gas line connected to the drain tanks and analyzed. High concentrations of F_2 and UF_6 were found in both of the samples (see Table 1), confirming that the annual annealing operations had not been successful in recombining the fluorine with the fuel salt and, more importantly, that the temperature gradient created during the annealing operation had surely contributed to the displacement of UF_6 from the fuel salt.

Table 1. Analysis of two samples taken from the MSRE off-gas system

Species	Samples	
	First	Second
UF_6	70 mm Hg (0.9 g/L)	68 mm Hg (0.9 g/L)
HF	1200 ppm	1000 ppm
MoF_6	10 mm Hg	*a*
CF_4	5 mm Hg	*a*
F_2	*b*	350 mm Hg
He, Ar, N_2, O_2 [c]	305 mm Hg	305 mm Hg

[a]Present as in first sample.

[b]Not determined analytically but assumed to be the same as second sample.

[c]Quantity determined by difference from total sample pressure. Qualitative identification by mass spectroscopy.

The 70-mm-Hg partial pressure of UF_6 is close to the saturation vapor pressure of solid UF_6 at temperatures that could plausibly exist in cooler regions of the MSRE off-gas system piping. Though UF_6 gas (particularly this highly radioactive isotopic mix) is subject to alpha radiolysis,[2–4] the presence of F_2 gas appears to protect it from net decomposition (promoting recombination of reaction products to UF_6) before decomposition products can precipitate.[5] The combination of these factors prevented any accurate prediction of the quantity of uranium that might have been converted to the mobile, gaseous UF_6.

On further investigation, it was found that the gas line from the drain tank also ran to the auxiliary charcoal bed (ACB), which was not isolated because a shutoff valve had failed in the open position. Gamma scan and thermal analyses indicated that more than 2.5 kg of the uranium from the drain tanks had deposited in the ACB, which, along with the fluorine also expected to be present, presented a chemical condition of considerable concern.

Oxidizing fluorine gases such as F_2 and UF_6 are known to react with activated charcoal to produce carbonfluorides of varying composition. Of particular concern is the potential for the explosive decomposition of carbon-fluorine compounds when they are heated or shocked. The consequences of such an explosion would be to scatter the radioactive materials laden in the charcoal and thus result in an unacceptable radiological hazard.

Because the chemical form of the fluorinated, uranium-laden activated carbon was not known, early safety analyses took the (very conservative) assumption that the potential chemical energy that could suddenly be released was represented by the complete reaction of molecular fluorine with carbon. Under that assumption, the energy released would be substantial and produce temperatures and gas pressures that could not be contained by the ACB or its containment. To move the analyses away from the extremely conservative bounding case and closer to reality, there was an urgent need to fully understand the carbon fluorine chemistry in the charcoal beds. With a better understanding of the physical and chemical condition of the ACB, the hazards could be more realistically evaluated, and an effective means of nullifying the hazards through chemical treatment or physical removal could be successfully developed.

This report addresses the carbon-fluorine-uranium chemistry of the ACB via laboratory tests designed to reproduce as closely as possible the conditions present in the beds. Laboratory analysis of the reaction products has been extensive and includes electron spectroscopy for chemical analyses (ESCA), nuclear magnetic resonance (NMR), Fourier transform infrared (FTIR) and Raman spectroscopy, thermogravimetric and differential thermal analyses (TGA-DTA), as well as a host of other techniques. This work has produced a more accurate description and a useful understanding of the chemistry in the ACB and is the basis upon which remediation is proceeding.

2. MATERIALS, INSTRUMENTATION, AND METHODS

2.1. ACTIVATED CHARCOAL

The coconut-based activated charcoal[6,7] samples were provided by Calgon Carbon Corporation. According to the MSRE and manufacturer records, the physical-chemical characteristics of this activated charcoal are quite similar to tthose of the material that was originally used by the MSRE experiment for the ACB. The properties provided by the manufacturer are shown in Table 2. The initial samples tested had a 4 by 10 mesh size. Since further information indicated that the MSRE ACB contained 6 by 16 mesh size particles, further tests were conducted using this smaller screened fraction.

Table 2. Physical-chemical properties of the activated charcoal

Total surface area [N_2, Brunauer-Emmett-Teller (BET) method], m^2/g	1150–1250
Density, g/cm^3	
Apparent (bulk) density	0.44
Particle density (Hg displacement)	0.85
Real density (He displacement)	2.2
Pore volume (within particle), cm^3/g	0.72
Voids in dense-packed column, vol %	50
Iodine number (minimum), mg/g	1200
Carbon tetrachloride adsorption, wt %	60
Ash, %	2.62
Total iron, wt % of ash	0.94
Total sulfur, % of carbon	0.03
Hardness number	92

Source: Calgon Corporation, P.O. Box 717, Pittsburgh, PA 15230-0717.

According to the manufacturer's data, a large portion of the volume of the micropores consists of pores in the range 1.5 to 2.0 nm (Fig. 1). In addition to the micropore structure, this type of activated charcoal has a system of macropores larger than 100 nm that interconnects the micropore structure and allows a rapid diffusion of gaseous species.

2.2 REAGENTS

Fluorine gas having a purity of 97% was procured from Air Products. The concentration of hydrogen fluoride (HF) was determined to be about 30 ppm using an infrared (IR) gas cell fitted with zinc selenide (ZnSe) windows. Since HF was also detected in the MSRE gases (see Table 1) that migrated to the ACB, no attempt was made to further purify the fluorine stream.

The helium used, also provided by Air Products, had a 99.99% purity. The preparative manifold has a titanium getter heated at 450 °C. The getter is routinely used to remove any water, oxygen, or nitrogen impurities. The vacuum line has soda-lime and liquid-nitrogen traps connected in a series to remove reactive and condensable impurities to protect the oil of the mechanical vacuum pump. The UF_6 used was provided by the Oak Ridge K-25 Site (currently East Tennessee Technology Park), and the uranium isotopic distribution was depleted in ^{235}U with respect to the natural abundance.

2.3. PREPARATION OF FLUORINATED CHARCOAL

The reaction between activated charcoal and fluorine is highly exothermic.[8–11] The unrestricted reaction can proceed briskly, thus causing a rapid heating that can easily inflame the activated charcoal to form carbon-fluorine compounds that further decompose into gaseous by-products such as carbon tetrafluoride (CF_4), hexafluorethane (C_2F_6), tetrafluorethylene (C_2F_4), carbonyl fluoride (COF_2), and carbon monoxide and dioxide (CO and CO_2, respectively).[12–17] The latter species originate from oxygen moieties present at the rim of the charcoal platelets (see Sect. 3.4).

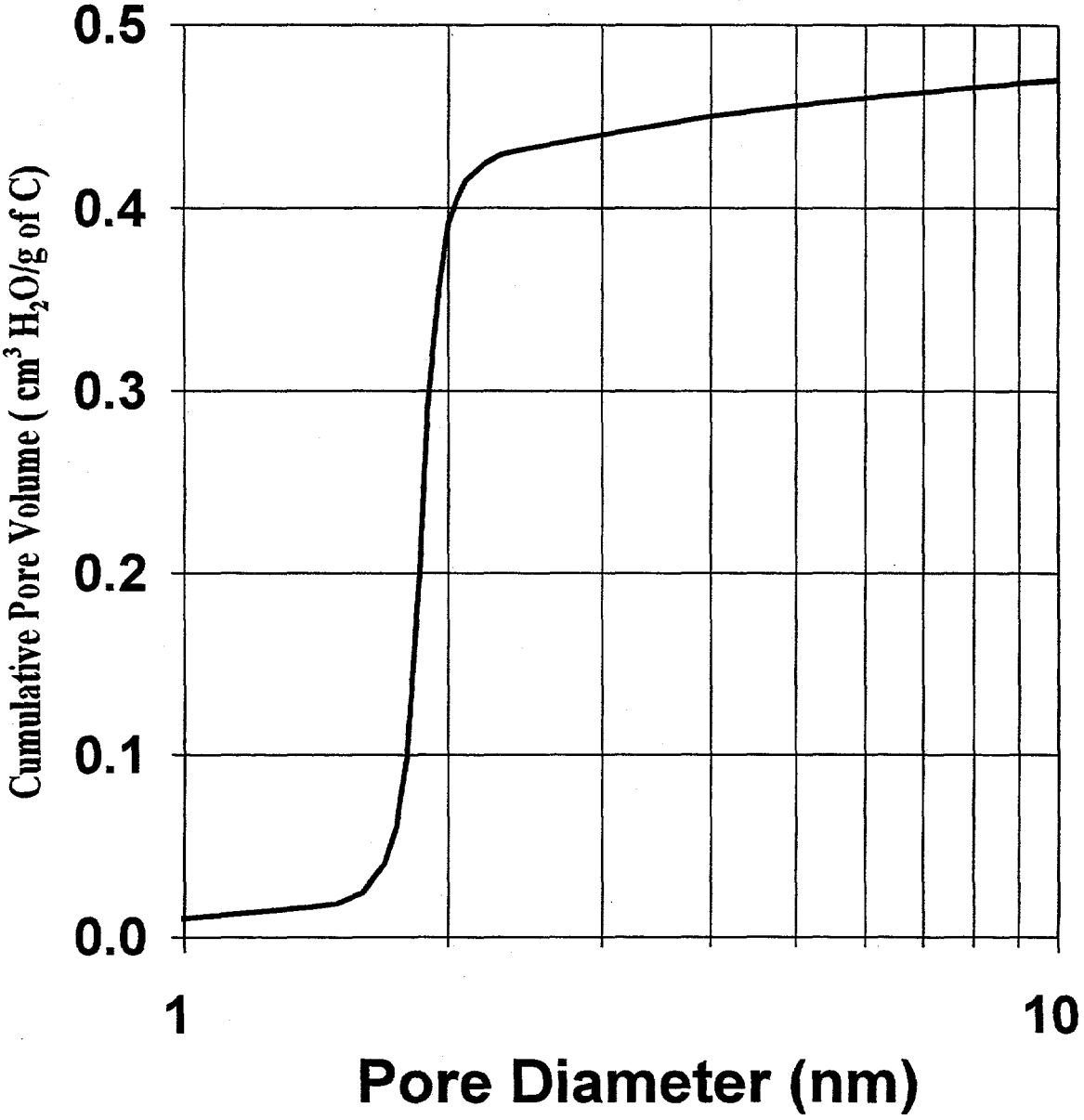

Fig. 1. Pore size distribution in the activated charcoal obtained from the water desorption isotherm. Source: Calgon Carbon Corporation.

In order to obtain reproducible carbon-fluorine compounds, it was necessary to control the speed of the fluorination and allow the heat of reaction to dissipate by diluting the F_2 stream with helium. A 5 vol % F_2-He mixed gas was prepared using a 3-L F_2-passivated vessel constructed of nickel. To obtain homogeneous mixing, the gases were introduced through the bottom. The heavier fluorine gas was introduced first.

Initially, 1-g activated charcoal samples were fluorinated using a small annular reaction tube made of quartz. The vessel was preheated to about 300°C under vacuum to remove hydroxyl sites from the quartz surface. Ace®-type vacuum valves (Teflon® piston with Viton® O rings) were used as input and output valves.

Type K thermocouples connected to a personal computer (PC)–based data acquisition system were used to continuously record the charcoal bed and wall temperatures for all preparations. The annular tube was fully immersed in the appropriate media to maintain the desired temperature. A Dewar filled with a methanol–dry-ice slush was used to prepare samples at about −78°C. Water and ice were used for 0°C, and for higher temperatures, a thermostatic bath was used.

To avoid contamination with silicon tetrafluoride (SiF_4), the quartz vessel was replaced by a passivated-nickel U tube (0.5-in. OD) having monel bellows valves at each end. Temperature control was as described previously except for the above-100°C preparations that used a hollow-tube furnace. Ten- to 15-g batches of activated charcoal were fluorinated using the U tube.

Before fluorination, the activated charcoal samples were preconditioned in their respective vessel (quartz or nickel tube) by heating to about 200–250°C under helium flow to simulate the conditions used for the conditioning of the actual MSRE auxiliary charcoal bed. After the pretreatment, the F_2-He gas mixture was dispensed at a very low flow rate. No attempt was made to measure the actual flow rate. Instead, a long Teflon tube was connected to the vessel outlet and used to bubble the gases through a sodium hydroxide solution. The flow of the F_2-He mixture was controlled such that the charcoal temperature was only slightly above the wall temperature (1 to 3°C). The flow of reactive gases was maintained for several days, depending on the batch size, until the internal and wall temperatures were equalized. After equalization, a slow flow of pure fluorine for 2 h ensured a complete reaction.

After completion, the preparative manifold was purged with helium for a few minutes. Then, the fluorinated samples were transferred to a dry-helium glove box and weighed.

2.4 THERMAL AND SHOCK STABILITY OF THE FLUORINATED CHARCOAL

Since several accidents have occurred at different facilities during the use or handling of partially fluorinated carbon, one of the most important issues was to determine the general stability of the fluorinated charcoal.[18–26]

In the earliest trials, several small samples consisting of a few charcoal granules with different fluorine contents were rapidly heated inside a heavy-wall, open quartz tube, using a torch to simulate a very fast temperature rise. These tests were followed by a small mixed bed having a few particles of fluorinated charcoal at the top and a couple of pieces of nonfluorinated activated charcoal at the bottom of a quartz tube. The quartz tube was protected by a heavy-wall Lucite tube and connected to a gas manifold using an Ace-type O-ring cap. Fluorine was rapidly introduced through the top of the mixed bed. The object of this test was to simulate a sudden entry of fluorine into the ACB system.

Controlled heating of different fluorinated charcoal samples was also done using 1-g samples, at rates between 5 and 20°C/min, both under vacuum and with a helium atmosphere. The pressure was continuously recorded using a pressure transducer connected to a PC-based data acquisition system. The gases were collected and analyzed by FTIR spectroscopy.

Ad hoc shock tests were done by simply hammering a few particles of fluorinated charcoal against a vise. Sparking using a Tesla coil was also used to test the stability toward electrical arcing.

2.5 TGA-DTA

TGA-DTA analyses were conducted on fluorinated charcoal samples prepared at different temperatures. The specimens were ground into fine powder under a helium atmosphere inside a dry glove box. Samples ranging from 100 to 250 mg were measured using a Harrop Industries TGA-DTA analyzer.

Samples and a blank were heated using alumina crucibles at 10°C/min under a nitrogen flow of 0.5 L/min. The weight and differential temperature were continuously recorded. The heat released as a function of the temperature was compiled by calibration using known standards, which included the heat of fusion of pure zinc metal (7.32 kJ/mol at 419.6°C) and the two phase transitions of $BaCO_3$ (α, NaCl-type cubic, to β, calcite-type rhombohedral, to γ aragonite-type orthorhombic ; $\alpha \Leftrightarrow \beta$, 3.13 kJ/mol at 1079 K, and $\beta \Leftrightarrow \gamma$, 17.56 kJ/mol at 1241 K).

2.6 ELECTRON SPECTROSCOPY FOR CHEMICAL ANALYSIS (ESCA)

ESCA, also known as X-ray photoelectron spectroscopy (XPS), is a high-vacuum technique that probes the surface of a material by bombarding the sample with an X-ray source. Because of the X-ray bombardment, photoelectrons are ejected from the sample. Since the energy levels of the various electrons are shifted depending on the chemical environment of their parent atom, the energy of the photoelectrons can be used to differentiate atoms of the same element in different bonding environments.

Following the initial ejection of a core electron, a valence electron can fall down to fill the vacancy. This decay process can release sufficient energy such as to eject another valence electron, thus generating a doubly charged ion. The electrons ejected by this process are called Auger electrons. Because they involve outer electron orbitals, Auger electron energy shifts are more sensitive to the chemical environment that surrounds the atoms.

The ESCA spectra were obtained using a PHI (Perkin Elmer) 5000 series spectrometer equipped with a dual anode (Al: $h\nu$ = 1486.6 eV and Mg: $h\nu$ = 1253 eV). For this experiment an aluminum anode was used at a power of 400 W (15 kV). The instrument was operated in the fixed analyzer transmission (FAT) mode with a pass energy of 17.9 eV for high-resolution scans. The background pressure was $<10^{-7}$ torr. The instrument was interfaced to an Unix-based Apollo 3500™ PC for data collection. In order to be consistent, binding-energy values for all samples were referenced to the O 1*s* line (532.5 eV).

ESCA is a surface analysis technique because only those photoelectrons generated near the surface (1–5 nm deep) can escape without energy loss. For the surface analysis to be representative of the entire sample, it was necessary to check the homogeneity of the fluorination. For that purpose small chunks of fluorinated material consisting of 4 × 6 × 2 mm platelets were tested first at the surface, then sliced in approximately half, and measured at the newly exposed surface. Additionally, activated charcoal samples were ground to a fine powder having uniform consistency. Double-sided carbon sticky tape was mounted onto a ESCA sample holder. The activated charcoal powder was then applied to the carbon sticky tape so that it uniformly and completely covered the tape.

All ESCA samples were prepared in a dry-helium glove box, and exposure to air was minimal. Loss of physically adsorbed gases (if any) under vacuum during the analysis, however, could not be avoided. Adsorbed F_2 and UF_6 will be seen by ESCA only if the species (assuming they are present initially) survive in quantity in the analyzed surface region for a time comparable with the sample evacuation and analysis time. Thus, molecular F_2, probably not a species that adsorbs strongly, is unlikely to be seen in room-temperature ESCA samples. Similarly, UF_6 might be difficult to detect. The UF_5, U_2F_9, and related compounds are subject to disproportionation to UF_6(gas) and UF_4 (solid) in a vacuum. Consequently, even if present, they will likely appear as UF_4.

Data analysis of each C 1*s* and F 1*s* spectrum included the application of a deconvolution procedure and a nonlinear least-squares curve-fitting (NLLSF) routine. Deconvolution was carried out using the point simultaneous overrelaxation Jansson algorithm.[27–28]

Deconvolution can enhance the resolution of a given ESCA spectrum by removing instrumental and intrinsic broadening effects. Broadening of an ESCA spectrum occurs because the intrinsic ESCA signal is convoluted with several broadening functions that are either Gaussian or Lorentzian in nature. Examples of these functions include the natural line width (because of the lifetime of the core hole), the exciting X-ray line shape, the detection system, and sample charging (a major factor with insulators).

To carry out the deconvolution properly, each broadened spectrum was pretreated. Pretreatment includes the removal of background by using a Shirley-type integral[29] and spectral smoothing by means of the modified least-squares correlation approach of Savitsky-Golay.[30] For this experiment, a correlating filter of 11 data points was used.

Curve fitting was accomplished by using the Levenberg-Marquardt damping method.[27] All peaks were fitted using a Voigt function with 20% Lorentzian character. The background was assumed to be integral, and it was applied individually to each peak.

2.7 IRRADIATION EXPERIMENTS

In order to test the stability of the fluorinated charcoal, C_xF samples prepared at different temperatures (Sect. 2.3) were subjected to intense gamma irradiation using a ^{60}Co source.[31]

Four C_xF samples prepared at −80, 0, 23, and 45°C were independently irradiated under 1 atm of helium for 40 days using a dose rate of 4000 R/min. The specimens prepared at −80, 0, and 45°C consisted of 1 g of the particular C_xF contained in separate, vacuum-tight F_2-passivated Monel tubes. For the C_xF prepared at room temperature, a larger amount of material (10 g) was used, and a pressure transducer was connected to the tube. The pressure inside the tubing was continuously monitored by a data acquisition system for the generation of any gaseous by-product that could be formed as a result of the irradiation.

At the end, each container was opened inside a helium-filled glove box (<1 ppm O_2 and water) and the specimens were weighed again. The results showed weight differences of less than 0.1%. The gas atmosphere of the tube containing the 23°C sample was analyzed using an FTIR instrument. The irradiated samples were also analyzed by ESCA, as described in Sect. 2.6.

2.8 FLUORINE (^{19}F) AND CARBON (^{13}C) NMR SPECTROSCOPY

Fluorine is easily detected by ^{19}F NMR spectroscopy.[32,33] It also provides a useful polarization source for investigating carbon structure by transferring the magnetization to the ^{13}C, ^{19}F-^{13}C cross-polarization (CP), NMR.[34] The combination of ^{19}F NMR and ^{19}F-^{13}C CP NMR can be used as a powerful tool to study the structure and chemical nature of the fluorinated charcoal prepared at different temperatures.[35-36]

The spectra were obtained using a Bruker MSL100™ spectrometer in a 2.35-T field. Samples, 50–100 mg, were packed in 5-mm Torlon rotors and spun in a doubly tuned, single-coil, magic-angle-spinning (MAS) probe. The 5-mm supersonic HFC probe (Doty Scientific) was constructed without fluoropolymers. Single-pulse ^{19}F spectra were acquired at 94.200 MHz and at MAS = 12 kHz ^{13}C spectra were obtained at 25.184 MHz by ^{19}F-^{13}C with ^{19}F decoupling during acquisitions. Dipolar dephasing delays in the range of 0–100 μs were used to aid the assignment of fluorinated groups, while 0 to 2-ms delays were used for graphitic carbon.

Quantitative CP data were obtained using variable contact times (VCTs). Contact times chosen were sufficiently long such as to allow maximum transfer of polarization from the abundant spin (in this case ^{19}F) to the dilute spins (^{13}C) before spin relaxation processes degraded the signal.

Signal intensity is highly dependent on both the location and dynamics of the abundant spin (^{19}F) so that remote carbon nuclei build intensity more slowly. If relaxation processes prevent the signal intensity from reaching the full value at the selected contact time or if the contact time is too short to allow full intensity to be generated, these species will be underrepresented in the spectra.

To obtain quantitative compositional data from these CP experiments, VCT was performed on the series of fluorinated charcoals. Signal intensity (I) is plotted vs contact time (τ) over a wide range of times (25 μs to 100 ms) and fit to Eq. (1) to determine the initial areas and time constants for each carbon resonance in the spectra. While I_0 represents the full intensity of the resonance, T_{CF} and $T_{1\rho}$ represent, respectively, the time constants governing the buildup and decay of signal intensity by dipolar interactions between ^{13}C and ^{19}F nuclei. Fitting was accomplished by least-squares minimization. Data for each carbon type are then reported as a percentage: I_0 for each species divided by the sum of the I_0 values of all species observed:

$$I(\tau) = \frac{I_0}{T_{CF}} \cdot \frac{e^{-\frac{\tau}{T_{1\rho}}} - e^{-\frac{\tau}{T_{CF}}}}{\frac{1}{T_{CF}} - \frac{1}{T_{1\rho}}} \qquad (1)$$

Typically, 25–40 contact times were used for each fluorinated charcoal sample. In every case more than 10 contact times were selected in the very short (10- to 200 μs) and long (10- to 100-ms) contact time regions. In these regions, signal intensity is affected by only one dipolar interaction, either buildup or decay; therefore, these regions are more important in the accurate determination of either T_{CF} or $T_{1\rho}$ by the fitting procedure. The precision of the signal intensities reported is on the order of 5%, primarily because of low signal-to-noise ratios and difficulties in maintaining the match conditions over the many hours of acquisition. The compositions determined by NMR are on the same order. The time constants produced by the fitting procedure are reliable to a single digit.

3. RESULTS

3.1 STOICHIOMETRY OF ACTIVATED CHARCOAL EXPOSED TO F_2

One of the most important characteristics observed for all the fluorinated samples was a smooth and continuous change in the physicochemical properties according to the temperature used during the fluorination.

The experimental results shown in Fig. 2 indicate that the carbon:fluorine ratio, which is determined by weight difference, changes according to the preparation temperature in a very reproducible fashion. It can also be observed that a plateau having a global C_2F composition exists in the temperature range between 50 and 150°C. The data include samples prepared using quartz and nickel containers. Since there were no appreciable differences based upon the container material, the contamination with SiF_4 from the pretreated quartz tubes was judged insignificant.

The calculation of the gravimetric C:F ratio assumes that the weight difference results only from the loading of fluorine. However, fluorine is probably displacing some oxygen and hydrogen from components such as hydroxyl groups located at the rim of the platelets. The actual carbon:fluorine ratios are slightly higher than those calculated by weight difference (see Sect. 3.4).

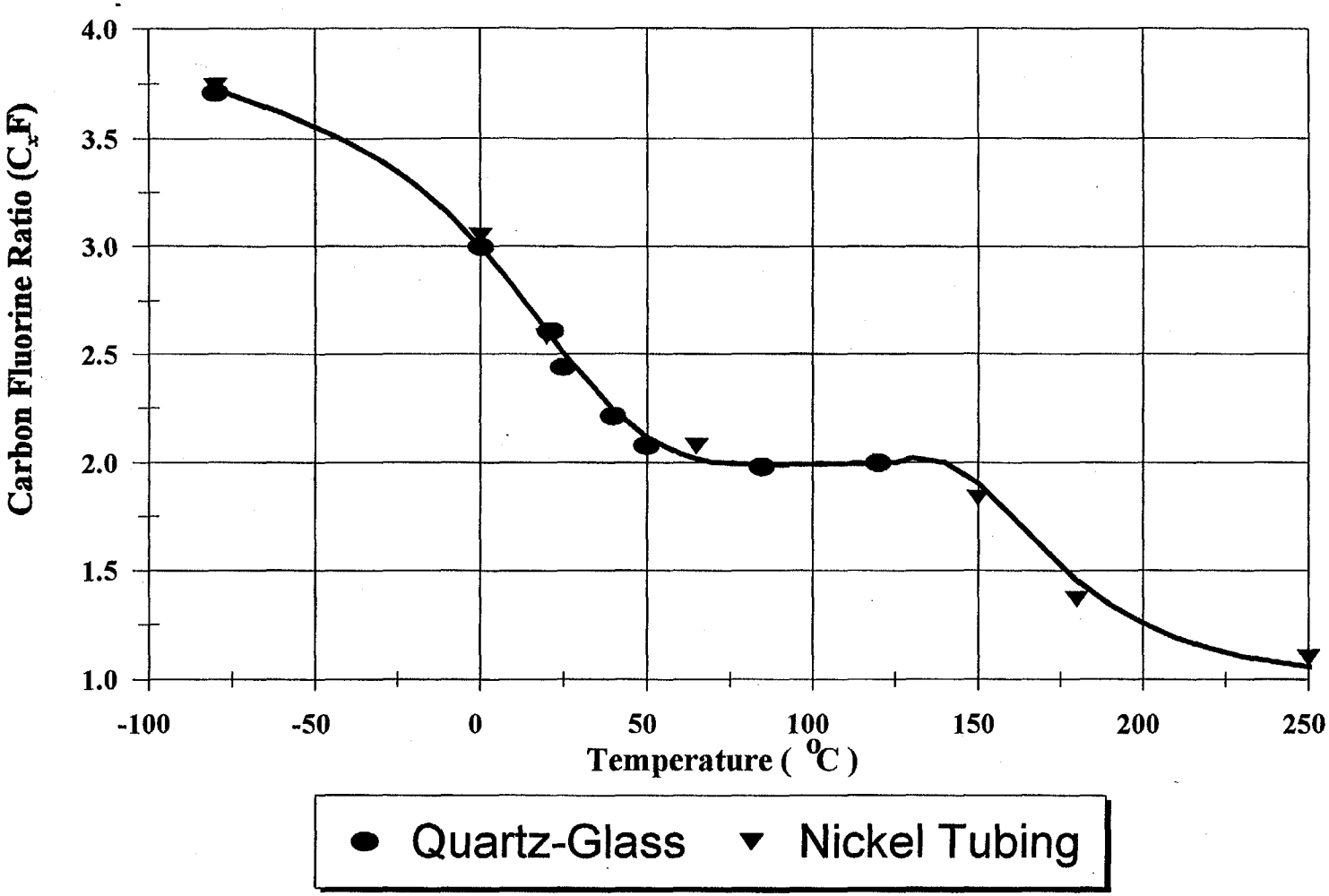

Fig. 2. Carbon:fluorine ratio (by weight difference) vs the fluorination temperature.

Several samples prepared at different temperatures were subjected to a prolonged overnight vacuum at room temperature, after which they showed a very slight weight loss. In all cases, the total weight loss was below 3%. Sorption experiments performed by prolonged contact of fluorinated charcoal with pure fluorine at the same temperature used during the fluorination showed a weight gain on the order of 2%. This finding is at least indirect evidence of adsorption of F_2, though other impurities cannot be definitively ruled out.

Fluorinated samples prepared at temperatures below 200°C were black and externally indistinguishable from the initial activated charcoal. The fluorinated particles became increasingly brittle with increased fluorination temperatures. The size of the particles remained essentially unaffected by the fluorination process at temperatures below 120°C. At higher fluorination temperatures, some of the initial chunks fractured into smaller pieces. The initial black color of the fluorinated samples changed at temperatures in excess of 200°C. They changed first from black to gray, then to brown, and finally to white at the highest temperature tested (350°C).

3.2 ESCA OF FLUORINATED SAMPLES

As mentioned in Sect. 2.6, ESCA is a surface technique during which a sample is bombarded by an X-ray source and photoelectrons are ejected from the sample. The energy of those electrons can be used to differentiate atoms of the same element in different bonding environments. Samples of fluorinated carbon prepared at the temperatures described in Sect. 2.3 were analyzed using ESCA. The main objective was to determine all the different environments for carbon and fluorine atoms in the different carbon-fluorine samples in order to understand the chemical nature of the fluorinated charcoal, C_xF.

The homogeneity of the samples was tested as mentioned in Sect. 2.6. The outcomes of the homogeneity tests are shown in Fig. 3. The spectra at normal beam incidence, 35° tilt, and a new cleaved surface were almost identical. The process was repeated for a second sample with the same results. The results were also compared with those for a ground sample without any significant difference. As a consequence, it can be concluded that the fluorinated charcoal samples are quite homogeneous along the volume of the particle.

The ESCA binding-energy regions of C 1*s* and F 1*s* as well as the $KL_{23}L_{23}$ Auger region of fluorine were analyzed for the fluorinated samples.

The original activated charcoal and the fluorinated samples prepared at the lower temperatures all contain a relatively small concentration of oxygen. NMR data (see Sect. 3.3) show the presence of different oxygenated moieties located at the periphery of the graphitic platelets.

3.2.1 C 1*s* Region

As seen in Fig. 4, the C 1*s* peak for the standard activated charcoal sample exhibits asymmetric tailing toward high binding energy. This behavior is typically seen in the ESCA spectra of conductive (metallic) materials. The tail is due to the interaction of the positive core hole, formed during the photoemission process, with the conduction electrons.

Another feature shown in Fig. 4 for the C 1*s* spectrum of activated charcoal is the presence of a plasmon satellite peak at ~6 eV from the main line.[27] The peak shape and satellite peak of the activated charcoal might cause some complications as well as possible error when curve fitting the spectra of the samples that have been fluorinated.

For consistency and to minimize errors when fitting the C 1*s* envelopes of the fluorinated samples, the area ratio and the binding-energy differences between the fitted peaks and the main C 1*s* peak, representative of activated charcoal, were kept constant. Also, the tailing parameter was fixed throughout the analysis of the fluorinated samples. However, the peak position of the main C 1*s* line was allowed to relax to its local minima when fitting the fluorinated samples spectra.

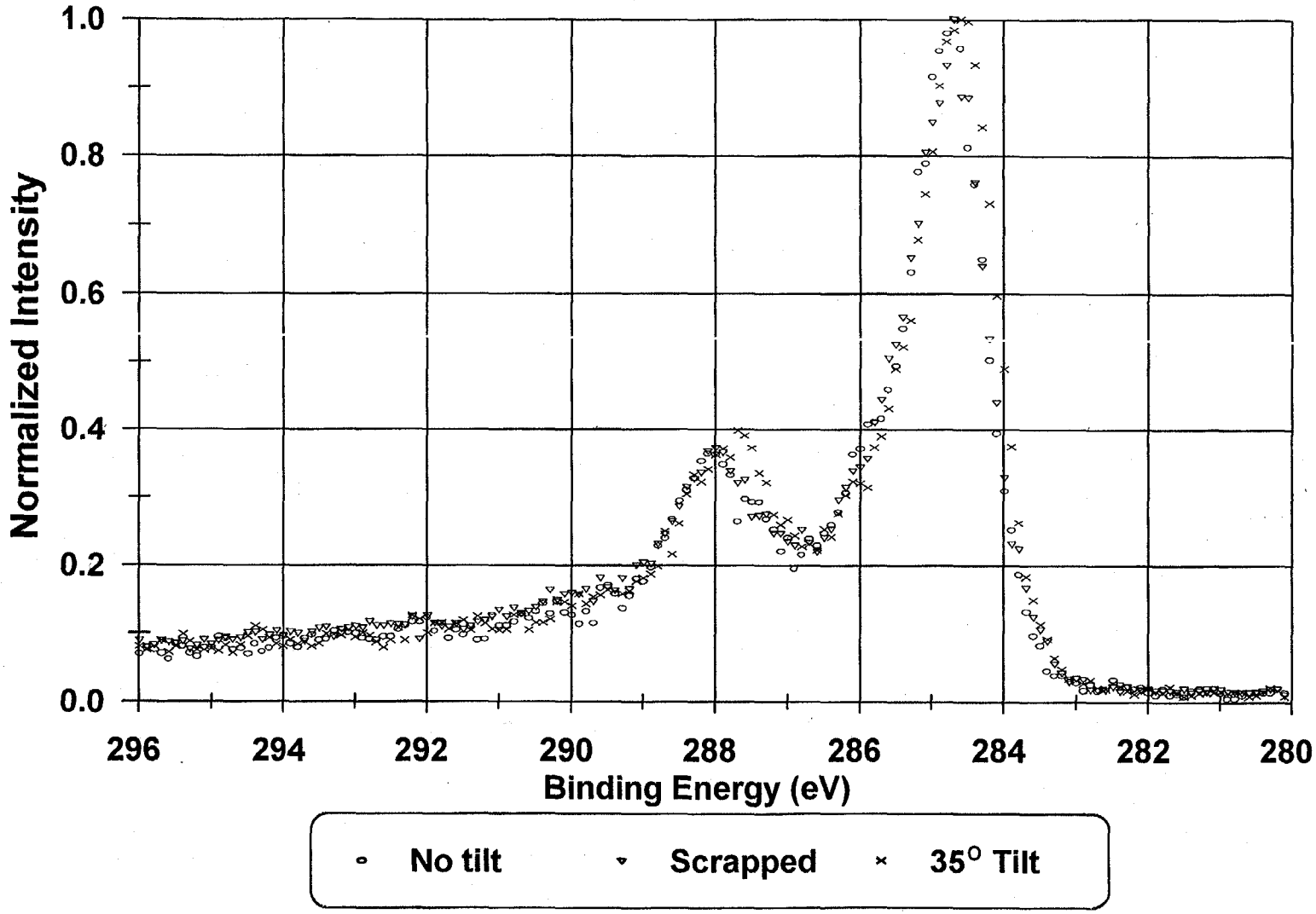

Fig. 3. ESCA spectra, C1*s* region of fluorinated charcoal at −80 °C, obtained using different incident angles and at different depths to confirm the homogeneity of the fluorination.

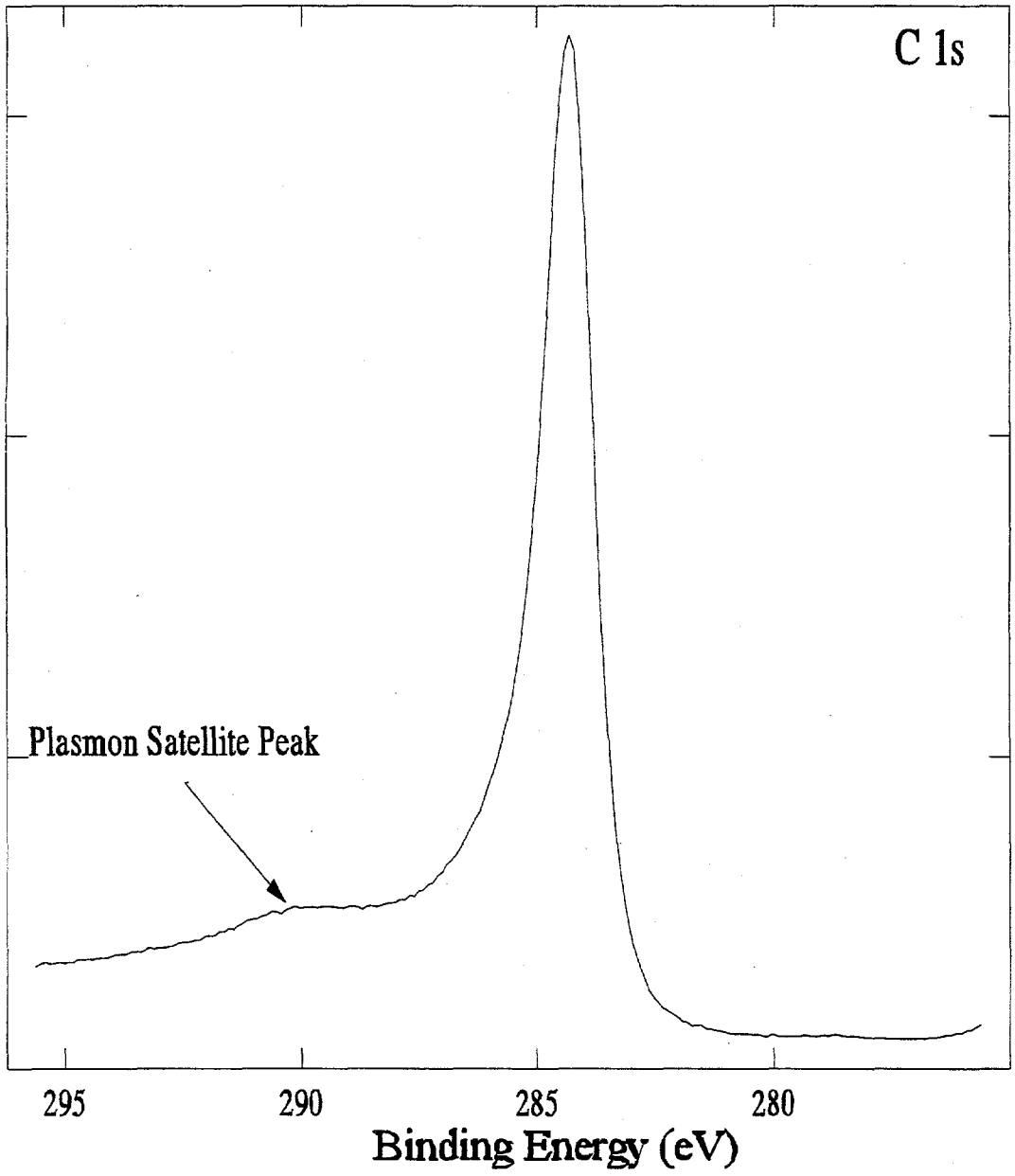

Fig. 4. ESCA spectrum, C 1*s* region, of activated charcoal at room temperature.

Figure 5 shows the series of C 1*s* envelopes obtained by fluorinating activated charcoal at various temperatures. The top plot of the figure displays the spectrum of the initial activated charcoal. The curve at the bottom corresponds to the spectrum of the residue from a fluorinated sample that was thermally decomposed by prolonged heating at 750°C.

It is clear that a new major peak emerges when activated charcoal is exposed to F_2 at –80 °C. This peak arises from fluorination of the charcoal. The figure distinctly indicates that the extent of fluorination increases with increasing fluorination temperature. It can also be seen that the peaks from samples fluorinated at higher temperatures are broader than those for the samples fluorinated at lower temperatures. This results because these samples exhibited a higher degree of electric charging than the samples fluorinated at lower temperatures.

The increase in charging is directly related to the destruction of the conductive graphitic microstructure of the samples as the fluorination temperature rises (see Sect. 4). The bottom spectrum demonstrates that prolonged heating of a fluorinated sample to 750°C removes the fluorine (as CF_4 or other volatile fluorocarbon) thus leaving a carbonaceous residue similar to the original material.

Figure 6 displays the ESCA data for the C 1*s* region for a fluorinated sample prepared at 180 °C that deflagrated after being rapidly heated. One can see that most of the fluorinated carbon disappeared and that the deflagrated sample resembles the initial activated charcoal (see Fig. 4).

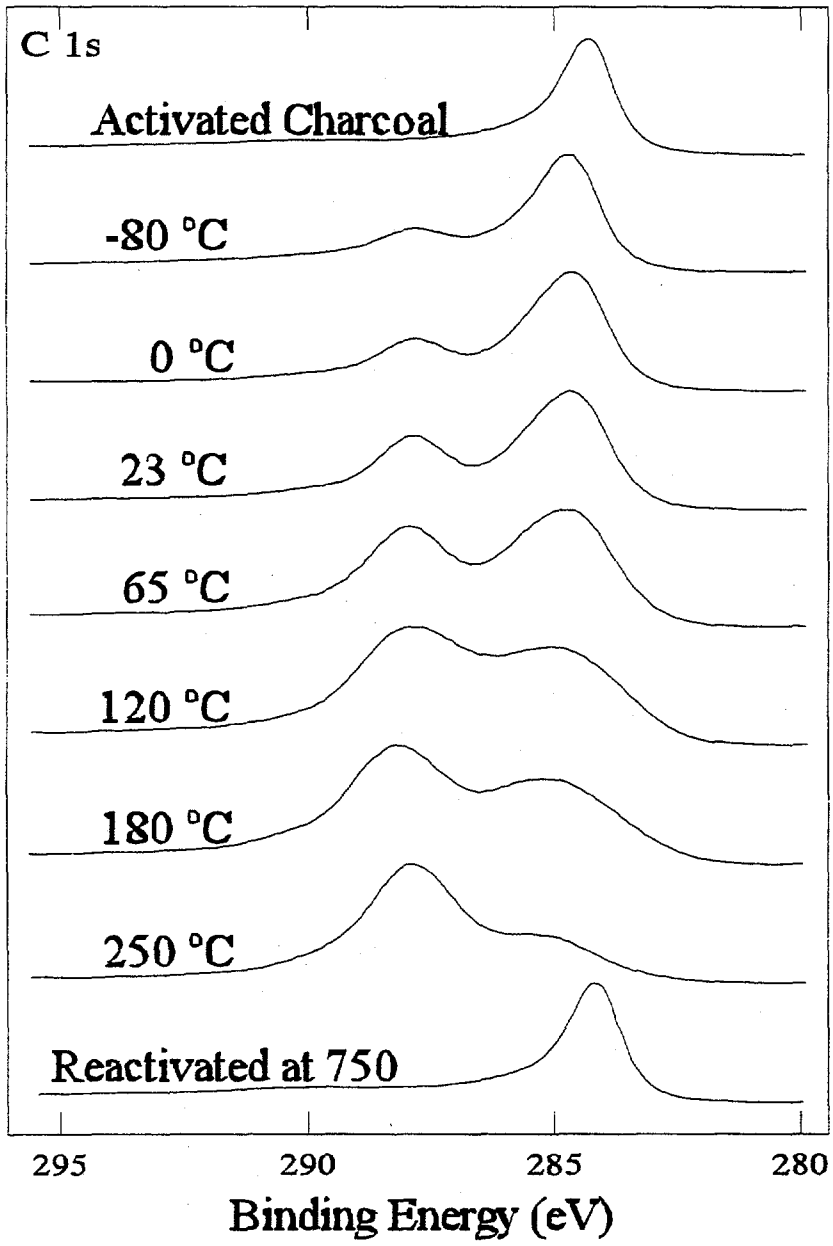

Fig. 5. ESCA spectra, C 1s region, for fluorinated charcoal at different temperatures.

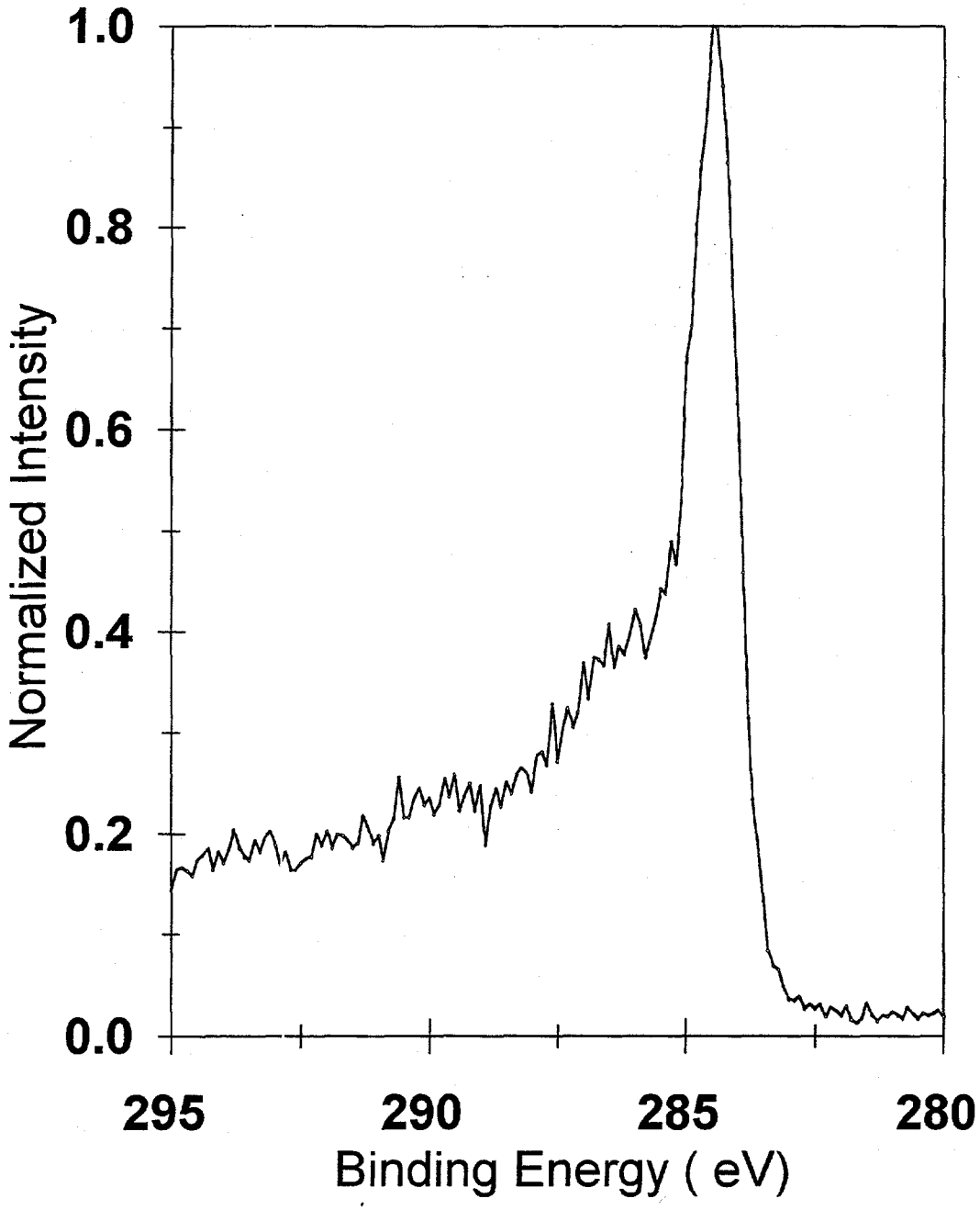

Fig. 6. ESCA spectrum, C 1*s* region, after deflagration of a fluorinated sample prepared at 180°C.

3.2.2 F 1*s* and Auger Regions

Figure 7 exhibits the series of F 1*s* ESCA envelopes for the samples fluorinated at various temperatures. Unlike the C 1*s* envelopes, the shape and position (~ 687.0 eV) of the F 1*s* peak remain relatively constant as the fluorination temperature is increased.

Figure 8 shows the series of F $KL_{23}L_{23}$ Auger envelopes for the fluorinated samples. As mentioned in Sect. 3.1, Auger electrons are more sensitive to the bonding environment than are the core photoelectrons. Therefore, if different bonding interactions exist as the fluorination temperature changes, the fluorine Auger envelopes will exhibit different shapes. It is clear from Fig. 8 that all the fluorine $KL_{23}L_{23}$ Auger peaks are very similar in shape.

The fundamental covalent nature of the carbon-fluorine bond in fluorinated charcoal was confirmed by the fluorine Auger spectral measurements. Figure 9 shows the F $KL_{23}L_{23}$ Auger peak for LiF, Teflon, and a representative fluorinated charcoal sample. LiF and Teflon were used as standards. The bonding in LiF is ionic, and the bonding in Teflon is covalent. It is evident that the shape of the F $KL_{23}L_{23}$ Auger for the fluorinated sample resembles that of Teflon. In fact, when the F $KL_{23}L_{23}$ Auger peak of the fluorinated sample was cross-correlated with the F $KL_{23}L_{23}$ Auger peak of Teflon, the cross-correlation response (r_o) was 0.992. (A perfect correlation is $r_o = 1.00$.)

3.2.3 Data Analysis and Carbon Speciation

Figure 10 exemplifies a deconvoluted ESCA spectrum for the C 1*s* region. The four peaks can be attributed to the following four environments for carbon atoms. The peak at the lowest energy corresponds to the planar graphitic-like structure (sp^2 hybridization) of the activated charcoal. The carbon atoms represented by this peak remain unaffected by fluorine atoms and display the same signature as in the initial activated charcoal.

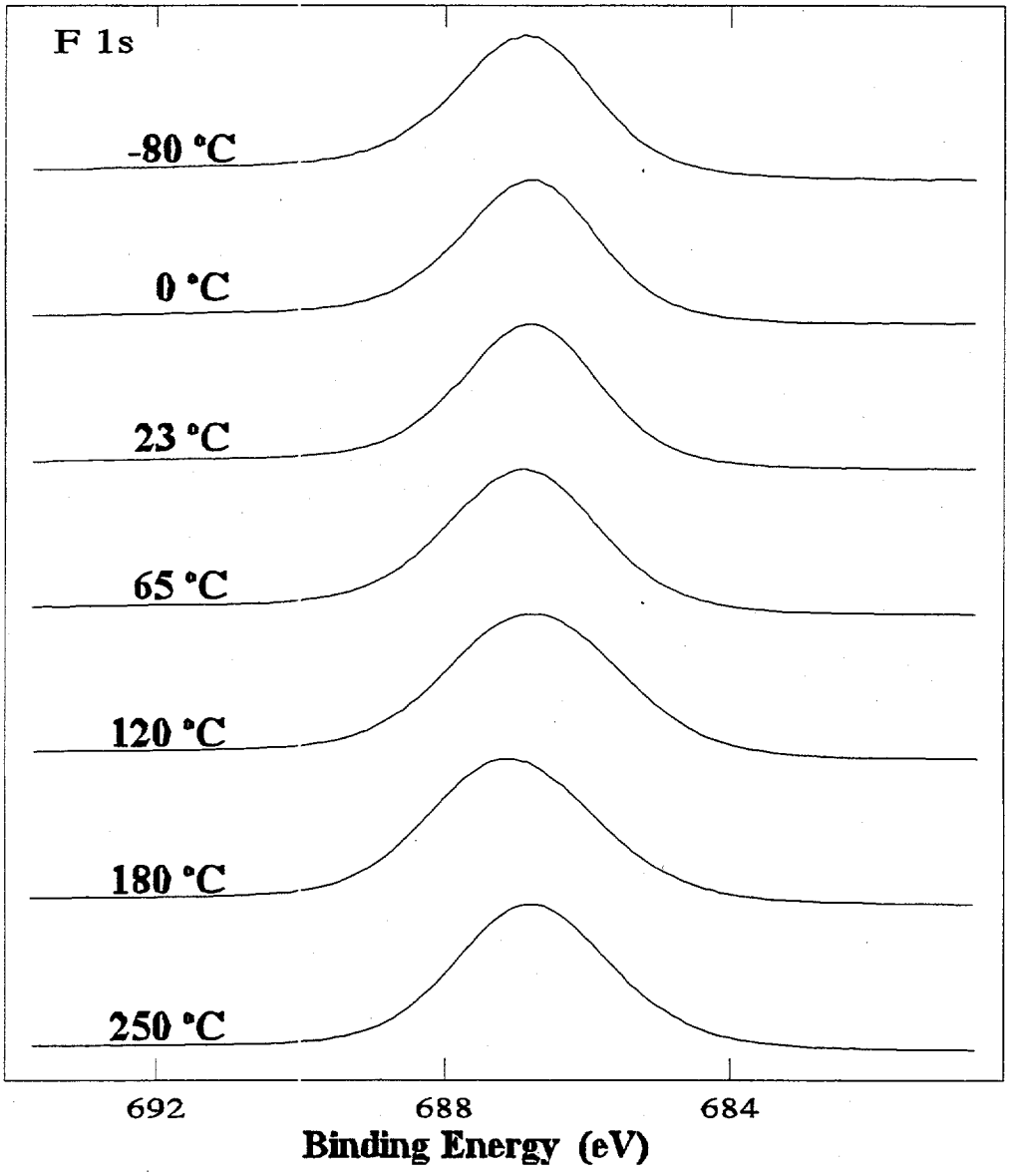

Fig. 7. ESCA spectra, F 1*s* region, for fluorinated charcoal prepared at different temperatures.

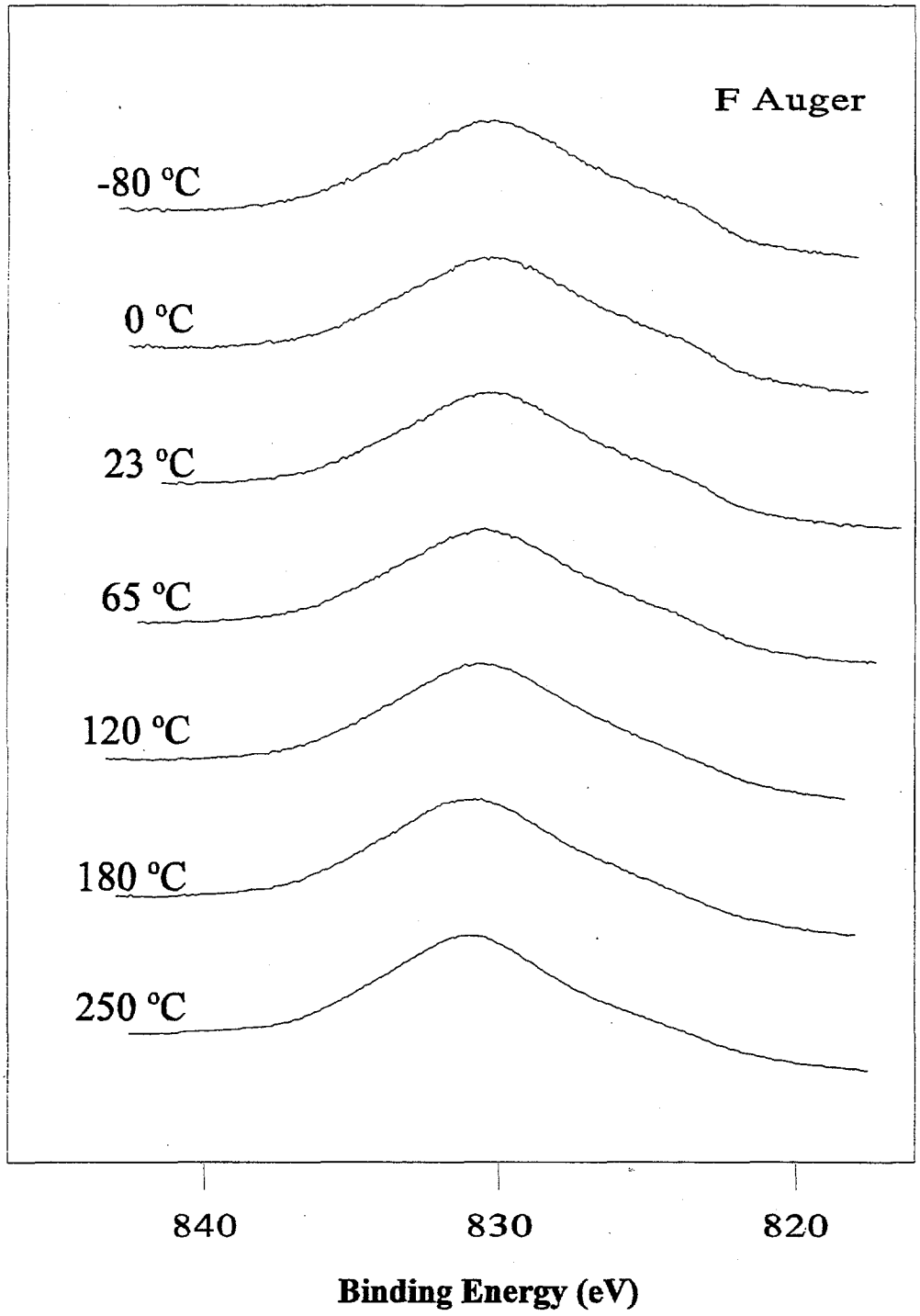

Fig. 8. Fluorine Auger electrons from fluorinated charcoal prepared at different temperatures.

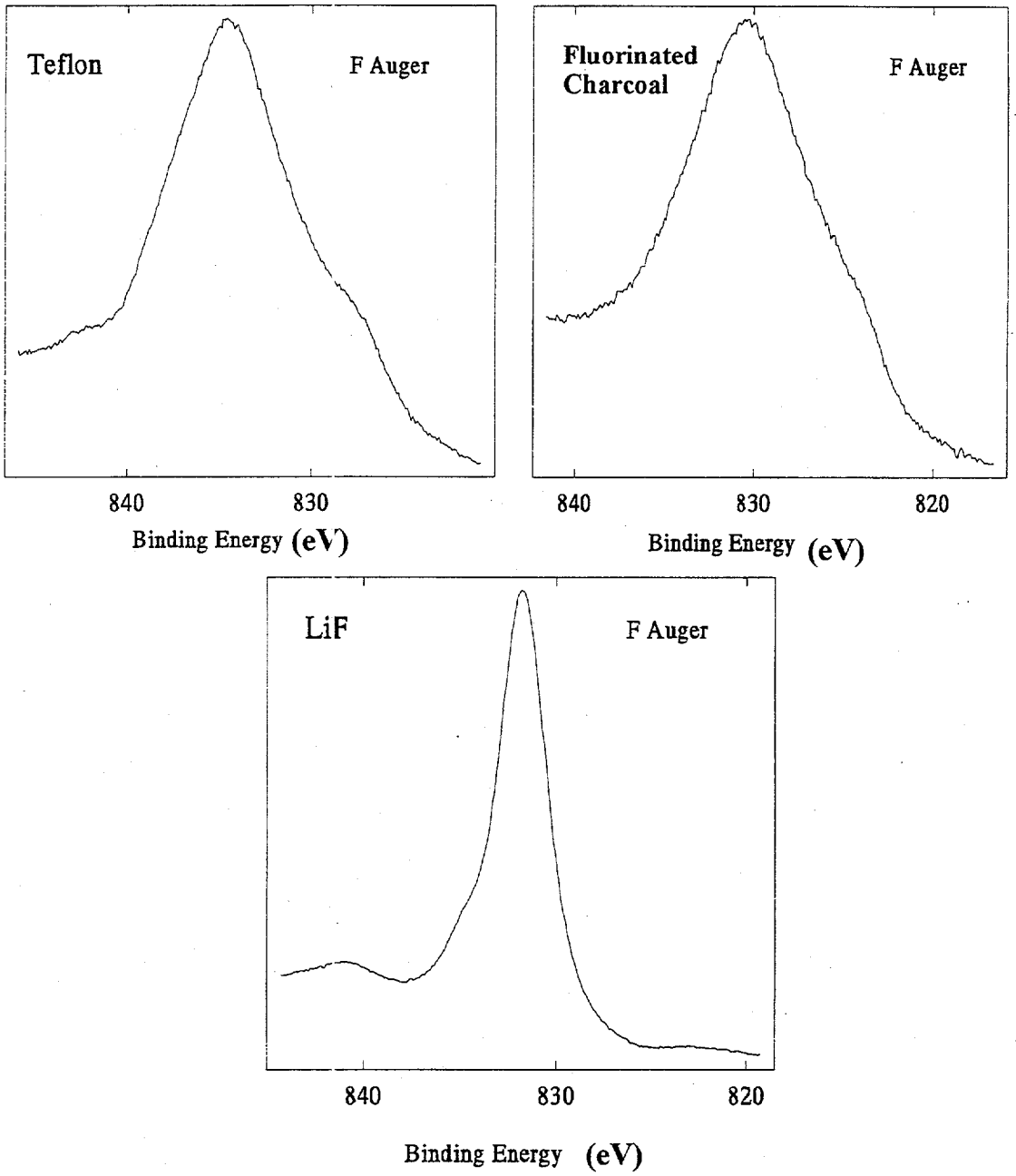

Fig. 9. Auger peak for fluorine ($KL_{23}L_{23}$) in Teflon, fluorinated charcoal, and LiF.

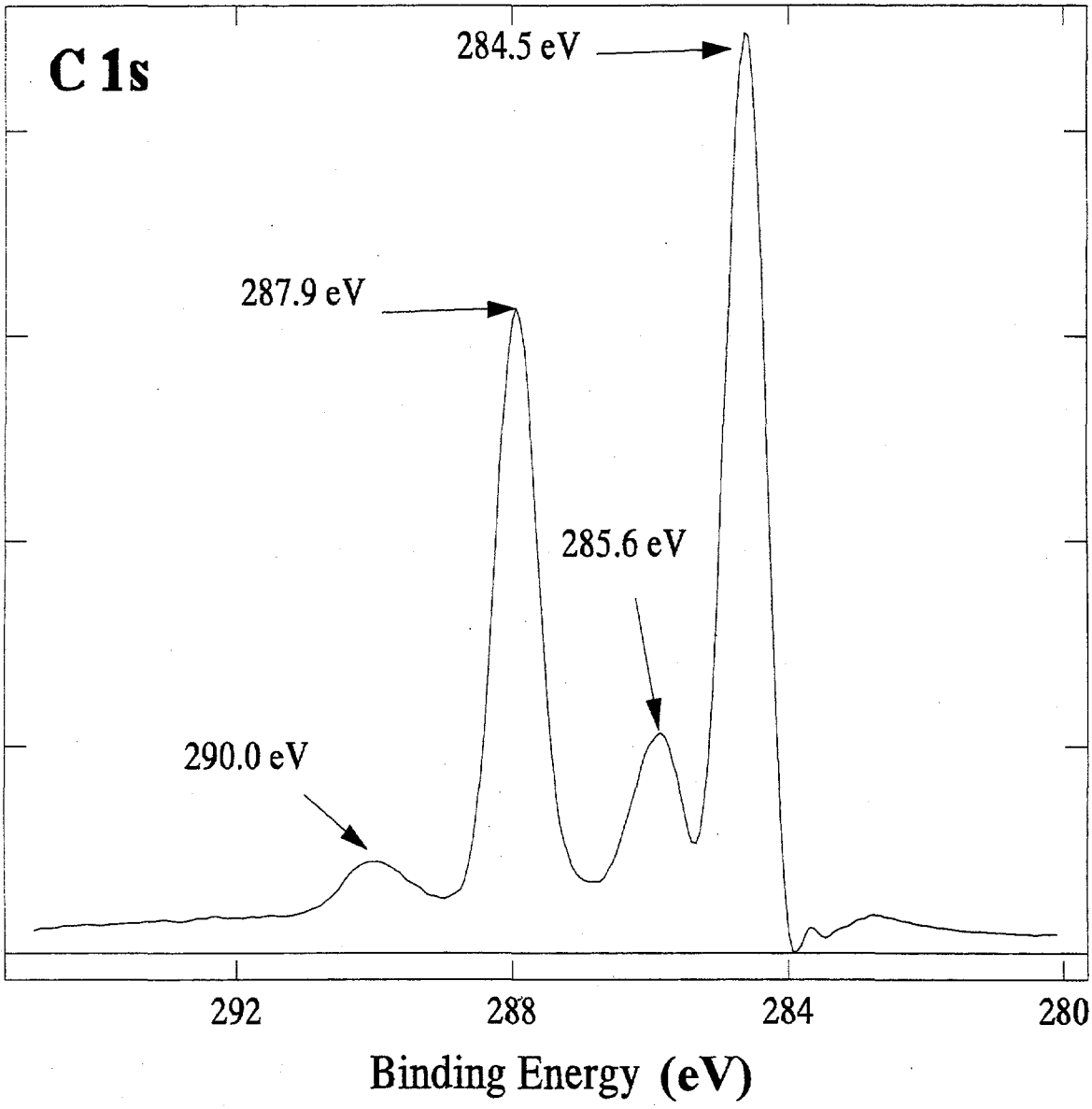

Fig. 10. Deconvoluted ESCA spectrum for the C 1*s* region.

The second peak originates from carbon atoms that are also bonded to other carbon atoms; however, they are experiencing the influence, intraplanar or interplanar, of fluorine atoms. The third peak represents carbon atoms directly bonded to fluorine atoms (fluoromethine CF, sp^3 hybridization). Finally, the fourth peak, at the highest binding energy, corresponds to carbon atoms bonded to two fluorine atoms (fluoromethylene CF_2, sp^3 hybridization). These carbon atoms are located at the rim of the micrographitic platelet (see Sect. 4). For the samples prepared at the highest temperatures, a fifth peak (~292 eV) corresponding to the end-of-chain trifluoromethyl groups (CF_3, sp^3 hybridization) was observed.

Figures 11 through 17 show the curve-fitted ESCA C 1*s* region for individual samples fluorinated at different temperatures ranging from −80 to 250°C. The fits include the different peak components and the residuals associated with the fit of the experimental data.

Table 3 summarizes all the fitted data. It can be observed that the peaks are wider at higher fluorination temperatures because of the increasing charge buildup resulting from the decreasing conductivity (loss of graphitic structure) of the fluorinated charcoal. There is also a small shift toward lower binding energies for the graphitic-like carbon atoms, while all the other carbon peaks shift toward higher binding energies as the fluorination progresses with higher temperatures.

As Figs. 11 through 17 and Table 3 indicate, the peak corresponding to "isolated" carbon diminishes while the fluoromethine (CF) carbon peak increases with increased fluorination temperatures.

Figure 18 displays a normalized distribution of the different carbon environments for the different fluorination temperatures. Again, it can be seen that the peak corresponding to "isolated" carbon diminishes while the fluoromethine (CF) carbon peak increases with increased fluorination temperatures.

Table 3. ESCA curve-fitting results[a,b]

Temp (°C)	Graphitic C			C-C			CF			CF_2			CF_3		
	Area	Position	FWHM	Area	Position	FWHM	Area	Position	FWHM	Area	Position	FWHM	Area	Position	FWHM
-80	84,115	284.4	1.1	66,660	284.8	2.03	37,950	287.6	1.9	4,537	289.9	1.6			
0	78,292	284.3	1.1	74,817	284.8	2.2	38,814	287.7	1.7	4,704	289.8	1.65			
23	76,797	284.4	1.3	72,417	284.8	2.43	50,737	287.7	1.6	6,260	289.7	1.61			
65	24,551	284.1	1.3	90,875	284.8	2.49	60,087	287.8	1.8	7,761	289.7	1.78			
120	19,148	283.7	1.7	82,469	285.0	2.85	84,346	287.8	2.3	4,618	290.2	1.60	1,633	291.9	1.90
180	26,121	283.8	1.7	99,606	285.1	2.85	116,465	288.0	2.2	9,495	290.2	2.0	2,826	291.6	2.0
250	217	283.8	1.7	79,696	285.2	2.85	144,005	287.8	2.1	12,309	290.1	1.75	2,026	291.7	1.80

[a] Graphite area includes graphite plasmon plus oxides.

[b] Full-width half-maximum.

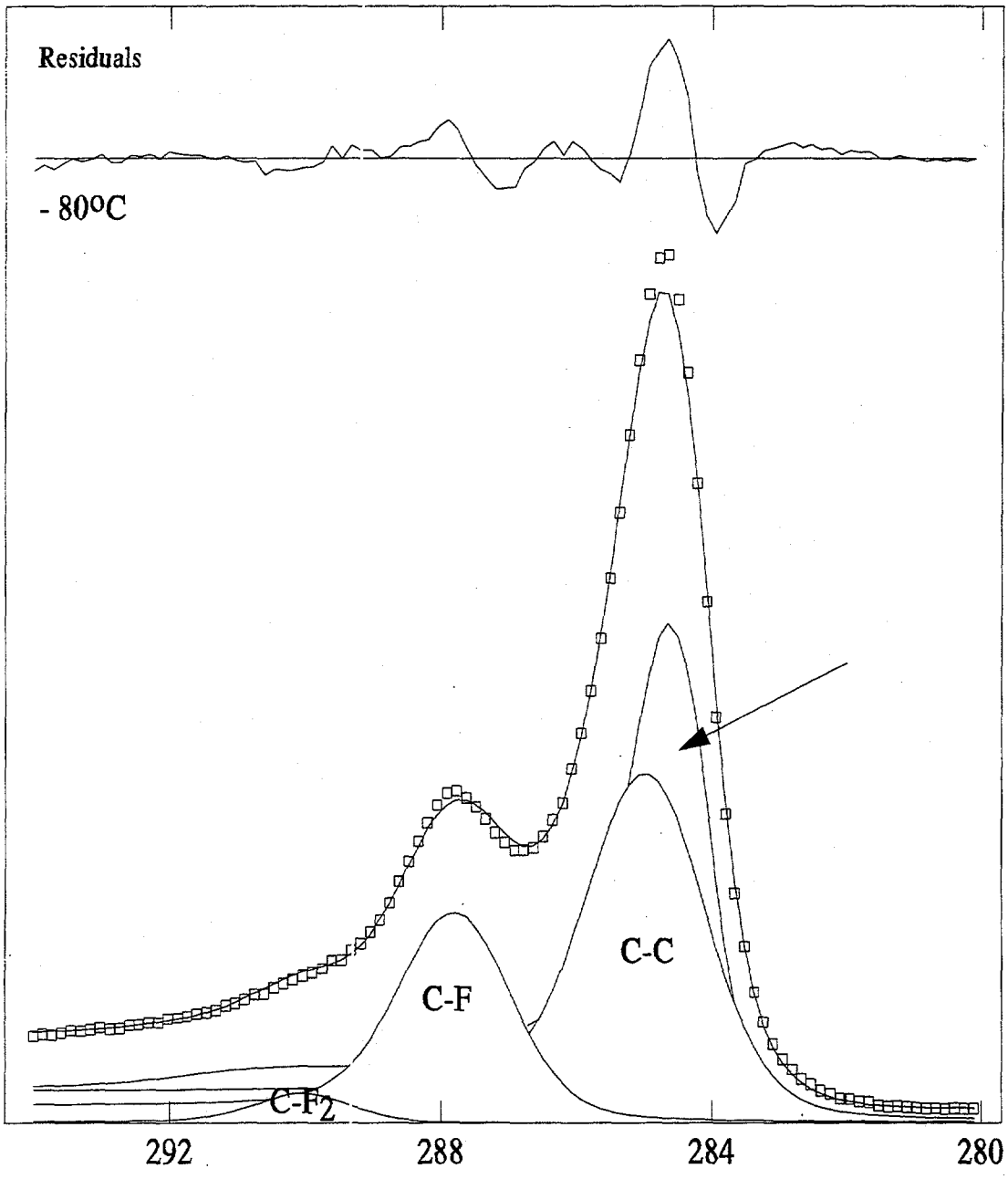

Fig. 11. ESCA spectra, C 1*s* region, of fluorinated charcoal prepared at -80°C.

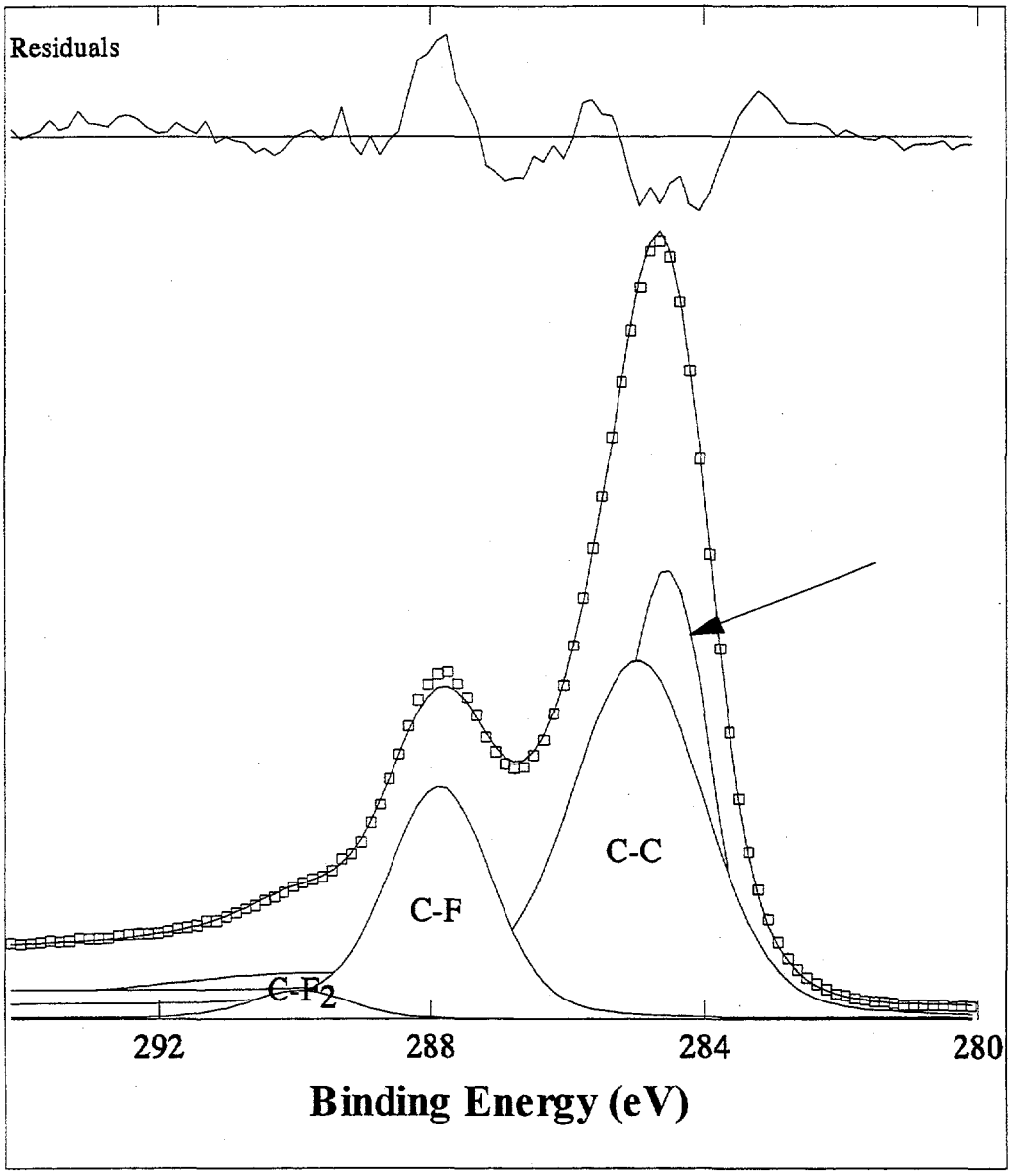

Fig. 12. ESCA spectra, C 1*s* region, of fluorinated charcoal prepared at 0°C.

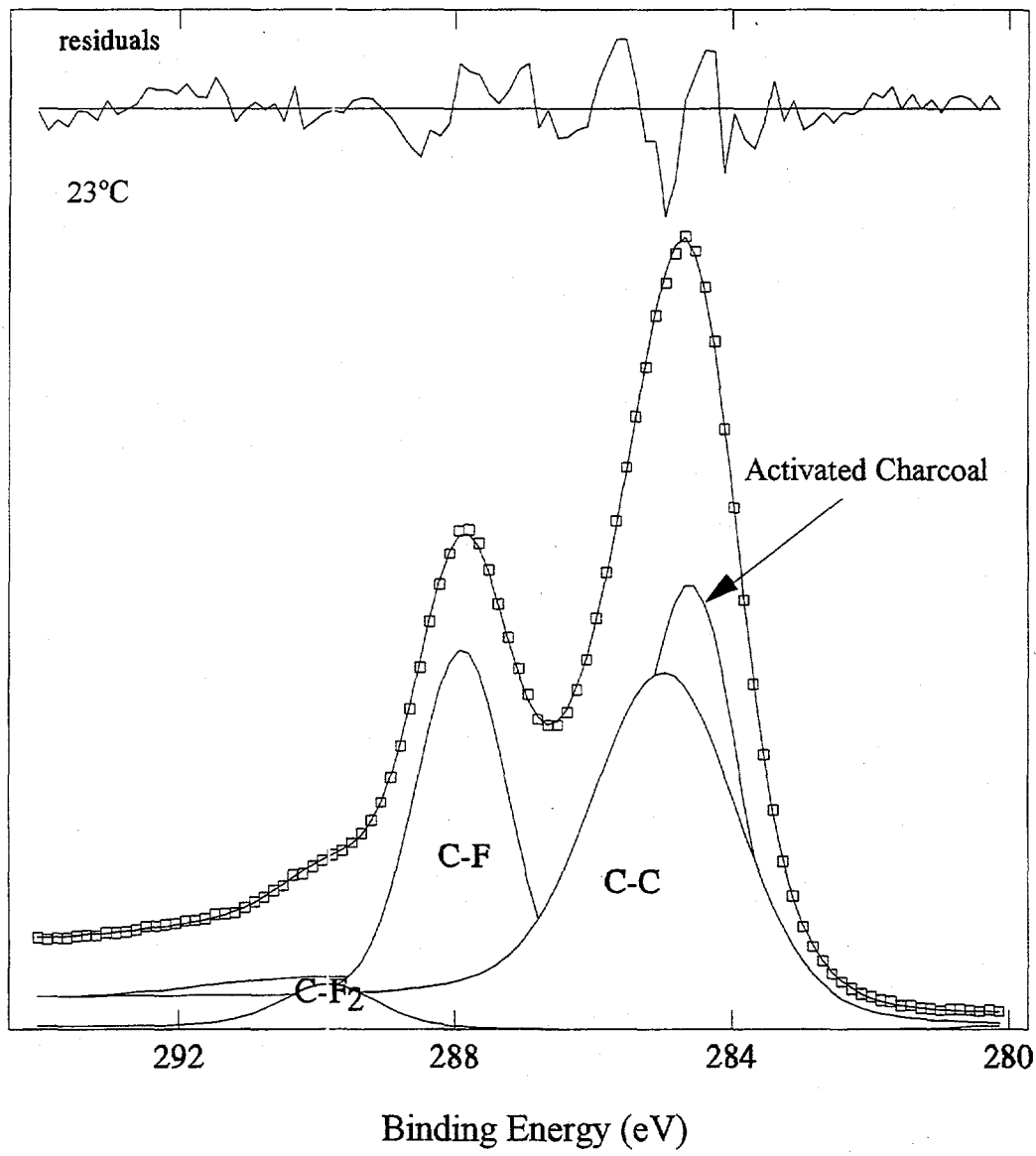

Fig. 13. ESCA spectra, C 1*s* region, of fluorinated charcoal prepared at 23 °C.

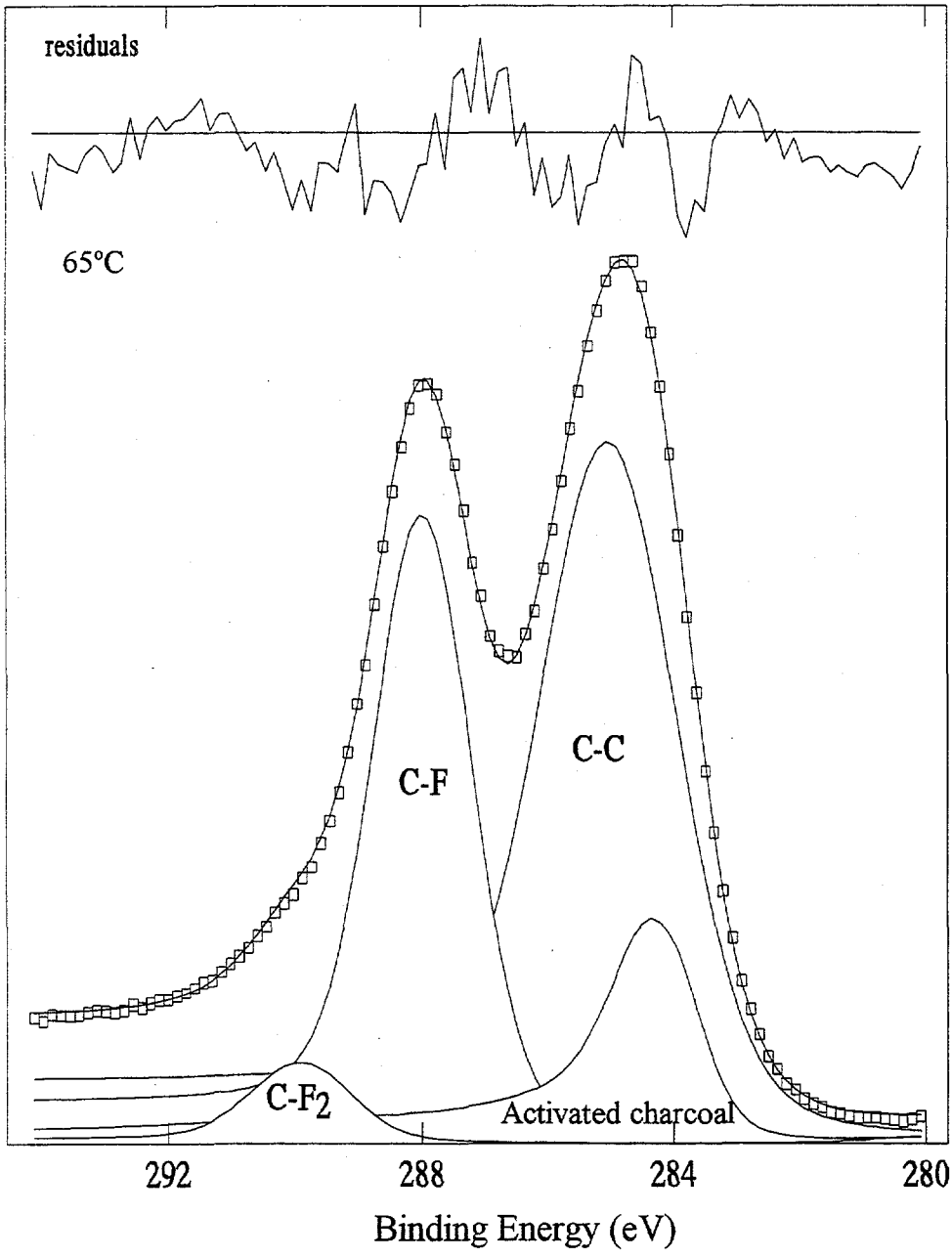

Fig. 14. ESCA spectra, C 1*s* region, of fluorinated charcoal prepared at 65°C

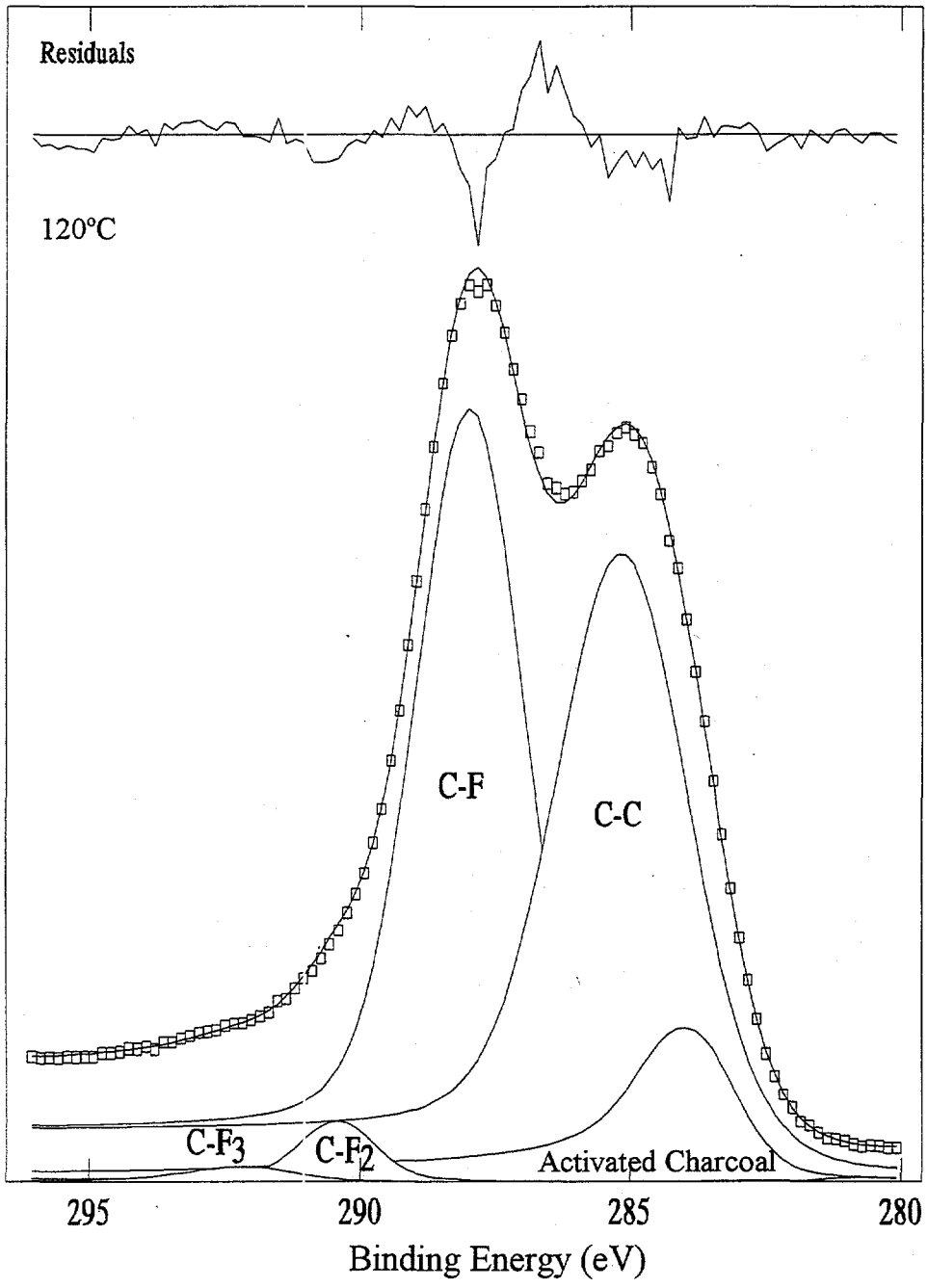

Fig. 15. ESCA spectra, C 1*s* region, of fluorinated charcoal prepared at 120°C.

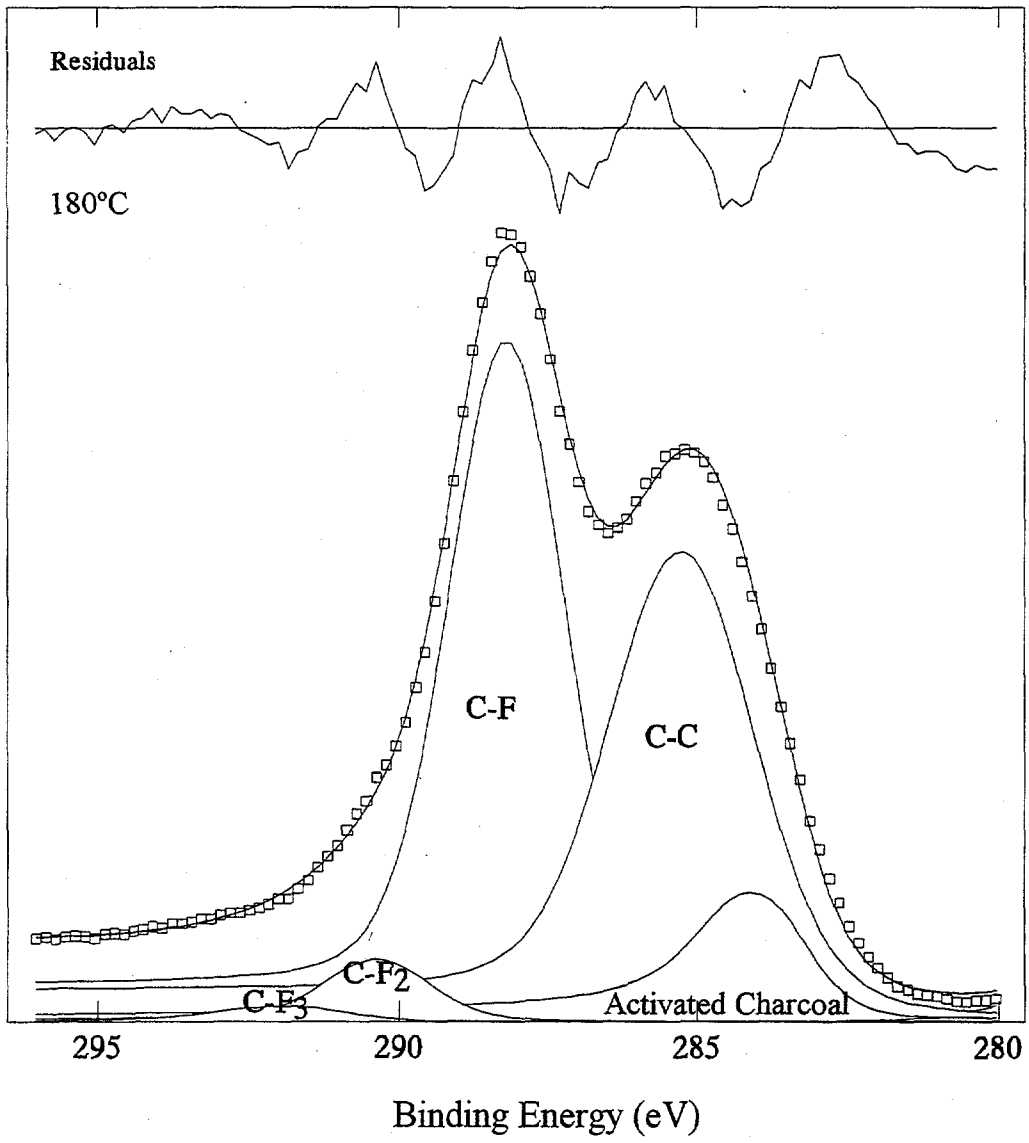

Fig. 16. ESCA spectra, C1*s* region, of fluorinated charcoal prepared at 180°C.

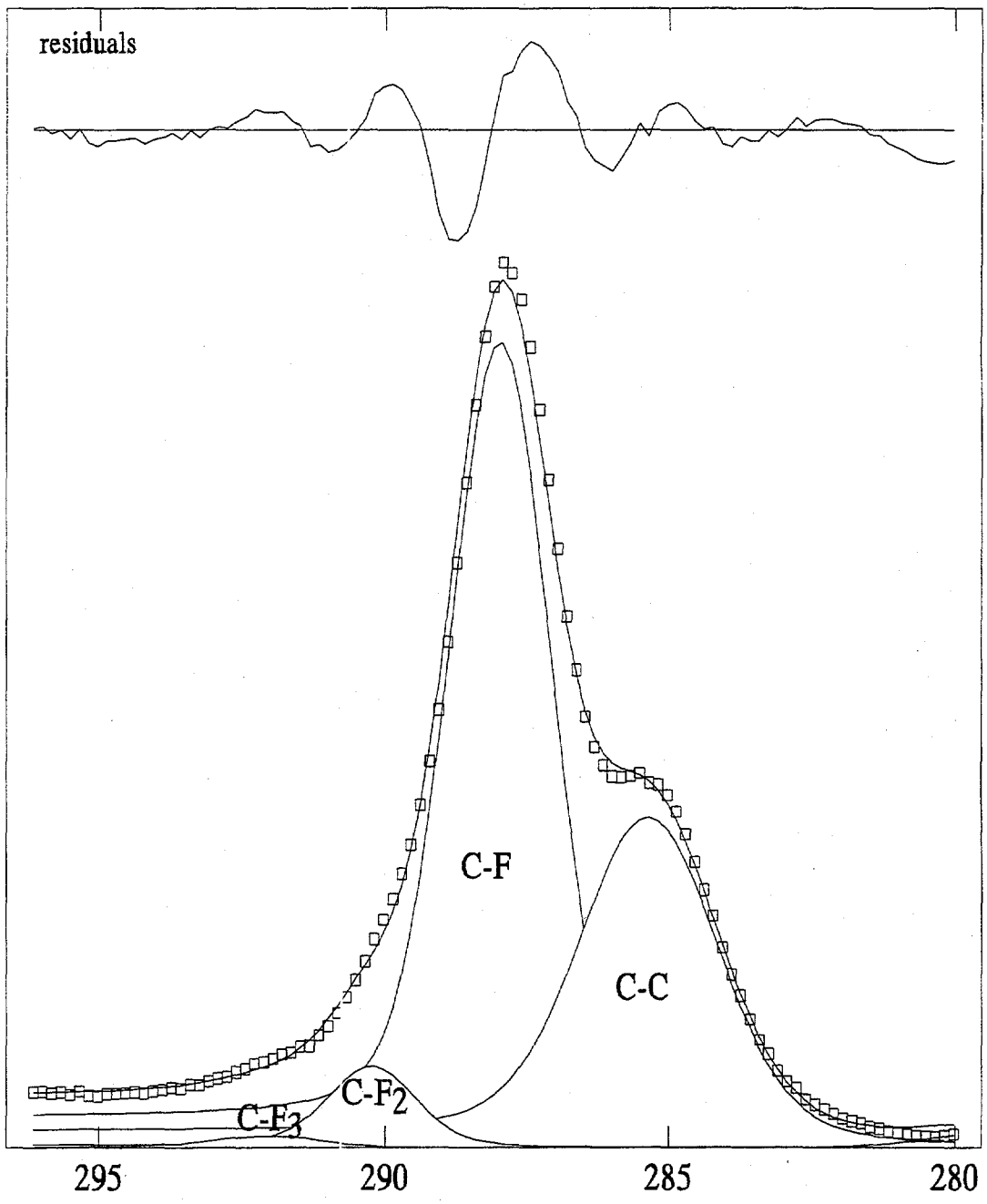

Fig. 17. ESCA spectra, C1*s* region, of fluorinated charcoal prepared at 250°C.

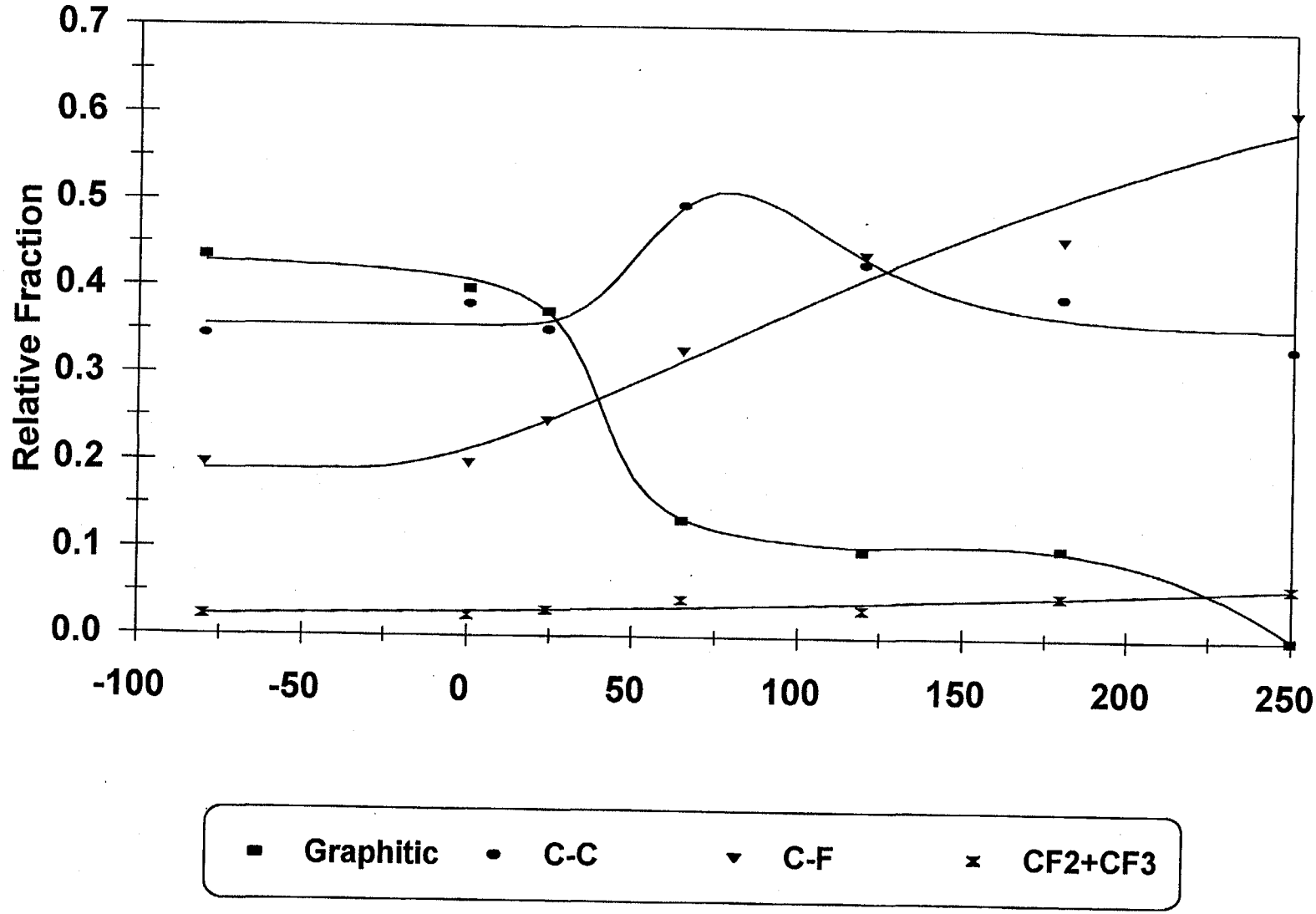

Fig. 18. Normalized distribution of the different carbon (C 1*s*) environments for C_xF prepared at different temperatures.

Additionally, it is noticeable that the carbon-bonded-to-carbon peak atoms influenced by neighboring fluorine atoms remains approximately constant with a maximum centered in the region attributed to the C_2F stoichiometry (see Fig. 2). These distributions along with NMR data will be used to propose a model for the fluorinated charcoal (Sect. 3.7).

Figure 19 compares the carbon:fluorine ratios obtained by weight difference during fluorination with the ratios obtained using the fitted C 1*s* ESCA data. The carbon to fluorine ratios from ESCA data were calculated in the following manner: (1) the carbon concentration is proportional to the total C 1*s* area, including all the peaks; (2) the fluorine concentration was estimated by adding the area corresponding to CF, plus two times the CF_2 area and three times the CF_3 area; and (3) the carbon:fluorine ratio was then calculated by dividing (1) by (2).

The carbon:fluorine ratios obtained from the ESCA C 1*s* data are not expected to be highly accurate because the method involved the use of several areas estimated by peak fitting. However, it is reassuring to note that the general trend of the ESCA ratios is consistent with the more precisely determined gravimetric ratios. It will also be shown in Sect. 3.7 that the carbon:fluorine ratios obtained by NMR are similar.

3.3 GAMMA IRRADIATION OF FLUORINATED CHARCOAL

As mentioned in Sect. 2.7, several C_xF samples prepared at different temperatures were subjected to intense gamma-irradiation using a ^{60}Co source, including a 10-g C_xF sample prepared at room temperature and enclosed in a vacuum-tight Monel tube with a pressure transducer connected at the top. For this sample, the pressure slightly decreased during the first week (~3% integrated decrease). This phenomenon was probably caused by a slightly enhanced sorption of helium by the irradiated C_xF sample. After the first week, the pressure remained essentially constant for the entire irradiation period.

At the end of the irradiation period, each container was opened inside a dry-helium glove box, and the specimens were weighed again. The results showed weight differences less than 0.1%. The gas atmosphere of the tube containing the 10-g sample was analyzed using FTIR and showed only vestiges of carbon dioxide.

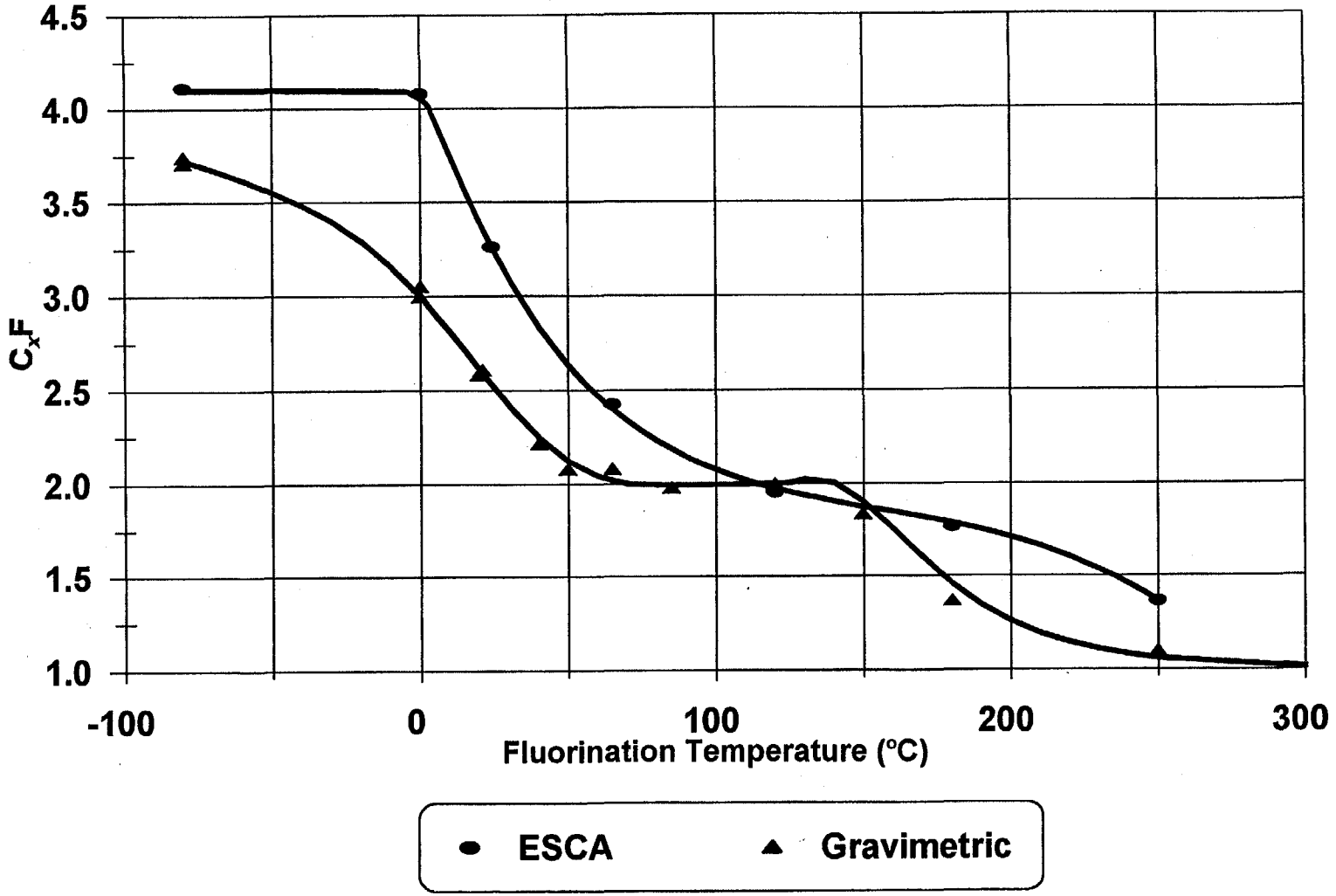

Fig. 19. Comparison of gravimetric and ESCA carbon:fluorine ratios.

All irradiated samples were also analyzed by ESCA (Sect. 2.6). Comparison of the irradiated and unirradiated samples showed no significant differences. As an example, Figs. 20 and 21 display the C 1*s* spectra for irradiated and nonirradiated C_xF samples prepared at –80 and 65°C, respectively. The results indicate that the fluorinated charcoal samples are quite stable when exposed to gamma irradiation because there were no discernible effects after total integrated gamma doses of 2.30×10^8 rad. This corresponds to the integrated dose the ACB deposit would experience for the first 10 years after deposition.

Accordingly, it can be assumed that no significant changes should be expected in the physicochemical behavior of the fluorinated charcoal as a result of the gamma self-irradiation at the MSRE ACB. It should be pointed out, though, that the bulk of the self-irradiation of a uranium deposit of MSRE assay (ca. 95% of adsorbed energy) will result from alpha particles rather than from beta or gamma radiation.

After 30 years, the accumulated dose in the ACB was calculated to be 2×10^{10} rad alpha, 8×10^8 rad beta, and 6×10^8 rad gamma. The ^{60}Co exposures subjected the test material to a total dose of 2.3×10^8 rad.

3.4 STABILITY OF THE FLUORINATED CHARCOAL AND TGA-DTA ANALYSIS

Fluorinated charcoals can be typically described as quite stable materials. Our tests showed that mechanical shock, smashing, sparking, etc., will not promote decomposition reactions. However, rapid heating of the material can result in a very fast decomposition of near-explosive characteristics with formation of gaseous products. All the C_xF samples tested "deflagrated" when rapidly heated. However, this effect was more significant for the samples prepared between 65 and 180°C. The fluorinated samples prepared at the highest temperatures (~C_1F stoichiometry) displayed an increased thermal stability.

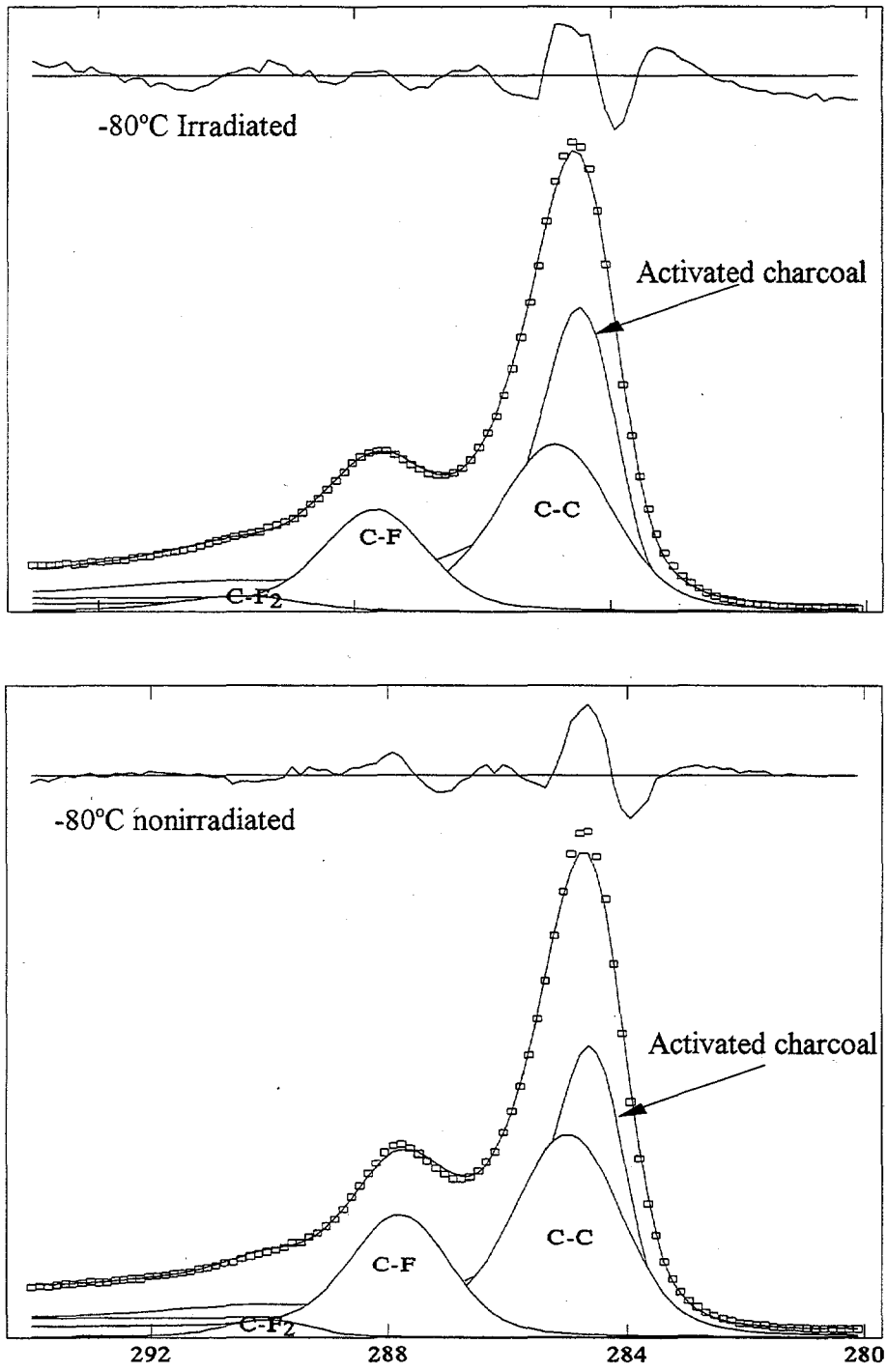

Fig. 20. ESCA spectra, C 1s region, for irradiated and nonirradiated C_xF prepared at -80°C.

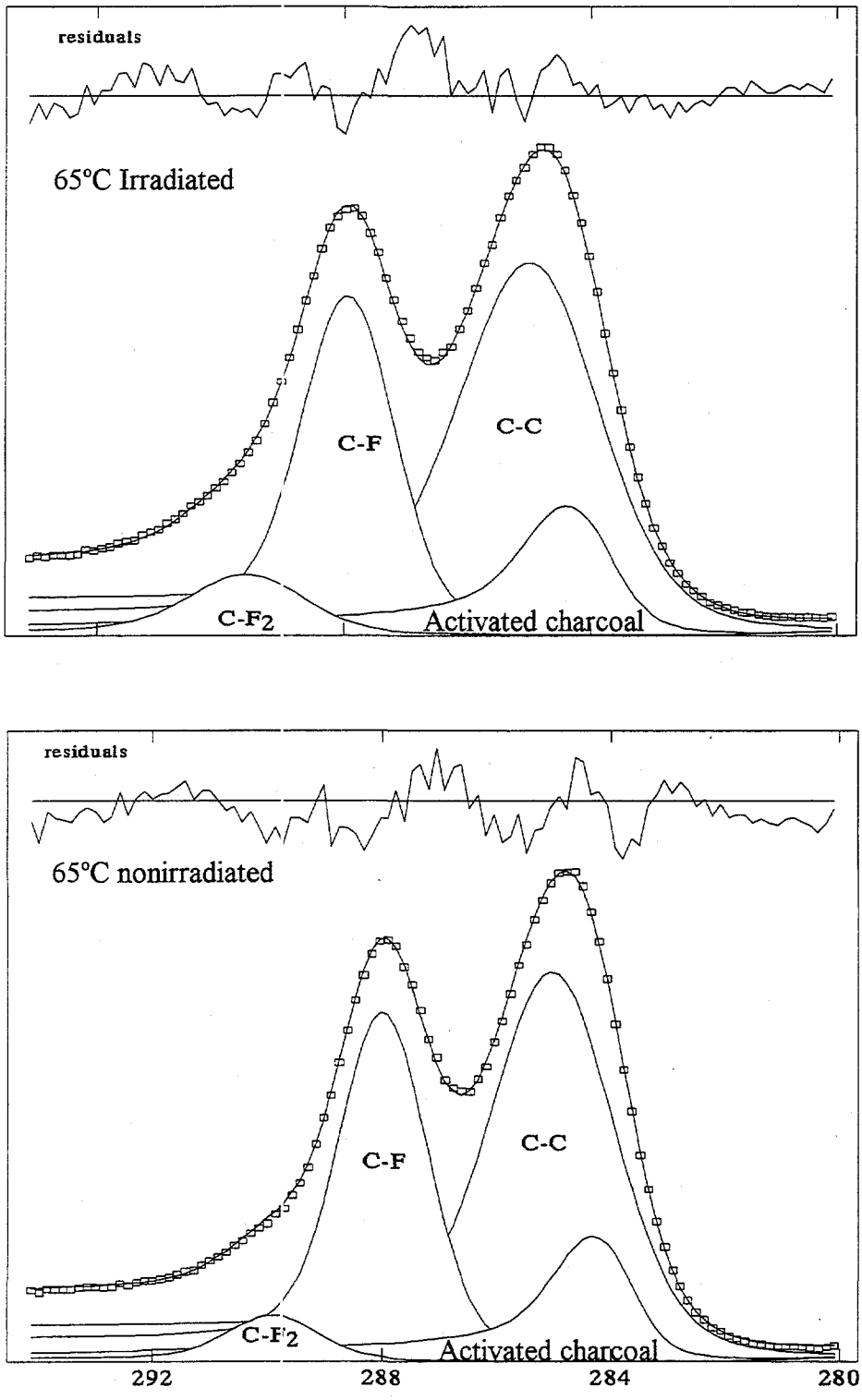

Fig. 21. ESCA spectra, C 1*s* region, for irradiated and non irradiated C_xF prepared at 65°C.

Samples of C_xF can be handled in air without noticeable short-term changes provided that the sorbed fluorine is removed by inert gas purge or vacuum. However, after prolonged storage of several weeks, partial hydrolysis occurred with trace formation of hydrogen fluoride detected as vapor.

Several TGA-DTA analyses were conducted on fluorinated charcoal samples prepared at different temperatures as mentioned in Sect. 2.5. The temperature profiles, Figs. 22 through 29, show that heating promoted the exothermic decomposition of C_xF.

The thermal decomposition of C_xF samples prepared at low temperatures started at temperatures slightly above 100°C (see, for example, Figs. 22 – 24). The heating curve for the sample prepared at –80°C (Fig. 22) was very broad and almost featureless except for a shoulder at about 475°C. This shoulder grows to a peak for the sample prepared at 0°C (Fig. 23).

The decomposition process continued over a wide range of temperatures and was completed at temperatures in excess of 600°C. As the fluorination temperature used to prepare the C_xF samples increased, the bulk of the weight loss and heat release occurred during an increasingly narrower temperature range centered at about 550°C (Figs. 25 – 28). The C_xF prepared at 350°C (white color with ~C_1F stoichiometry) was quite stable (Fig. 29) and started to decompose only at temperatures in excess of 500°C. Of course, almost by definition, any sample prepared at a given temperature cannot be expected to exhibit thermal instability below the preparation temperature.

During the heating tests of samples prepared at temperatures between 85 and 180°C, there were several instances during which the specimens "deflagrated" and part of the sample spilled out of the crucible. To avoid this problem, the tests were repeated and smaller volumes of sample were loaded.

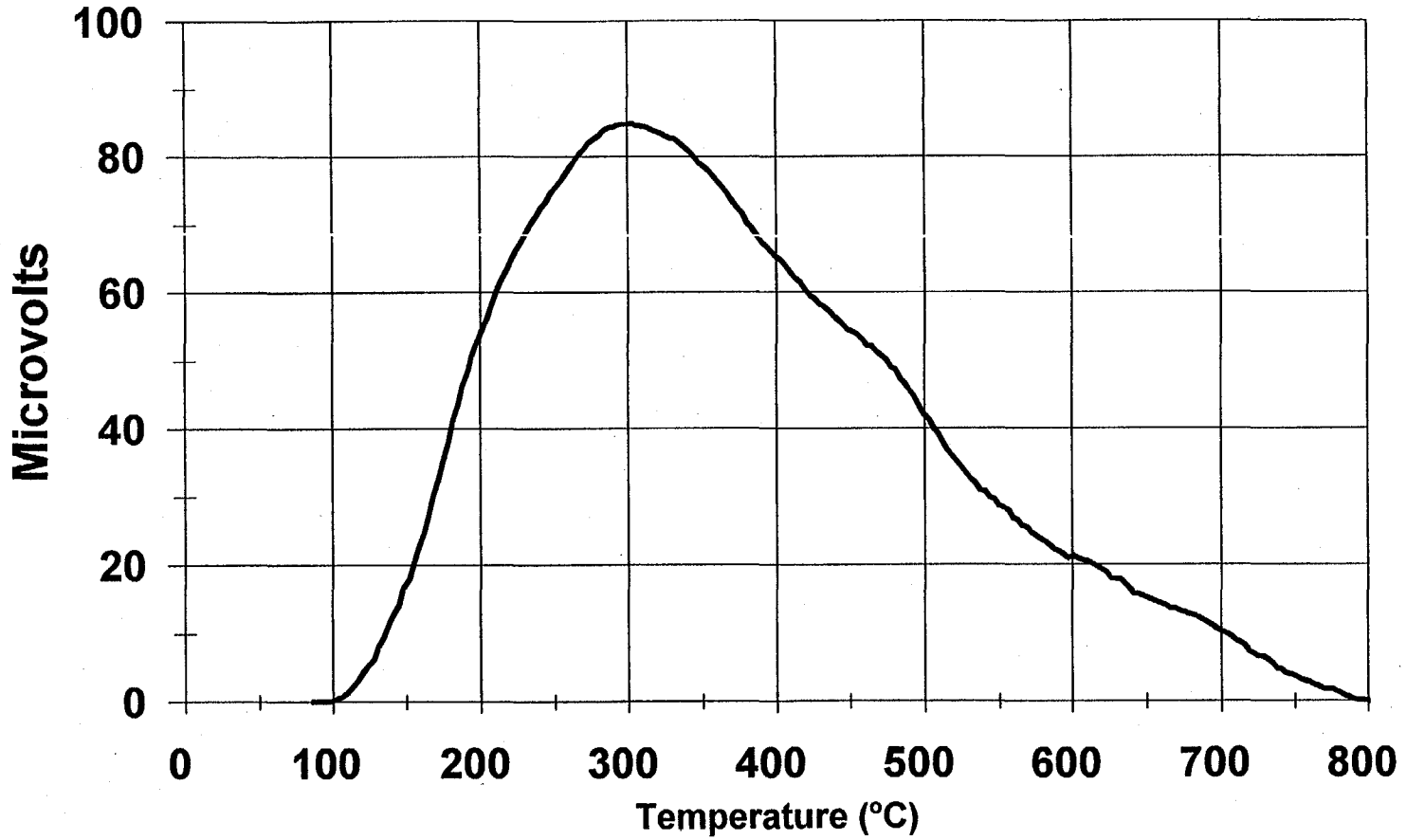

Fig. 22 . DTA analysis of a C_xF sample prepared at −80°C.

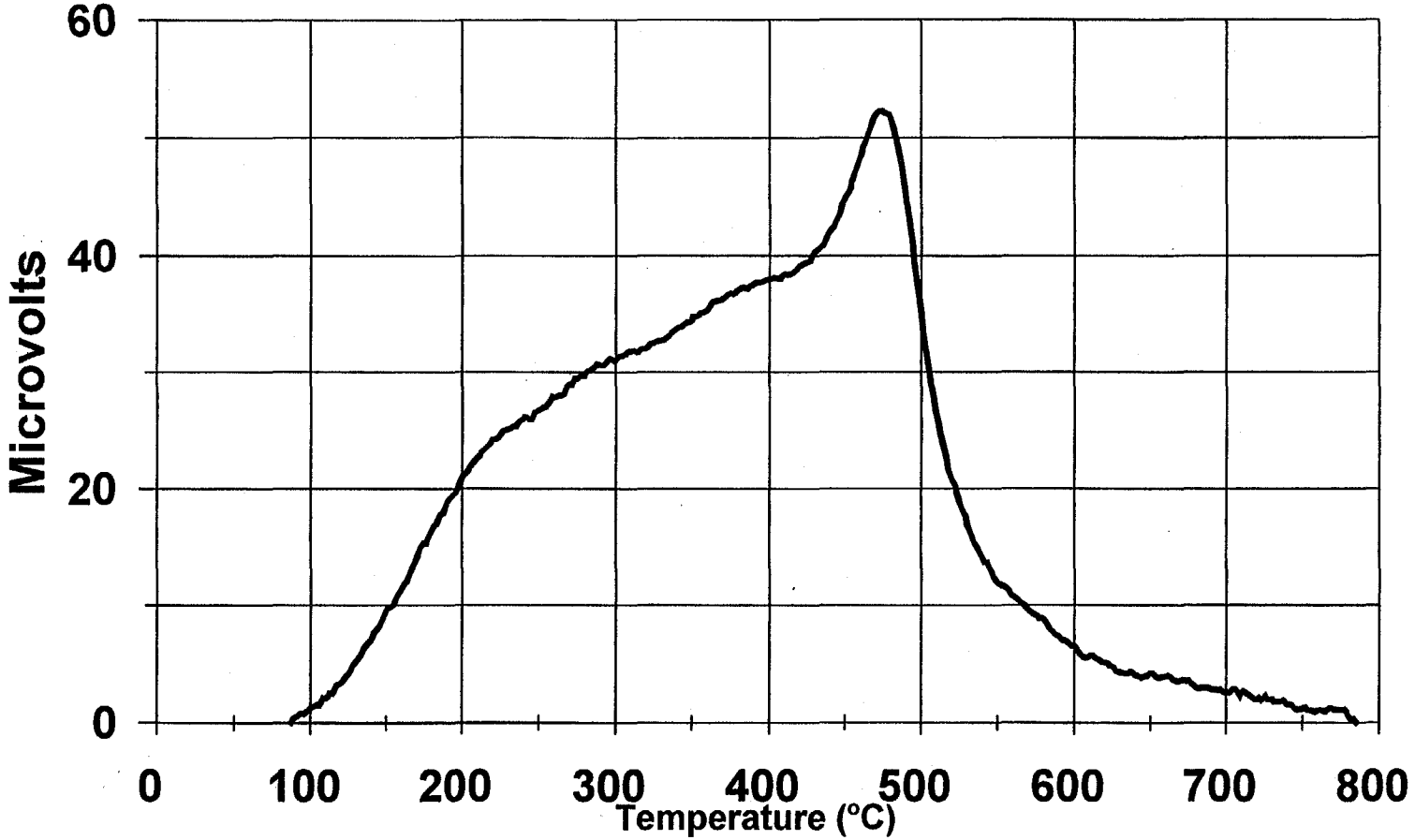

Fig. 23. DTA analysis of a C_xF sample prepared at 0°C.

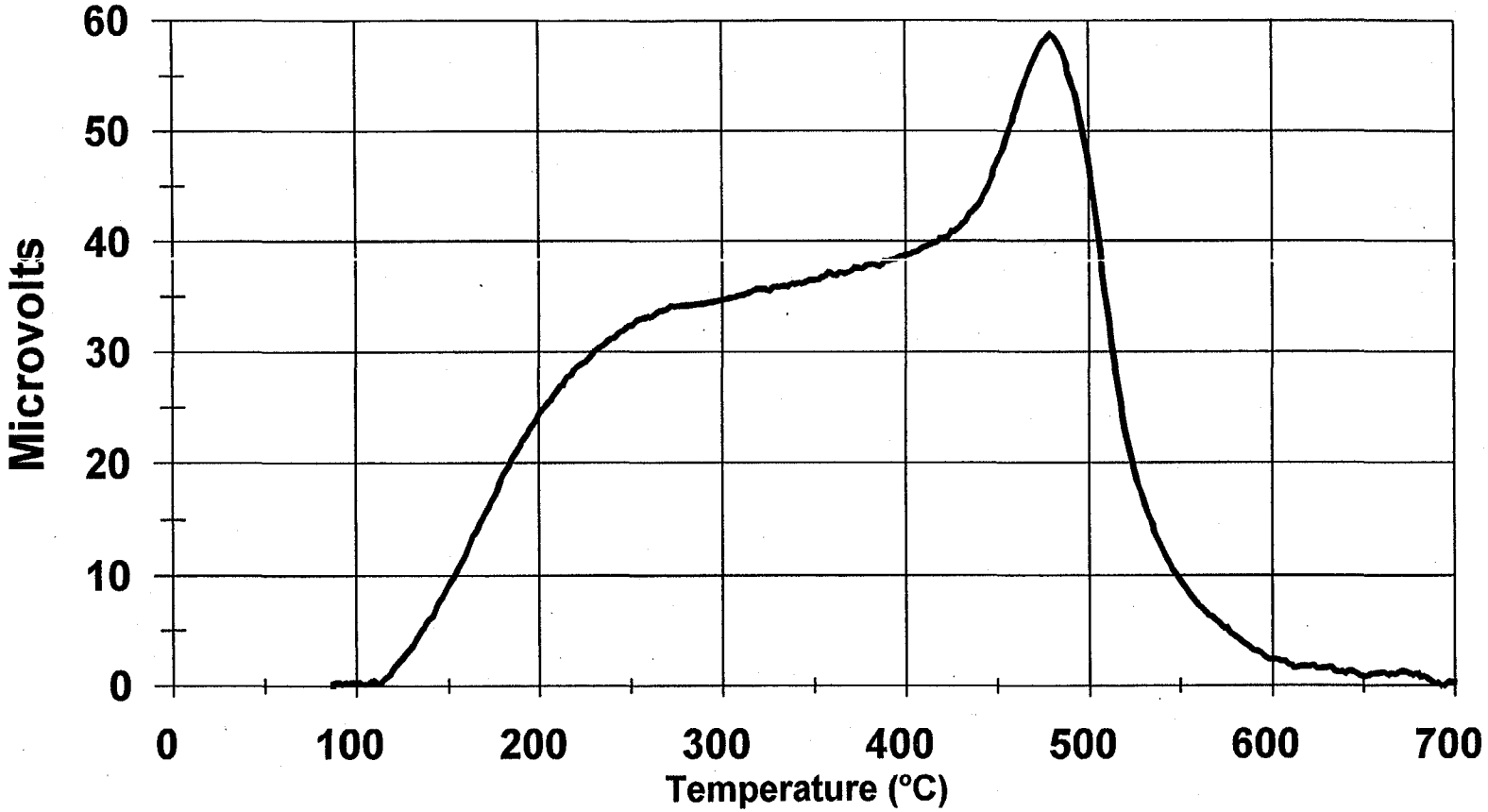

Fig. 24. DTA analysis of a C_xF sample prepared at 23°C.

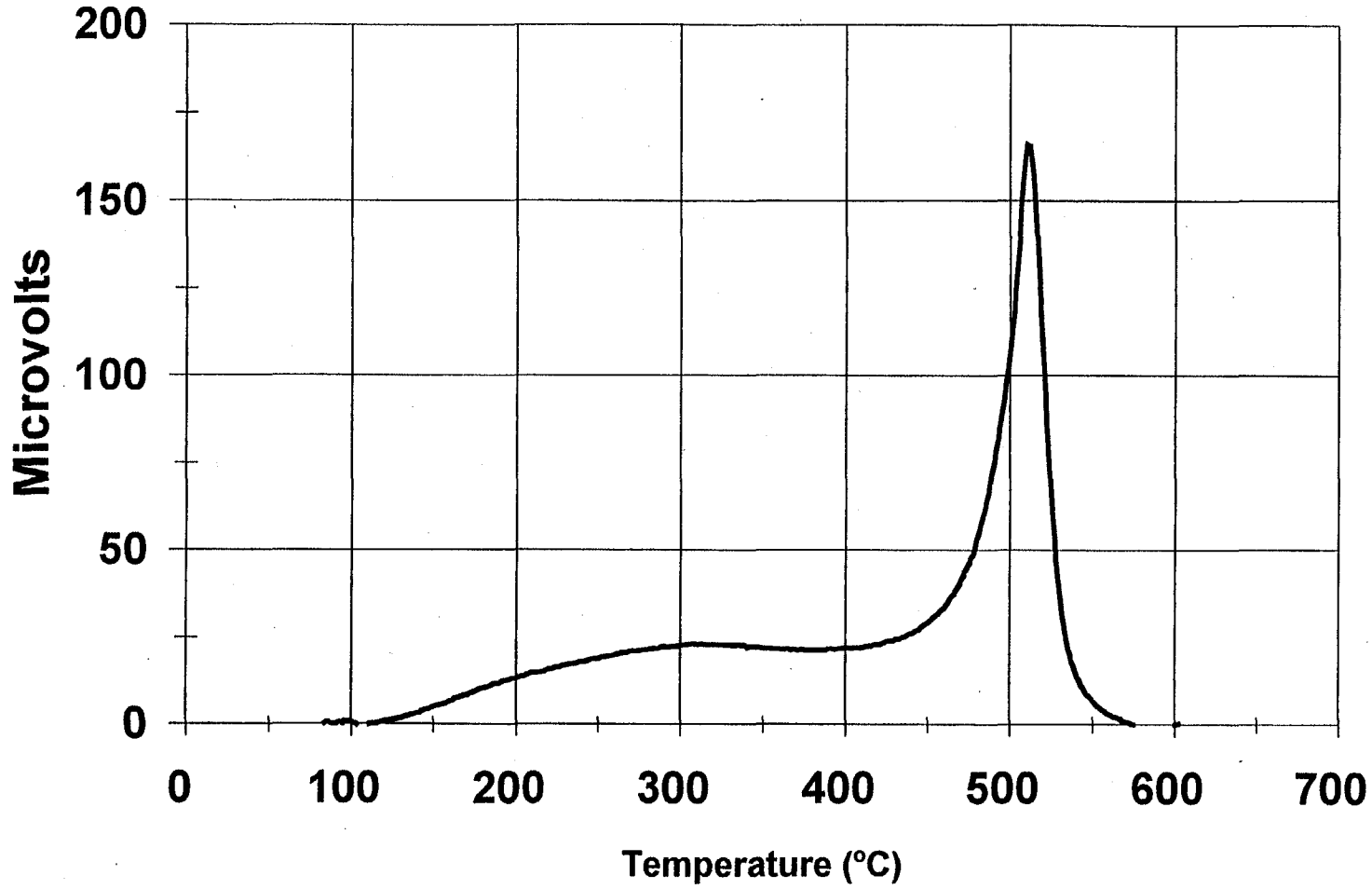

Fig. 25. DTA analysis of a C_xF sample prepared at 65°C.

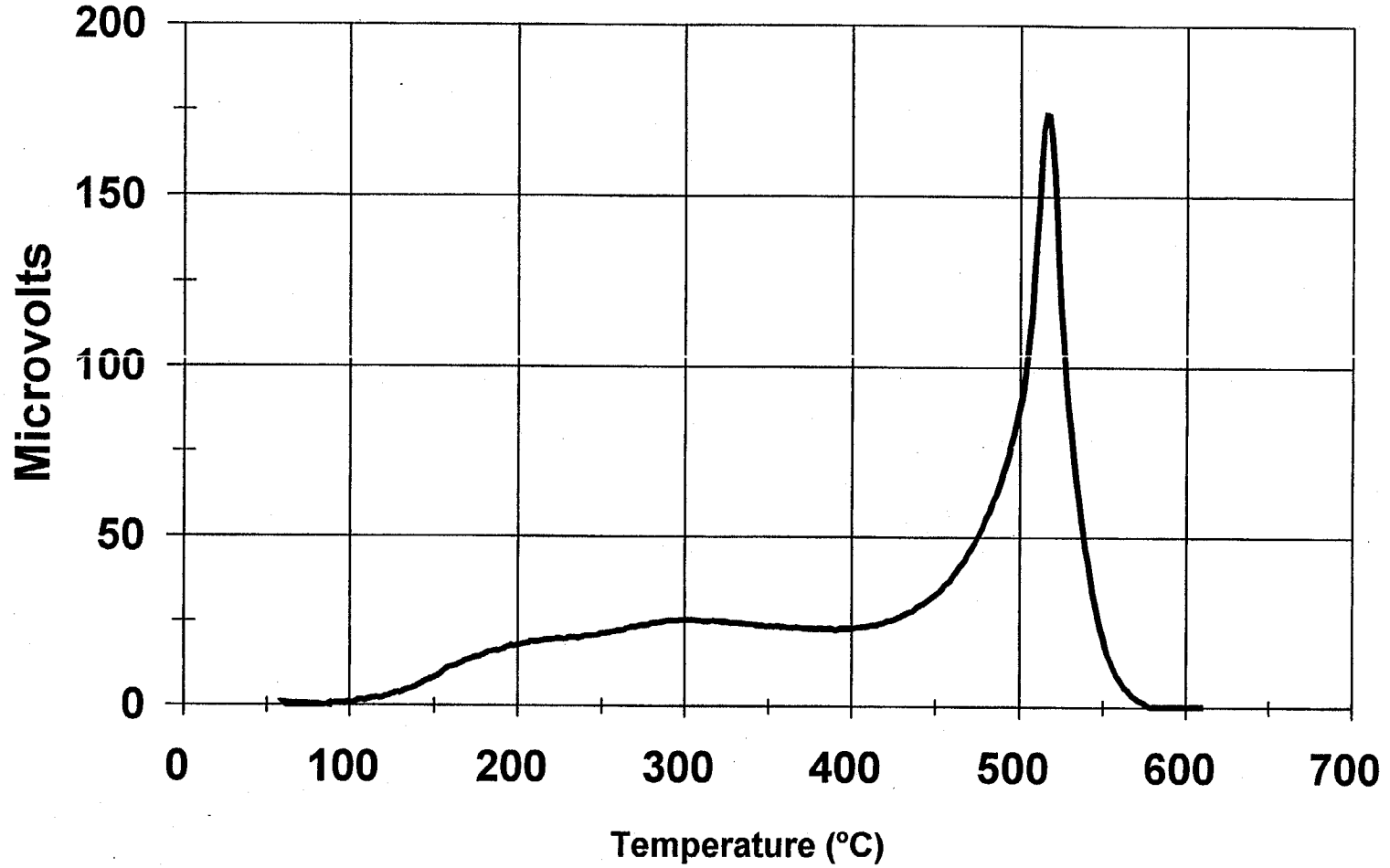

Fig. 26. DTA analysis of a C_xF sample prepared at 120°C.

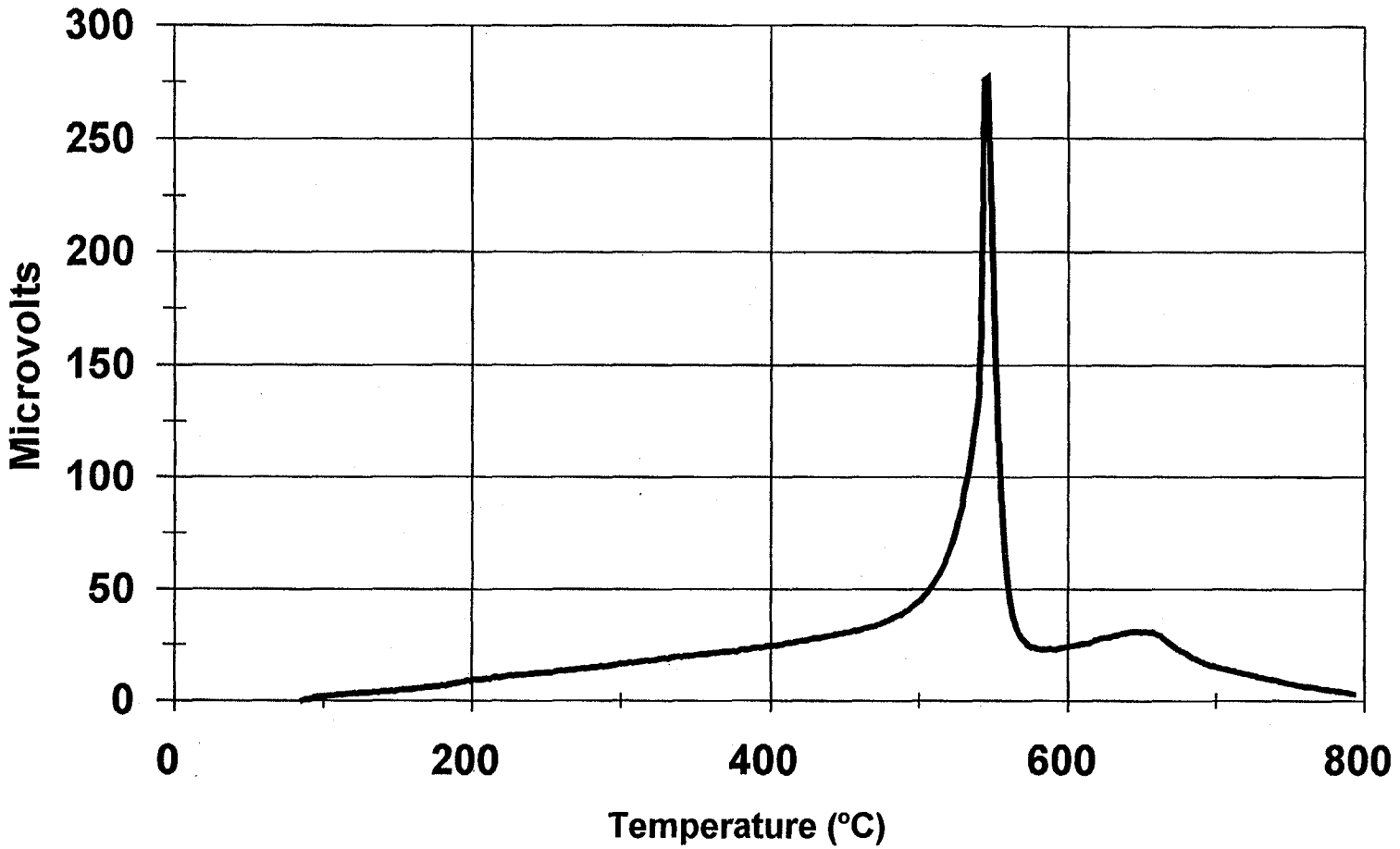

Fig. 27. DTA analysis of a C_xF sample prepared at 180°C.

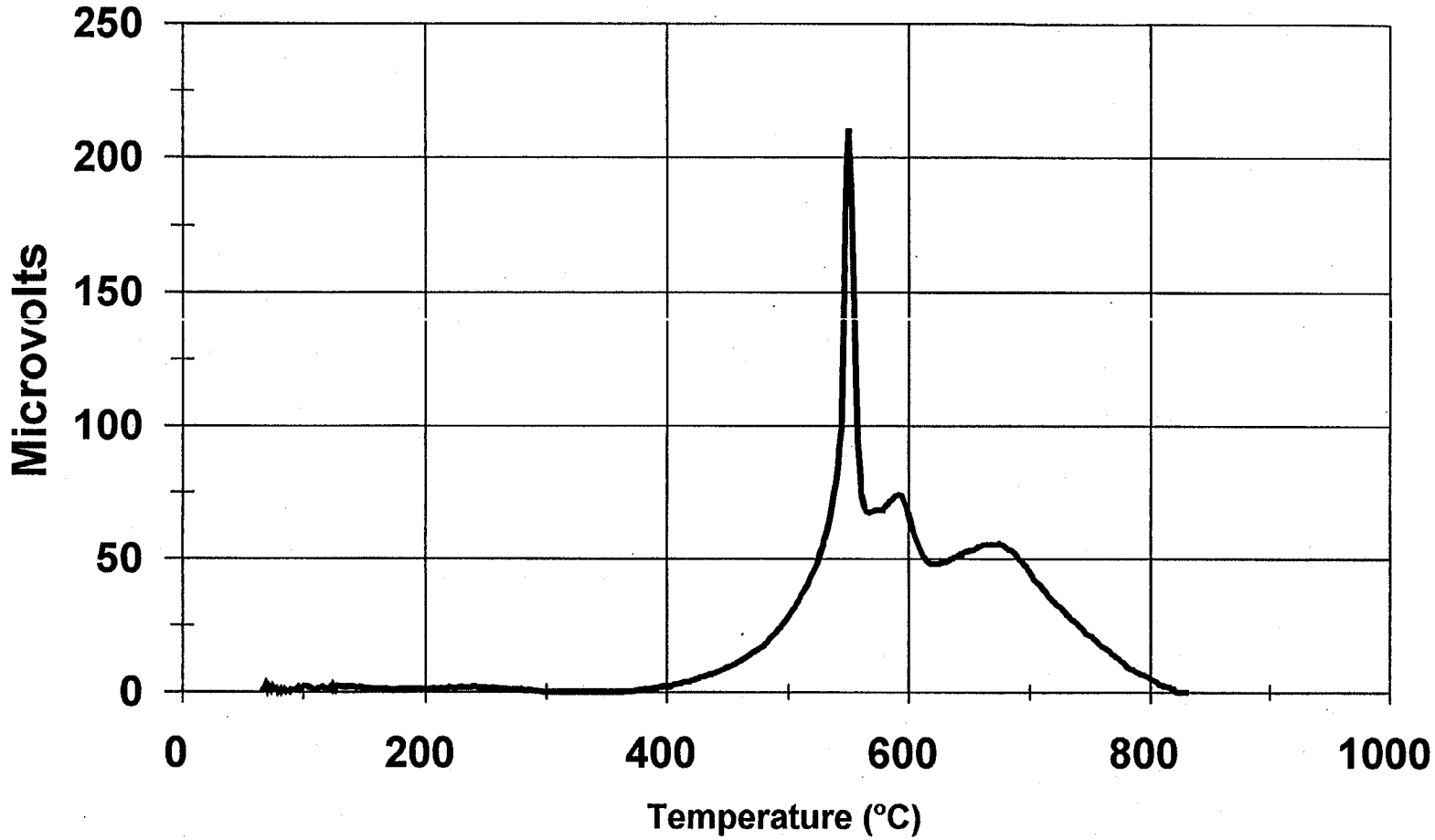

Fig. 28. DTA analysis of a C_xF sample prepared at 250°C.

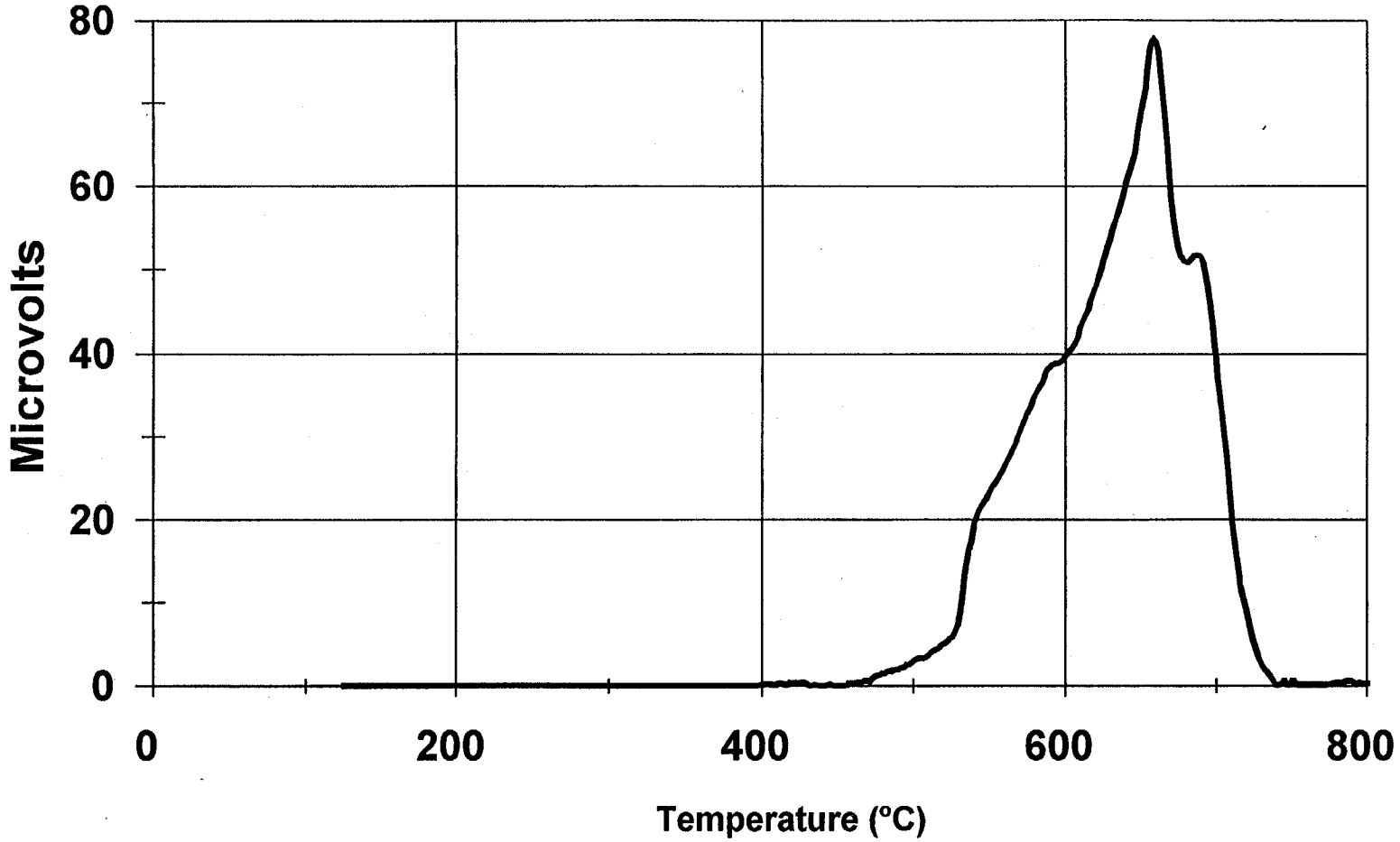

Fig. 29. DTA analysis of a C_xF sample prepared at 350°C.

Table 4 and Fig. 30 and show the integrated heat released during the decomposition process. The enthalpy values were calculated using the gravimetric C_xF stoichiometry. Since it is necessary for the calculation to apply a baseline correction over a wide temperature range ($\Delta t \approx$ 500-to-600°C), the experimental uncertainty for the absolute values is relatively high (25 to 50%).

Table 4. Experimental enthalpy values for the decomposition of C_xF

Fluorination temperature (°C)	ΔH (kJ/mol F)	C:F
–80	121	3.7
0	103	3.1
23	81	2.6
40	53	2.2
65	55	2.1
120	55	2.0
250	55	1.1
350	26	1.0

Experimental enthalpy values for decomposition of C_xF are consistent with values in the literature for heat of formation of C_xF. These values range from –107 to –173 kJ/mol.[37] The heat of decomposition of $C_{2.6}F$ should be approximately

$$C_{2.6}F \longrightarrow 2.35\ C + \tfrac{1}{4}CF_4,\ \Delta H = -67\ \text{kJ/mol F}.$$

While substantial, this value is much smaller than that derived from the original assumption that the available energy was represented by the reaction

$$\tfrac{1}{4}C + \tfrac{1}{2}F_2 \longrightarrow \tfrac{1}{4}CF_4\ \Delta H = -232\ \text{kJ/mol F}.$$

Clearly, much of the potential chemical energy was released as the F_2 arrived at the ACB and reacted with carbon years ago.

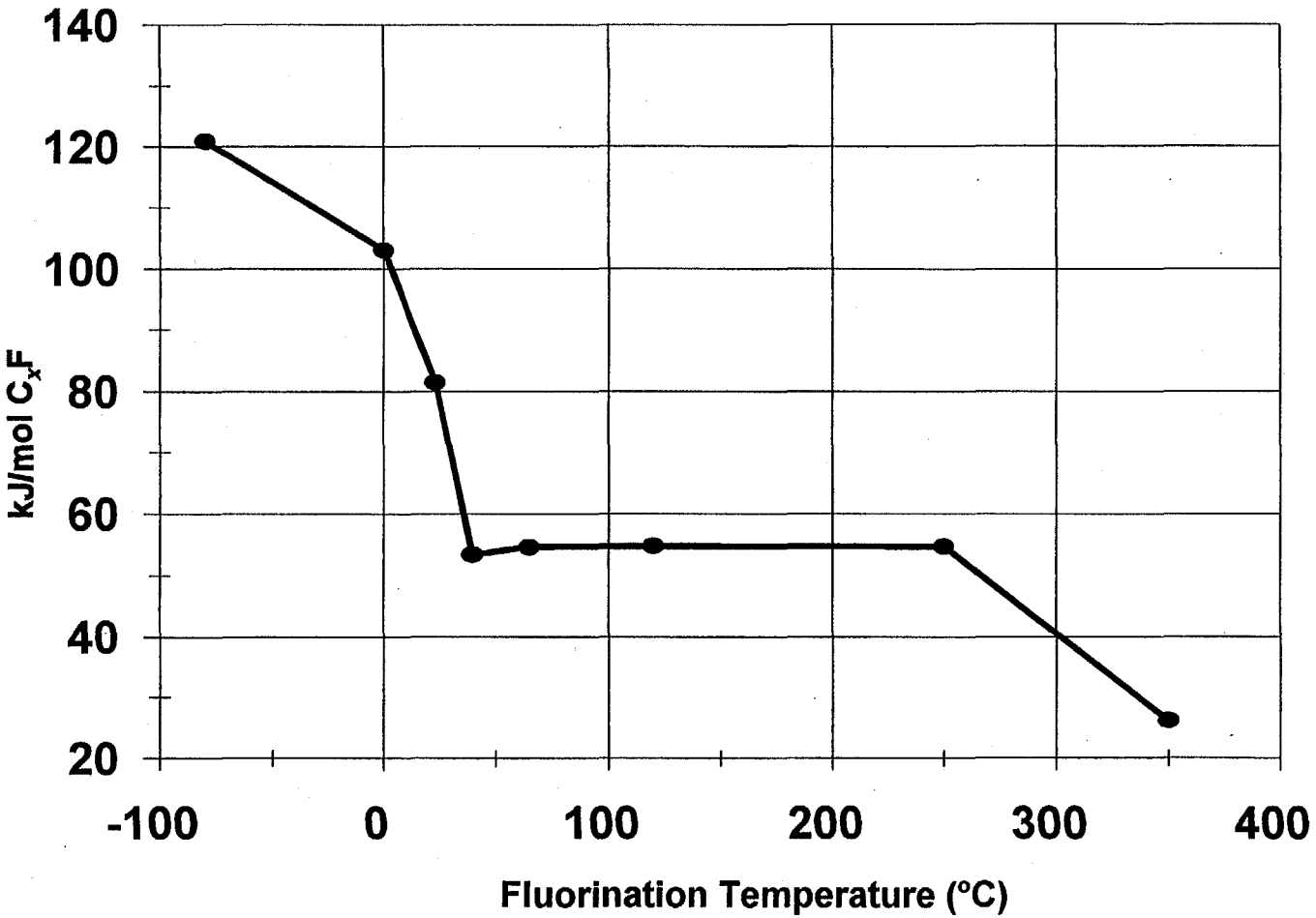

Fig. 30. Integrated heat released during thermal decomposition of C_xF samples prepared at different temperatures.

The weight loss recorded during heating was consistent with the DTA curves. The loss occurred slowly during a very wide range of temperatures for the C_xF samples fluorinated at low temperature. On the other hand, most of the weight loss for C_xF samples fluorinated at higher temperatures occured during a narrow range of temperatures coinciding with the "heat peak" at about 550°C. As an example, Fig. 31 contrasts the weight loss for a C_xF sample prepared at -80°C showing "broad decomposition" with a C_xF sample prepared at 180°C showing "sharp decomposition."

Figures 32 and 33 show the results of the heating tests using 1-g samples of fluorinated charcoal prepared at 0 and 120°C. The specimens were heated inside a quartz vessel. A type K thermocouple and a pressure transducer connected to a data acquisition system were used to continuously and simultaneously record the pressure and temperature values. At the end of each test, the gas liberated during the heating was analyzed by FTIR.

In agreement with previous tests (see Fig. 23), the sample prepared at 0°C thermally decomposed over a wide range of temperatures (100–500°C) as indicated by the gradual pressure rise (left scale) because of the slow accumulation of the gaseous species. Also, as according to previous experiments (see Fig. 26), the sample prepared at 120°C sharply decomposed at about 500°C. This fast decomposition is consistent with the behavior observed during the DTA-TGA analysis of fluorinated charcoals prepared in the 85–180 °C temperature range.

The FTIR analysis of the gases formed during the thermal decomposition of the C_xF samples indicated the presence of carbon tetrafluoride (CF_4) and hexafluorethane (C_2F_6) as the major species and trace levels of tetrafluorethylene (C_2F_4), carbonyl fluoride (COF_2), and carbon monoxide and dioxide (CO and CO_2). The latter species originate from oxygen moieties present at the rim of the charcoal platelets (see Sect. 3.4).

The decomposition of C_xF prepared at low temperatures (-80 to 45 °C) also produced some heavier fluorocarbons that condensed on the vessel walls as liquid drops or very small, thin solid flakes. The formation of condensed fluorocarbons was also observed in early trapping experiments of F_2 gas onto charcoal at the Oak Ridge Gaseous Diffusion Plant.[21]

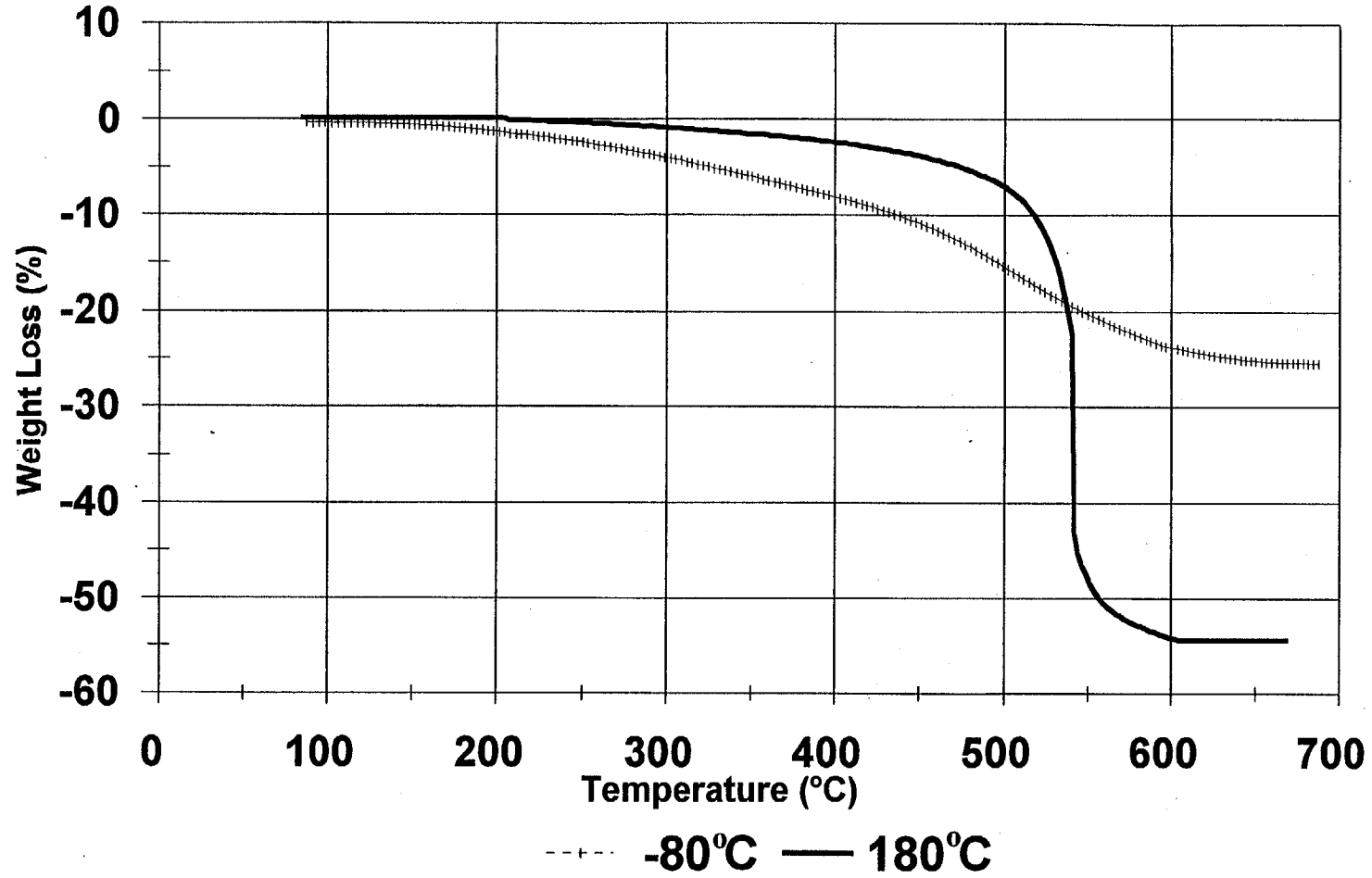

Fig. 31. TGA comparison between C_xF samples prepared at −80 and 180°C, showing, respectively, broad and sharp thermal decomposition.

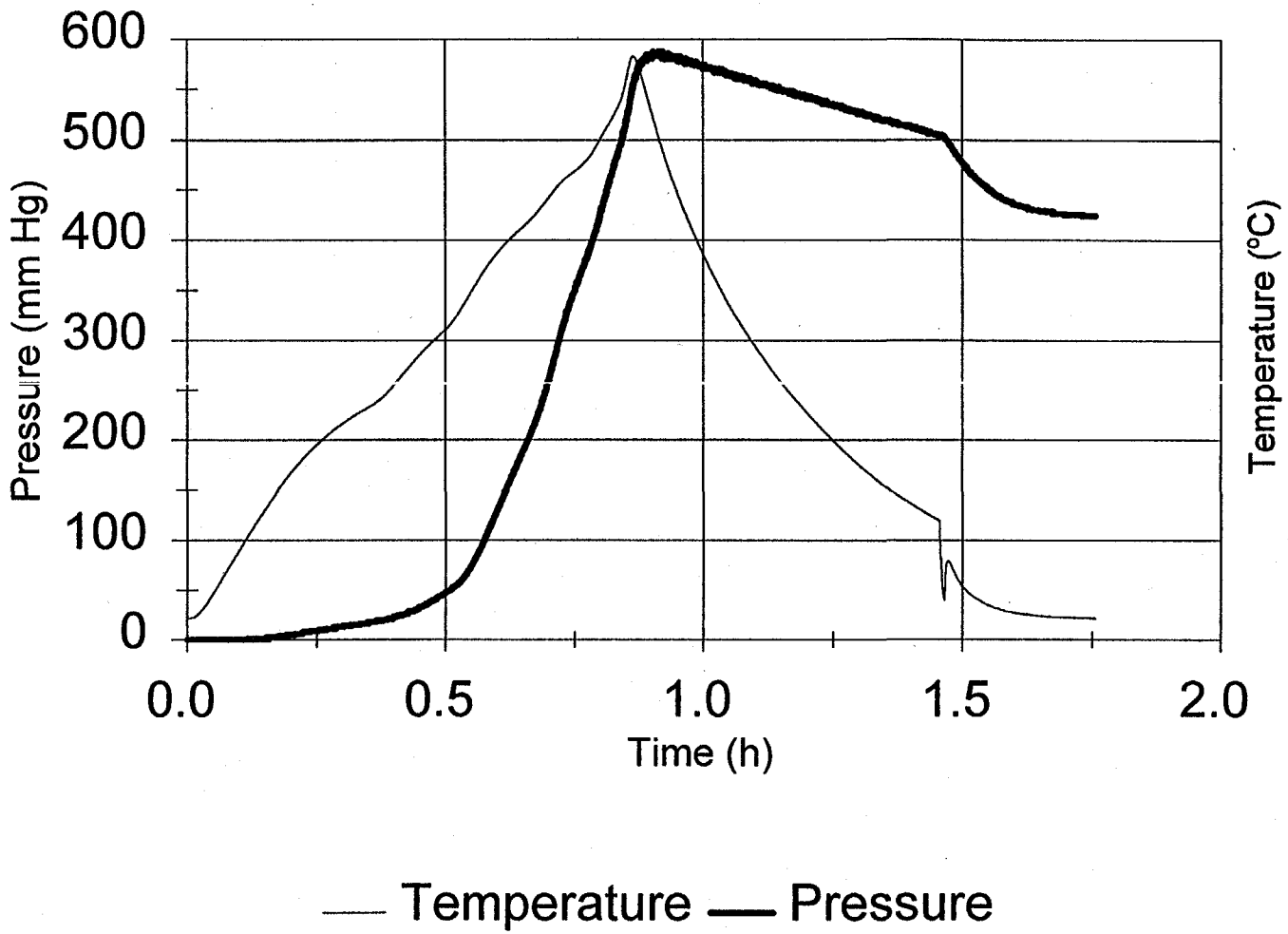

Fig. 32. Thermal decomposition of 1-g sample prepared at 0°C.

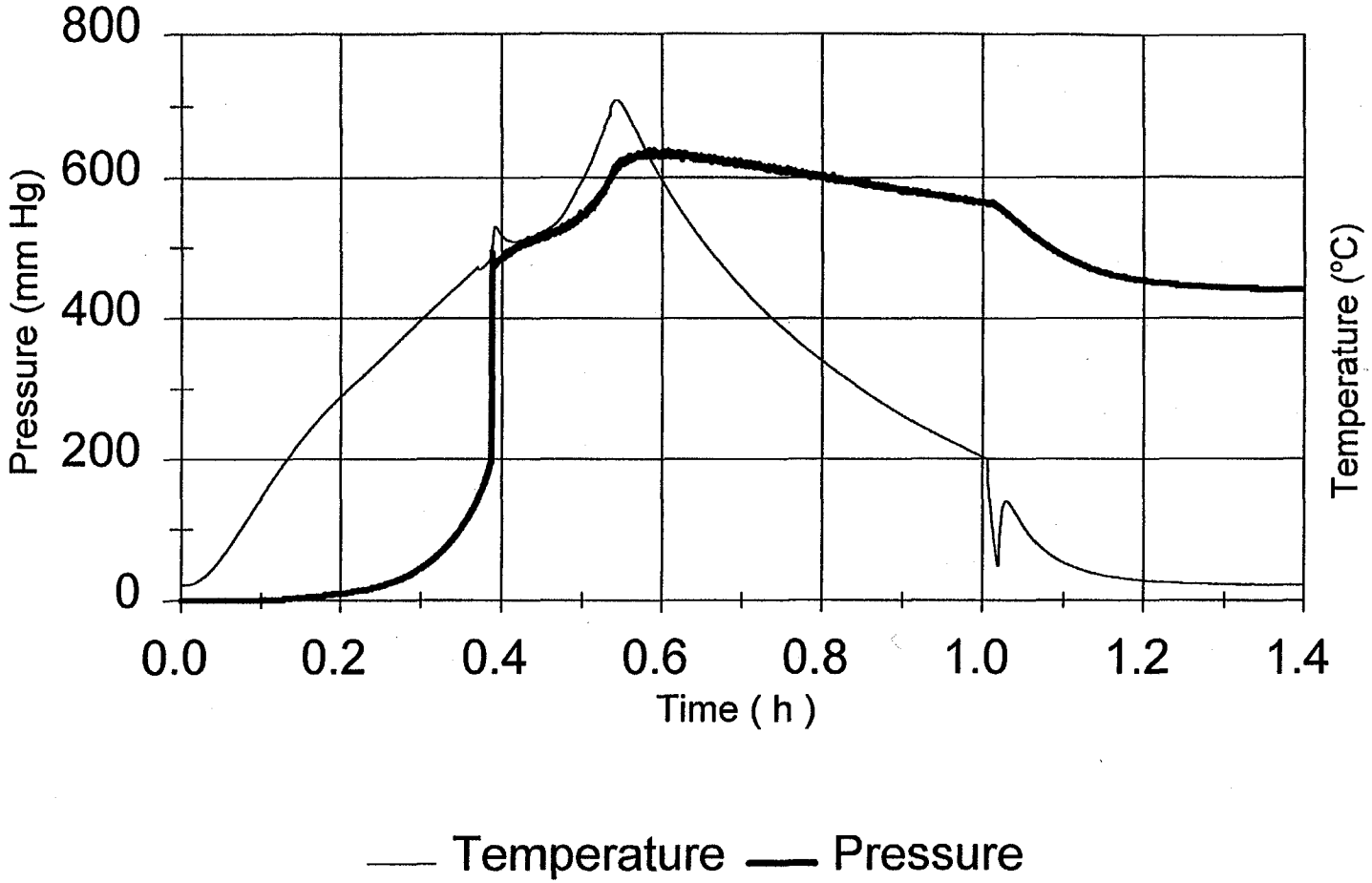

Fig. 33. Thermal decomposition of 1-g sample prepared at 120°C.

3.5 PASSIVATION OF THE ACB

As mentioned in Sects. 2.4 and 3.3, fluorinated charcoal, when subjected to rapid heating, can decompose and produce gaseous products (CF_4, C_2F_6, etc.). Under confined conditions, the sudden exothermic decomposition can produce high temperatures and pressures of near-explosive characteristics.

To proceed with the planned remediation and uranium recovery activities at the MSRE, it will be necessary to tap into the ACB to allow the installation of piping and instrumentation. The drilling and tapping operations could conceivably result in local heating in excess of 100°C.

As shown in Sect. 3.3, fluorinated charcoal starts to thermally decompose at temperatures above 100°C, and it is not clear how much hotter a region of the ACB deposit could get before undergoing a thermal runaway leading to deflagration. Consequently, it is necessary to chemically transform the reactive fluorinated charcoal into a more stable material to safely conduct the remediation and recovery activities.

As indicated in Sect. 3.3, partial hydrolysis of the fluorinated charcoal with HF formation was observed after prolonged storage in humid air. Also, Watanabe et al.[14] found that fluorinated "carbon black" partially reacted with a potassium iodide (KI) solution, forming iodine (I_2) according to the reaction

$$2(C...F) + 2\,KI \rightarrow 2\,KF + I_2 + 2C\,,$$

where C...F represents absorbed or "weakly bonded" reactive fluorine. Our sorption studies of pure fluorine on fluorinated charcoal indicated a 1 to 3 wt % gain after prolonged exposure of C_xF to fluorine at atmospheric pressure. This gained weight is lost after prolonged evacuation or inert gas purging.

Those known reactions suggested the idea of using "reactive" gases such as NH_3, HI, NO, NO_2, CO, $CH_2{=}CH_2$, $CH{\equiv}CH$, H_2O, H_2, CS_2, B_2H_6, BCl_3, etc., to transform the C_xF materials into a stable inert material that could be heated without danger of a sudden decomposition.

After extensive testing of a variety of candidate reactants, anhydrous ammonia gas proved to be the only reactant that converted C_xF to benign compounds per the reaction

$$C_xF + 4/3NH_3 \rightarrow xC + NH_4F + 1/6N_2$$

at a rate that was sufficiently rapid for operational practicality but slow enough that thermal control could readily be achieved. Testing and evaluation of the reaction of NH_3 with C_xF are treated in a separate report.[26] The ammonia treatment process, termed "denaturing" in the MSRE project lexicon, has since been successfully applied to the ACB.

3.6 LOADING OF UF_6 AND F_2 ON ACTIVATED CHARCOAL

Several scoping tests were performed to understand the behavior of activated charcoal when contacted with UF_6 or a F_2-UF_6 "MSRE" blend (5:1 volume ratio of F_2 toUF_6) at room temperature. These experiments included batch static and dynamic loading through columns filled with activated charcoal. The tests showed that the loading of pure UF_6 on activated charcoal results in the intercalation of uranium fluorides and oxyfluorides in the micrographitic structure.

The uranium-laden activated charcoal will not "deflagrate" when heated rapidly. The ESCA analysis of the laden samples shows no appreciable fluorination of carbon atoms (no carbon-fluorine bonds). This finding explains the increased thermal stability.

The experiments also indicated that the reaction between charcoal and the F_2-UF_6 MSRE blend produces C_xF that contains intercalated uranium fluorides and oxyfluorides. The ESCA analysis of the samples contacted with the F_2-UF_6 MSRE blend shows that the concentration of fluorine atoms directly bonded to carbon is lower than for the samples contacted with pure fluorine. This observation correlates with the milder decomposition of the F_2-UF_6 –laden samples when rapidly heated (mild deflagration).

The dynamic loading of the F_2-UF_6 MSRE blend through columns filled with activated charcoal showed that the fluorine front moves ahead of the uranium front. Based upon our laboratory experience, the measured MSRE ACB uranium front (C_xF plus intercalated uranium compounds) extends about 1 ft from the top of the ACB and followed by a C_xF front spanning a few feet further downstream. The rest of the ACB, about 80 ft, most probably consists of unreacted activated charcoal.

From the different tests, samples were taken for ESCA analysis. As mentioned in Sect. 2.6, the ESCA data can be used to differentiate atoms of the same element in different compounds (different bonding environments). Consequently, the ESCA data can provide information on the nature of the chemical species formed by reaction of charcoal, F_2, and UF_6. The analysis of the ESCA data is presented in the appendix.

It is important to mention that when water was completely excluded from the system, the visual appearance of the charcoal particles after the loading of UF_6 remained the same as free-flowing, "virgin" activated charcoal. Consequently, the laden charcoal particles could be easily removed from a column by gravity or vacuuming as planned for the actual ACB removal. However, in the presence of humidity, the charcoal particles become cemented by interstitial uranyl fluorides. These cemented chunks of laden charcoal are quite hard and require a significant mechanical force for the particles to be separated.

The significance for the planned ACB planned remediation is that hardened chunks of material could be present. The removal of those chunks would require a special tool to break the chunks into "vacuumable" particles. The visual appearance of the uranyl-laden charcoal has the distinctive yellow-orange color characteristic of the uranyl fluoride. A visual inspection of the top of the ACB could give an indication of the presence of interparticle uranyl fluoride.

3.7 SOLID-STATE ^{13}C AND ^{19}F NMR CHARACTERIZATION OF FLUORINATED CHARCOAL

The chemical nature of the different samples of fluorinated charcoal was also studied using solid-state ^{13}C and ^{19}F NMR spectroscopy. The complete discussion of the results was published separately.[35,36] NMR results along with gravimetric and ESCA results (Sects. 3.1 and 3.2) provide a new insight into fluorocharcoal structure.[36]

NMR experiments involving ^{19}F-^{13}C CP MAS, determined the extent of fluorination as a function of reaction temperature. Three types of carbon species were observed and assigned to graphitic carbon (C), CF, or CF_2 on the basis of chemical shift. These assigments were confirmed by measurements of CP and dipolar dephasing time constants, T_{CF} and T_{DD}, respectively.

The fluorinated carbons fully cross-polarize in tenths of milliseconds, while polarization transfer among graphitic carbon is slower and is explained by a two-component model. One component, with T_{CF} less than 1 ms, is assigned to sp^2 hybridized carbons adjacent to fluorinated carbons, viz., interfacial graphitic carbon (C_i). The other component, with T_{CF} on the order of milliseconds, is assigned to more remote carbon species, viz., bulk graphitic carbon (C_b). The concentrations of CF and CF_2 found in the ^{19}F-^{13}C CP MAS experiments were confirmed by direct measurement of the ^{19}F NMR spectrum (see Table 5).

At the lowest fluorination temperature, –80 °C, the fluorinated charcoal is diamagnetic, as is carbon monofluoride (CF), the white end product from complete fluorination at 350°C . The low free-electron density in these materials stands in stark contrast to that of the charcoal and fluorinated charcoal prepared at intermediate temperatures.

The CF_2:CF ratio for fully fluorinated materials is a measure of edge (CF_2) to interior fluorinated carbon (CF) and can be used, with an assumed two-dimensional particle geometry, to estimate platelet size. Using fully fluorinated coronene ($C_{24}H_{12}$), with two fluorines per peripheral carbon and one fluorine per internal carbon (center circle of Fig. 34) as the model for platelet geometry, larger platelets can be created by "growing" the two-dimensional platelet isotropically by adding rings to the carbon skeleton (Fig. 35). The dashed circle surrounding the central coronene structure identifies an element that we label a crown ring. Proportionately larger platelets can be created by adding successive crown rings to the perimeter.

Using n to denote the number of crown rings in a substance, Table 6 shows the particle diameter and CF_2:CF ratio for fully fluorinated platelets and values of $n \leq 7$ (for coronene $n = 1$). With the addition of crown rings, the diameter increases and the ratio of edge to interior carbon decreases. The CF_2:CF ratio obtained from ^{13}C NMR analysis of the sample prepared at 250 °C is 0.19 ± 0.09 and 0.21 ± 0.02 from the ^{19}F NMR spectrum.

Table 5. Concentrations (mole percent) and ratios of carbon components in fluorinated charcoal as determined by ESCA

Carbon component	Binding energy[a] (eV)	Fluorination temperature (°C)							
		-80	0	23	65	120	180	250	350
C_b	284.4	44	40	37	13	10	10	0	0
C_i	284.8	34	38	35	50	43	39	34	14
$C = C_i + C_b$		78	78	72	63	53	49	34	14
CF	287.6	20	20	25	33	44	46	60	67
CF_2	289.9	2	2	3	4	2	4	5	19
CF_3	291.9	0	0	0	0	1	1	1	0
C_i/CF		1.6	1.7	1.3	1.3	0.9	0.8	0.5	0.2
CF_2/CF		0.1	0.1	0.1	0.1	0.05	0.1	0.1	0.3
F/C		0.24	0.24	0.31	0.41	0.51	0.57	0.73	1.05

[a] Binding energies derived from the -80 °C fluorination charcoal, except for CF_3 which is referenced to the charcoal fluorinated at 120 °C.

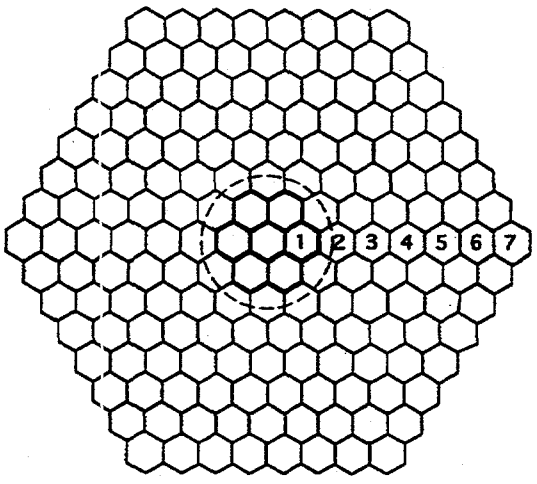

Fig. 34. Modeling of the charcoal platelet based on coronene.

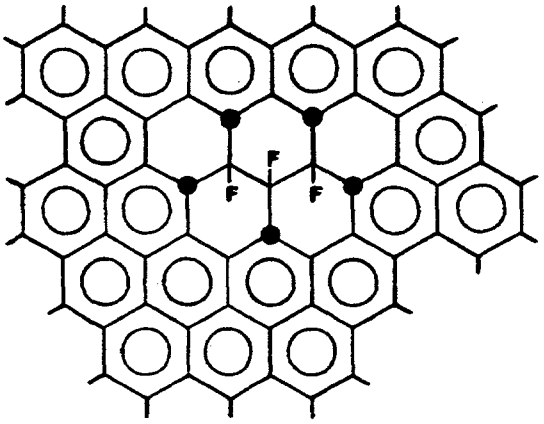

Fig. 35. Modeling of the CF cluster (3 CFs surrounded by 5 C_is).

Table 6. Modeling of the fully fluorinated charcoal platelet[a]

Number of rings (n)	Diameter (nm)	CF_2:CF ratio
1	0.74	1.00
2	1.2	0.50
3	1.7	9.33
4	2.2	0.25
5	2.7	0.20
6	3.2	0.17
7	3.7	0.14

[a] The edge-to-interior CF_2:CF ratio decreases as the platelet grows. The MSRE charcoal platelet is estimated at 2–4 nm

A platelet with $n = 5$ has a CF_2:CF ratio of 0.20, which matches the average experimental value (an average over shape and size distributions). It contains 216 carbon atoms and has a 2.7-nm diam. This particle diameter is consistent with the average platelet size of 1.9 ± 0.8 nm obtained from the broadening of the X-ray diffraction line of the MSRE Calgon charcoal.

The C_i:CF ratio illuminates the fluorination process. Formation of a single isolated CF species, as might occur if $F^{\cdot}$ reacts with a carbon, converts three adjacent sites from C_b to C_i. The C_i:CF ratio is a measure of CF cluster size. A ratio of 3 indicates clusters containing one isolated CF. Lower ratios reflect larger clusters where new CF sites are adjacent to other CF, rather than Ci sites..

As illustrated in Fig. 35, where the • indicates C_i, a cluster containing three CF moieties will have five associated C_i sites for a C_i:CF ratio of 1:6. This ratio (Table 5) is the measured value for the sample prepared at −80°C. Decreasing C_i:CF ratios are observed in the samples prepared at higher temperatures, reflecting increases in the average CF cluster size.

In Table 5, C_i remains relatively constant ($33 \pm 5\%$) for samples prepared over the temperature range from −80 to 120°C, while C_b decreases by a factor of 3. The constant C_i fraction is a statistical result that is obtained, independent of cluster size, if the clusters are considered to have nearly maximal packing density on the platelet and for F:C < 0.5.

The result of modeling fluorinated islands from 3 to 14 CF sites per cluster on a platelet having 216 total carbons predicts $C_i = 27 \pm 5\%$, which is in fair agreement with the NMR ratio. In the modeling, CF islands are prevented from merging by intact aromatic ring spacers. A construct assuming uniform cluster size is artificial but shows, for an assumed fluorination that is initiated at surface sites and occurs at maximum density over the entire surface of the particle, that a constant C_i is the anticipated result, at least until the platelet is half-fluorinated.

Based on the consistent trends in the C:F ratios obtained by gravimetric, ESCA, and NMR analysis, the following pictorial image can be envisioned for the fluorinated charcoal samples. Cluster fluorination occurs readily throughout the charcoal platelets. The undulant fluorinated islands (sp^2 flat graphitic rings replaced by tetrahedral sp^3 sites where fluorine atoms are located below and above the carbon plane) are separated by flat corridors of graphitic carbon. During this stage, the fluorinated charcoal still resembles charcoal. The repulsion between clusters is probably the limiting factor that stabilizes a given stoichiometry for a given temperature.

In this model, the relatively constant C:F ratio from ambient temperature to 150°C can be explained by a relatively high activation energy necessary to break the aromatic ring spacers. During this stage, there is probably a regrouping of the cluster into more-ordered three-dimensional structures. At higher temperatures, the graphitic valleys are gradually removed, and the fluorinated charcoal starts to change color from black to white (with gray and brown intermediates) until it completely transforms into the diamagnetic, alicyclic, white carbon monofluoride.

In short, the F:C ratio derived from NMR data is comparable with ratios obtained by ESCA and gravimetric methods. The distribution of carbon species observed over the preparation range supports radical fluorination throughout the carbon platelets. Fluorine (F_2) has a van der Waals radius of 0.28 nm and is small enough to diffuse between platelets. It is not limited to surface reaction in micropore void spaces.

The platelets spread out as CF regions are formed, increasing access to interior carbon. In X-ray diffraction studies of carbon monofluoride, platelet separation is 0.57 nm. This implies that F_2 is widely accessible throughout the stacked platelets, generating the family of fluorinated charcoal materials in which all ^{13}C are in the CP range (<0.5 nm) of ^{19}F nuclei. The unpaired electron density of the initial charcoal is altered by fluorination. With increasing fluorination, conductivity disappears and is replaced by localized free-spin density.

4. DISCUSSION OF THE DEFLAGRATION CHARACTERISTICS FOR FLUORINATED CHARCOAL

The reaction between fluorine and carbon was extensively used in the early days at the Oak Ridge Gaseous Diffusion Plant for fluorine disposal, but after several violent reactions during the period 1943 to 1950, the process was discontinued.[20,21] However, other facilities that also used charcoal for the disposal of fluorine did not report similar problems.[22,24]

Analyzing all the information gained from the present experiments, along with the previously reported experiences, a clearer understanding of the sometimes near-explosive character of the typically stable fluorinated charcoal has been developed to explain the apparent duality of behavior.

Fluorine will chemically react in a highly exothermic reaction to form nonstoichiometric C_xF compounds, where $1 \leq x \leq 4$. The value of x varies according to the temperature maintained during the fluorination, as shown in Figs. 2 and 19.

As mentioned in Sect. 2.3, if one seeks a material of a particular composition, great care is needed to control the rate of fluorination and to dissipate the generated heat. Increasing the temperature during the fluorination increases the amount of fluorine chemically bonded to the carbon up to the limit $C \approx F$ set by the formation at high temperature of the more stable, white, solid "carbon monofluoride." Uncontrolled fluorination produces high temperatures and pressures with the evolution of gaseous fluorocarbon species.

All our tests show that C_xF synthesized at low temperatures (Figs. 22–24) gradually decomposes at temperatures in excess of 100°C. As shown in Figs. 25 to 28, C_xF prepared at higher temperatures also starts to decompose at temperatures in excess of their preparation temperatures; however, the majority of decomposition occurs in a very narrow range of temperatures at around 500 °C. Finally, the white carbon monofluoride (CF) that is formed by fluorination at temperatures above 250 °C (Fig. 29) is a much more stable material that decomposes at around 700°C.

Fluorine sorption on fluorinated charcoal was mentioned as a possible explanation for unexpected violent decomposition reactions.[20,21] While we have no direct evidence for fluorine adsorption, indirect evidence suggests its presence at a relatively low level, 1 to 3 wt %. This level still may be sufficient to assist in initiating a deflagration reaction when heat is applied to the sample. However, this sorbed F_2 is easily removed by vacuum or by flowing an inert gas through the fluorinated charcoal.

Deflagration of near-explosive characteristics can be triggered in the presence of fluorine by any process or reaction that would rapidly elevate the temperature of the C_xF. The increased temperature would initiate a positive feedback sequence by the following processes: (1) exothermic formation of a more fluorinated C_xF by the fluorine sorbed onto the C_xF (1 to 3 wt %) and the fluorine present in the pores and void volume of the trapping column and (2) exothermic thermal decomposition of C_xF into gaseous fluorocarbons (CF_4, etc.) (Fig. 30).

Once the thermal excursion is initiated, the generation of heat and gases will propagate unless there is a mechanism in place to dissipate the heat. The presence of free fluorine is a main contributing factor for sudden decomposition events, while the total availability of fluorine, free and bonded, is the main limiting factor for the intensity of the deflagration.

Initially when the charcoal bed is far from saturation, the amount of readily available fluorine is low because fluorine reacts very fast with the available charcoal to form C_xF. The amount of chemically bonded fluorine will also be relatively low because most of the charcoal has not yet been fluorinated. However, when the charcoal is (locally) near saturation, fluorine can exist as a gas in pores and void spaces (about 50% of the column or reactor volume) and as an adsorbate on surfaces.

In the presence of any triggering reaction, a saturated trap presents the higher potential for an accident. Our laboratory experience showed that after removal of free fluorine (resident and sorbed F_2 gas) by vacuum or purging with an inert gas, the potential for a deflagration is greatly reduced. In all our tests, after removal of free fluorine, the deflagration is confined to a few particles near the initiation source (e.g., heating using a torch). However, in the presence of free fluorine, the thermal decomposition of C_xF will propagate and reach a significant volume of a reactor or trap, thus causing a near-explosive event.

Examples of heat-generating events that can trigger deflagration are (1) injection of a large amount of fluorine, (2) reaction between fluorine and water by opening a saturated trap in the presence of humid air, (3) accidental release of oil mists from a vacuum system into a trap having free fluorine, and (4) any other heat source that could not be dissipated fast enough. Most accounts of past accidents are anecdotal; however, they all seem to be explainable by the triggering events (1) through (3), and they all happened when the charcoal traps were near saturation with fluorine.

One phenomenon frequently noticed after sudden decomposition events is the presence of charcoal particles having a white coating. As mentioned in Sect. 3.1, charcoal fluorinated at temperatures above 200°C changes color from black to gray, then to brown, and finally to white (carbon monofluoride, $\sim C_1F$) at about 350°C. The reason for this color change is the gradual structural transformation from the delocalized graphitic electronic structure toward the "Teflon-like" aliphatic structure. The presence of charcoal particles having a white coating can be easily explained by the formation of carbon monofluoride at the surface of some particles. Carbon monofluoride is a much more stable material than C_xF and decomposes around 700°C (see Fig. 29).

5. CONCLUSIONS

The primary product from the reaction of fluorine with activated charcoal is fluorinated charcoal. The carbon:fluorine ratio, is a function of the fluorination temperature and ranges from ≈4 at –80°C to ≈1 at 250°C. Charcoal fluorinated at room temperature has a composition of about $C_{2.6}F$.

The stoichiometry that is established by the temperature of fluorination is reproducible and determines the thermochemical behavior and subsequent decomposition kinetics (upon further heating). Spectroscopic measurements (ESCA and NMR) indicate that the nonintegral stoichiometry is a reflection of the distribution of discrete carbon-bonding possibilities (C-C, C-F, $C-F_2$, and $C-F_3$) and that the lamellar structure of graphitic carbon plays a critical role in determining the extent of charcoal fluorination at any temperature.

The energy released during complete decomposition of fluorinated charcoal (as measured by DTA) ranges from 121 kJ/mol F for fluorination at –80°C to 26 kJ/mol F at 250°C. This decrease with the extent of fluorination agrees with established bond energies for the fluorination of carbon.[12] The energy of decomposition on a carbon basis is relatively constant at ~30 kJ/mol C and reflects the counterbalancing effects of fluorine content (increases with fluorination temperature) and fluorine decomposition energy (decreases with fluorination temperature). The values for material fluorinated at room-temperature are 81 k J/mol F and 31 kJ/mol C. The thermal decomposition kinetics is also primarily a function of the temperature of fluorination. For material fluorinated below 23°C, energy is released gradually over a broad temperature range, with a small distinct peak in the neighborhood of 475°C.

At higher fluorination temperatures (65 to 250°C), a large fraction of the energy release can be associated with a large, sharp energy peak around 500°C. The bulk of the decomposition of white carbon monofluoride occurs at temperatures in excess of 600°C. In all cases, some heating beyond the temperature of fluorination is required to initiate any decomposition, and for the material fluorinated at 65°C and below, the initial decomposition begins near 100°C. The visual observation of deflagration agrees with the limits established by these thermochemical measurements – deflagration can be precluded by limiting the temperature of fluorinated charcoal to less than 100°C.

A number of items that were considered to have an impact on a deflagration event were found to be insignificant or of secondary importance. Irradiation of fluorinated charcoal has no observable effect upon the properties of the material. Initiation of a deflagration event by mechanical shock or spark was tried and never found to be effective; only rapid heating produced such an event. Finally, we found that the fluorine sorption on fluorinated charcoal is less than 2 wt % and may help initiate deflagration events under some circumstances. This sorbed fluorine is rapidly removed by evacuation or an inert gas flow.

Another contributing factor in the initiation of deflagration is the presence of gaseous fluorine in the voids of the charcoal bed. However, the presence of unreacted fluorine in the ACB is not credible because the charcoal bed had been periodically purged during the cooling period after tank annealing and recently. Additionally, the large excess of unreacted charcoal present in the ACB would have scavenged both gaseous and sorbed fluorine. Thus, the only potential mechanism that could initiate a deflagration would be the sudden external heating of a portion of the ACB during drilling or tapping operations.

The uranium that is deposited in the activated charcoal from a UF_6/F_2 gas stream is in the form of nonvolatile uranium fluorides and uranium oxyfluorides that are intercalated in the micrographitic structure of charcoal. This material is less likely to deflagrate than fluorinated charcoal and decomposes with much less energy release. The fluorine front moves ahead of the uranium front producing fluorinated charcoal. The uranium-laden charcoal and the fluorinated charcoal are visually indistinguishable from virgin activated charcoal. Consequently, the laden charcoal particles can be easily removed from a column by gravity or vacuuming as planned for the actual ACB removal. However, in the presence of humidity, the charcoal particles become cemented by interstitial uranyl fluorides.[26] These cemented chunks of laden charcoal are quite hard and require a significant mechanical force for the particles to be separated. The potential presence of carbonaceous residues, derived from the reaction of pump oil vapors that might have been deposited in the charcoal and F_2, is another plausible source for lumping of the charcoal.

The significance of this laboratory observation for the ACB remediation is that hardened chunks of material could be present due to moisture intrusion. The removal of those chunks would require a special tool that could break the chunks into vacuumable particles. The visual appearance of charcoal with interstitial uranium oxyfluorides has the distinctive yellow-orange color characteristic of the uranyl fluoride. A visual inspection of the top of the ACB could give an indication of the presence of interparticle uranyl fluoride.

REFERENCES

1. D. F. Williams, G. D. Del Cul, and L. M. Toth, *A Descriptive Model of the Molten Salt Reactor Experiment after Shutdown: Review of FY1995 Progress*, ORNL/TM-13142, Oak Ridge National Laboratory, Oak Ridge, Tenn., 1996.

2. W. Wendolkowski and W. Davis, *Effects of Diluent Gases on Alpha Particle Decomposition of UF_6*, K-1142, Carbide and Carbon Chemicals Company, K-25 Plant, Oak Ridge, Tenn., 1954.

3. C. H. Shiflett et al., *The Chemical Effect of Alpha Particles on UF_6 at Room Temperature*, K-738, Carbide and Carbon Chemicals Company, K-25 Plant, Oak Ridge, Tenn., 1951.

4. F. D. Rosen et al., *The Temperature Dependence of the Decomposition of UF_6 under Alpha Particle Irradiation*, K-795 Carbide and Carbon Chemicals Company, K-25 Plant, Oak Ridge, Tenn., 1951.

5. E. W. Becker, W. Bier, P. Hagmann, and F. Mikosch, *Bedeutung der radiolytischen Selbstzersetzung von Uranhexafluorid bei der Anreicherung von Uran-235 nach dem Trenndüsenverfahren*, (Understanding of the Radiolytic Auto-Decomposition of Uranium Hexafluoride During the Enrichment of Uranium-235 by the Separation Jet Process), KFK 3332, Kernforschungzentrum Karlsruhe, Karslruhe, Germany, 1982.

6. M. Smíšek and S. Černý, *Active Carbon*, Elsevier Publishing Co., N. Y., 1970.

7. H. Jankowska, A. Świątkowski, and J. Choma, *Active Carbon*, Ellis Hordwood Limited, N. Y., 1991.

8. T. Nakajima and N. Watanabe, *Graphite Fluorides and Carbon-Fluorine Compounds*, Chapter 3, CRC Press, Boca Raton, Fla., 1990.

9. J. L. Wood, R. B. Badachhape, R. J. Lagow, and J. L. Margrave, "The Heat of Formation of Poly(Carbon monofluoride)," *J. Phys. Chem.* **73,** 3139–42, 1969.

10. J. L. Wood, R. J. Lagow, and J. L. Margrave, "The Heat of Combustion of Teflon in Fluorine, A Check on the Heat of Formation of Carbon Tetrafluoride," *J. Chem. & Eng. Data* **12**, 255–56, 1967.

11. J. H. Halloway, *Fluorine-Carbon and Fluoride-Carbon Materials,* Nakajima, T., ed., Marcel Dekker, Inc. N. Y., 1995.

12. P. Kamarchick and J. L. Margrave, "A Study of Thermal Decomposition of the Solid-Layered Fluorocarbon, Poly(Carbon Monofluoride)," *J. Thermal Anal.* **11**, 259–70, 1977.

13. N. Watanabe and S. Yoshizawa, "Reaction of Fluorine and Carbon," presented at the Symposium on Carbon, Tokyo, July 20–23, 1964.

14. N. Watanabe, Y. Kita, and O. Mochizuki, "Fluorination of Carbon Black," *Carbon* **17,** 359–6, (1979).

15. N. Watanabe, T. Nakajima, and H. Touhara, *Graphite Fluorides. Studies in Inorganic Chemistry 8*, Elsevier, Amsterdam, 1988.

16. N. Watanabe, S. Koyama, and H. Imoto, "Thermal Decomposition of Graphite Fluoride. I. Decomposition Products of Graphite Fluoride, $(CF)_n$ in a Vacuum," *Bull. Chem. Soc. Jpn.* **53**, 2731–34, 1980.

17. K. Kuriakose and J. L. Margrave, "Mass Spectrometric Studies of the Thermal Decomposition of Poly(carbon monofluoride)," *Inorg. Chem.* **8**, 1639–41 1965.

18. R. L. Farrar, Jr., and E. J. Barber, *Some Considerations in the Handling of Fluorine and the Chlorine Fluorides*, K/ET-252, Oak Ridge Gaseous Diffusion Plant, pp. 33-36, July 1979.

19. R. L. Farrar, Jr., and J. R. Merriman, Safe Handling of F_2 and ClF_3," Pp. 24–25 in *Program for Safety Steering Committee,* Oak Ridge Gaseous Diffusion Plant, 1980.

20. J. L. Madix and W. D. Goode, *Reactivity of Carbon and Graphite with Fluorine and Uranium Hexafluoride—A Review*, K-1790, 1970.

21. J. D. Navratil, *Disposal of Fluorine*, RFP-1200, 1968.

22. H. W. Schmidt, *Reaction of Fluorine with Carbon as a Means of Fluorine Disposal*, NASA-RM-E57E02, Cleveland, Ohio, 1957; NSA 12, 4726, 1958.

23. H. W. Schmidt, *Design and Operating Criteria for Fluorine Disposal by Reaction with Charcoal*, NASA-M-1-27-59E, Cleveland, Ohio, 1959; NSA 13, 14321, 1959.

24. H. W. Schmidt, *Fluorine Disposal Using Charcoal*, GAT-T-819, Portsmouth, Ohio, 1960; NSA 12, 4726, 1958.

25. Ozark-Mahoning Company, Tulsa, Okla., "Synthesis of Fluorographite," U. S. Patent 72-295675.

26. G. D. Del Cul, L. D. Trowbridge, D. W. Simmons, D. F. Williams, and L. M. Toth, *Passivation of Fluorinated Activated Charcoal*, ORNL/TM-13506, Oak Ridge National Laboratory, Oak Ridge, Tenn., October 1997.

27. P. A. Jansson, *Deconvolution with Applications in Spectroscopy*, Academic Press, Orlando, Fla., 1984.

28. W. E. Blass and G. W. Halsey, *Deconvolution of Absorption Spectra*, Academic Press, N.Y., 1981.

29. D. A. Shirley, *Phys. Rev. B* **5**, 4709 (1972).

30. A. Savintsky and M. J. E. Golay, *Anal. Chem.* **36**, 1627 (1964).

31. N. Watanabe, S. Koyama, Y. Kita, and M. Iwasaki, "Degradation of Graphite Fluoride by γ-Ray Irradiation," *Nippon Kagaku Kaishi*, **12**, 1618–22 (1978).

32. R. K. Harris and P. Jackson, *Chem. Rev.* **91**, 1427 (1991).

33. E. W. Hagaman and S. K. Lee, *Energy and Fuels* **9**, 727 (1995).

34. E. W. Hagaman and J. H. Burns, *Fuel* **72**, 1239 (1993).

35. D. K. Murray, E. W. Hagaman, and G. D. Del Cul, "An ^{19}F and ^{13}C NMR Study of C_xF Prepared by Variable Temperature Fluorination of Charcoal with Elemental Fluorine", presented at the 212th Annual National Meeting, American Chemical Society, March 24–29, San Francisco, 1997.

36. E. W. Hagaman, D. K. Murray, and G. D. Del Cul, "Solid State ^{13}C and ^{19}F NMR Characterization of Fluorinated Charcoal," *Energy and Fuels* **12**, 399 (1998).

37. P. Kamarchik and J. L. Margrave, "Poly(Carbon Monofluoride): A Solid, Layered Fluorocarbon," *Acct. Chem. Res.* **11**, 296 (1978).

APPENDIX:
ESCA ANALYSIS OF THE LOADING OF UF_6 AND F_2 ON ACTIVATED CHARCOAL

As mentioned in Sect. 3.6, the loading of pure UF_6 on activated charcoal results in the intercalation of uranium fluorides and oxyfluorides in the micrographitic structure. Loosely sorbed UF_6 could also be present but not as a major component; however, all samples were purged with helium and evacuated before handling to avoid the spread of contamination.

The experiments also indicated that reaction between charcoal and the F_2-UF_6 Molten Salt Reactor Experiment (MSRE) blend produces C_xF that contains intercalated uranium fluorides and oxyfluorides. [1,2] The electron spectroscopy for chemical analysis (ESCA) of the samples contacted with the F_2-UF_6 MSRE blend shows that the concentration of fluorine atoms directly bonded to carbon is lower than for the samples contacted with pure fluorine. This observation correlates with the milder decomposition of the F_2-UF_6–laden samples when rapidly heated (mild deflagration).

The dynamic loading of the F_2-UF_6 MSRE blend through columns filled with activated charcoal showed that the fluorine front moves ahead of the uranium front. Based upon our laboratory experience, the measured MSRE auxiliary charcoal bed (ACB) uranium front (C_xF plus intercalated uranium compounds) extends about 1 ft from the top of the ACB, and is followed by a C_xF front spanning a few feet further downstream. The rest of the ACB, about 80 ft, most probably consists of unreacted charcoal.

From the different tests, samples were taken for ESCA . As mentioned in Sect. 2.6, the ESCA data can be used to differentiate atoms of the same element in different compounds (different bonding environments). Consequently, the ESCA data can provide information on the nature of the chemical species formed by reaction of charcoal, F_2, and UF_6.[3-5]

The different regions related to fluorine, oxygen, carbon, and uranium atoms must be analyzed as a whole (e.g., F 1*s*, C 1*s*, F Auger, O 1*s*, U $4f_{7/2}$, U valence). The species assignments have to be consistent for all the ESCA regions. In other words, the species assignments and relative concentration obtained from the analysis of the fluorine region must be consistent with the species assignment based on the analysis of the uranium region. The following sections summarize the experimental conditions used to generate the samples and a preliminary analysis of the ESCA data.

A.1 ESCA OF CHARCOAL SAMPLES CONTACTED WITH UF_6 AND UF_6-F_2

Initially, a glass column with Teflon fittings (14.5 cm long, 1 cm ID) containing 4.41 g of activated charcoal was exposed to a slowly flowing He-UF_6 mixture (95.7 vol % He, 4.3 vol % UF_6) until breakthrough. A sample taken from the top of the column (gas input) was crushed inside a dry-helium glove box into a fine powder and mounted for ESCA (Sect. 2.6).

After the first experiment, the same column was refilled with 4.44 g of activated charcoal and slowly exposed to a flowing 5:1 mixture of F_2-UF_6 until breakthrough. Specifically, the gas mixture was 31.7 torr UF_6, 158.1 torr F_2, and the balance helium, all at a total pressure of 2300 torr. As in the first case, a sample taken from the top (the gas inlet end) of the column was crushed inside a dry-helium glove box into a fine powder and mounted for ESCA.

The uranium and fluorine-laden activated charcoal is a complex system. The ESCA of the samples included the binding-energy analysis for the core electronic levels of the atomic species present C 1*s*, F 1*s*, O 1*s*, U 4*f*) and the valence electron regions (U 7*s*, U 6*d*, U 5*f*, U $6p_{1/2}$, U $6p_{3/2}$, O 2*s*, F 2*s*). The consistent interpretation of the results and band assignments requires the simultaneous examination of all the regions.

A.1.1 ESCA Spectra, U 4*f* Region

As a general rule, the binding energies for a given element increase proportionally with its formal oxidation state.[3-5] The electronegativity of the ligands or counterions and crystal structure are also important factors in determining binding energies. Since fluorine is more electronegative than oxygen, the binding energy increases from the pure oxide to the pure fluoride $UF_6 > UO_2F_2 > UO_3$. The U 4*f* binding energy for UO_2F_2 is slightly lower than the binding energy for UF_5 and slightly higher than the binding energy for UF_4.

The characteristics of the binding-energy region for U 4*f* photoelectrons were quite similar for both treated samples. As an example, Fig. A.1 shows a curve-fitted spectrum for the charcoal sample contacted with F_2-UF_6. This U $4f_{7/2}$ envelope can be fitted with three components, designated as U_A, U_B, and U_C.

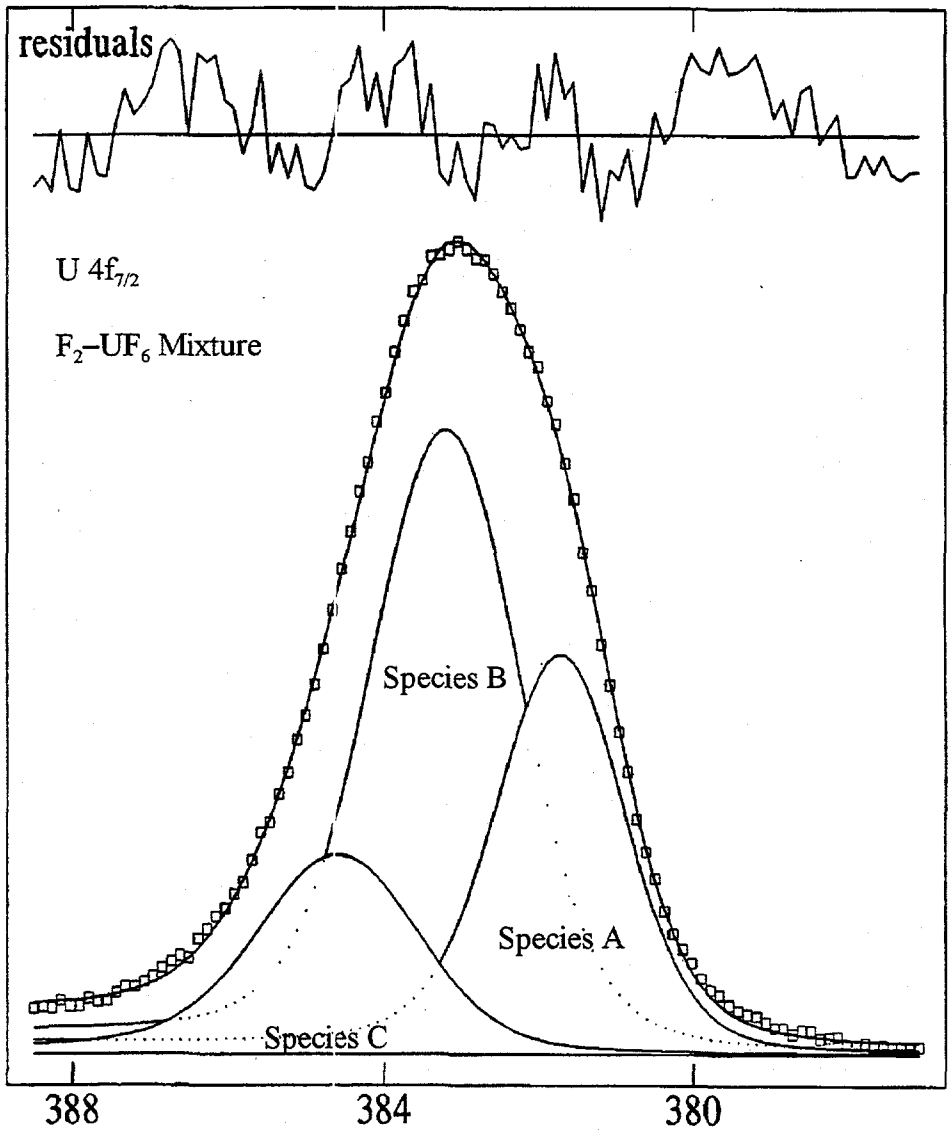

Fig. A.1. ESCA deconvoluted spectra, U $4f_{7/2}$ region, for charcoal contacted with F_2-UF_6.

The curve-fitted spectrum for pure UF_4, as shown in Fig. A.2, consists of a major component, U_B, along with the minor component, U_A. Therefore, the major band, U_B, having a U $4f_{7/2}$ binding energy of ~383.0 eV, can be identified as that associated with pure UF_4. The peak U_A (U $4f_{7/2}$ ~381.5 eV) which appears as a minor impurity in the UF_4 sample is probably caused by UOF_2 and UOF_4. The position of the U_C component (~384.5 eV), which is ~1.5 eV from that of UF_4, is consistent with higher fluorides, $UF_{x>4}$ (UF_5, U_2F_9, chemisorbed UF_6),[4] and UO_2F_2.[3]

According to the ESCA results for both samples, UF_4 is the major uranium species present in the uranium-laden activated charcoal, even in the presence of F_2. It should be noted, however, that the conditions the sample is subjected to in the course of ESCA will tend to convert fluorides higher than UF_4 (e.g., UF_5) to UF_4, either by disproportionation and volatilization of UF_6 or reduction by the X-ray and photoelectron flux.[4]

A.1.2 ESCA Spectra, F 1*s* Region

As shown in Fig. A.3, the curve-fitted ESCA F 1*s* region of the charcoal sample contacted with the F_2-UF_6 mixture consists of three components (labeled F_A, F_B, and F_C). The major peak, F_A (~684.5 eV), is consistent with fluorine bonded to uranium in UF_x (x = 4 to 6).[3,4] The F_B peak (~686.5 eV) corresponds to fluorine bonded to carbon (C-F) (Sect. 3.2.2) and UO_2F_2. The minor peak, F_C (~688 eV), corresponds to fluorine species with a higher than expected binding energy. Tressaud[6] assigned a peak at the same binding energy to a covalent C-F bond for fluorinated carbon fibers. This was the predominant peak for fibers having high carbon:fluorine ratios. This second C-F (F_C) peak could then be attributed to the presence of isolated C-F bonds, while the F_B corresponds to clustered C-F bonds.

Figure A.4 shows the same region for the sample reacted with pure UF_6. It can be seen that the F_B peak (C-F) is absent, thus indicating that UF_6 does not fluorinate the charcoal in any significant amount. This observation is consistent with the thermal stability of the uranium-laden charcoal. As mentioned in Sect. 3.6, activated charcoal contacted with UF_6 will not deflagrate when rapidly heated. This is in sharp contrast with the brisk thermal decomposition of C_xF under the same conditions.

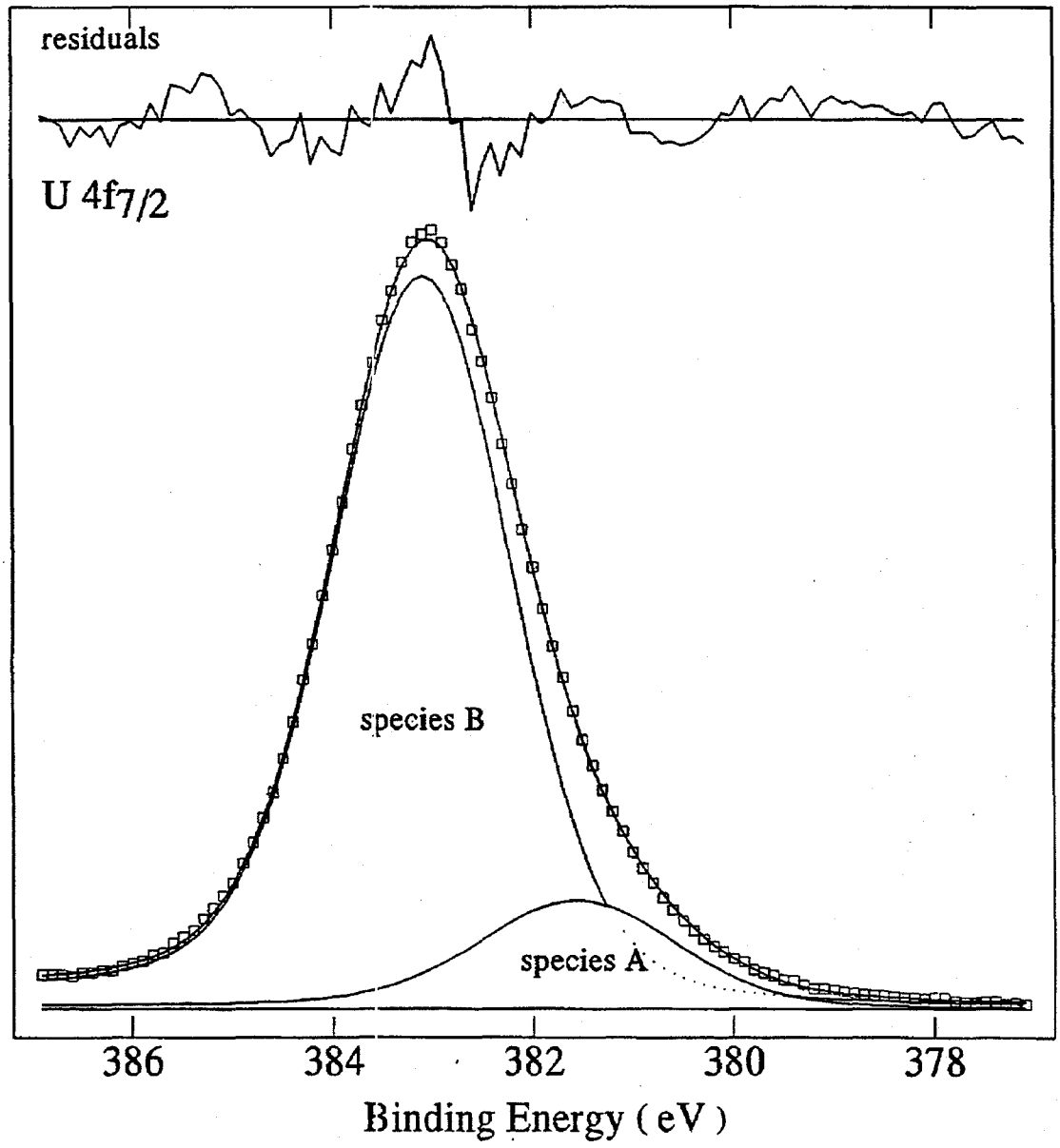

Fig. A.2. ESCA deconvoluted spectra U4$f_{7/2}$ region for UF_4.

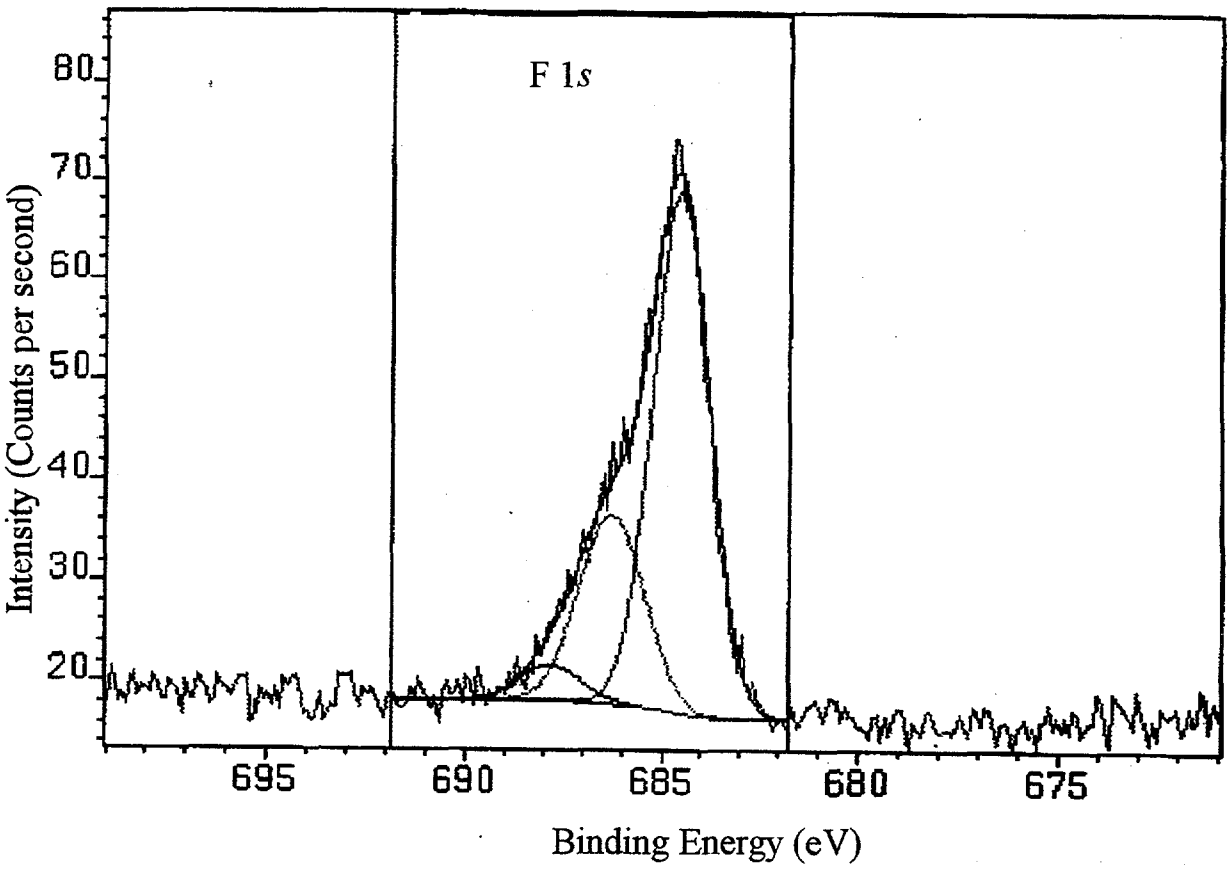

Fig. A.3. ESCA deconvoluted spectra, F 1*s* region, for charcoal contacted with UF_6-F_2.

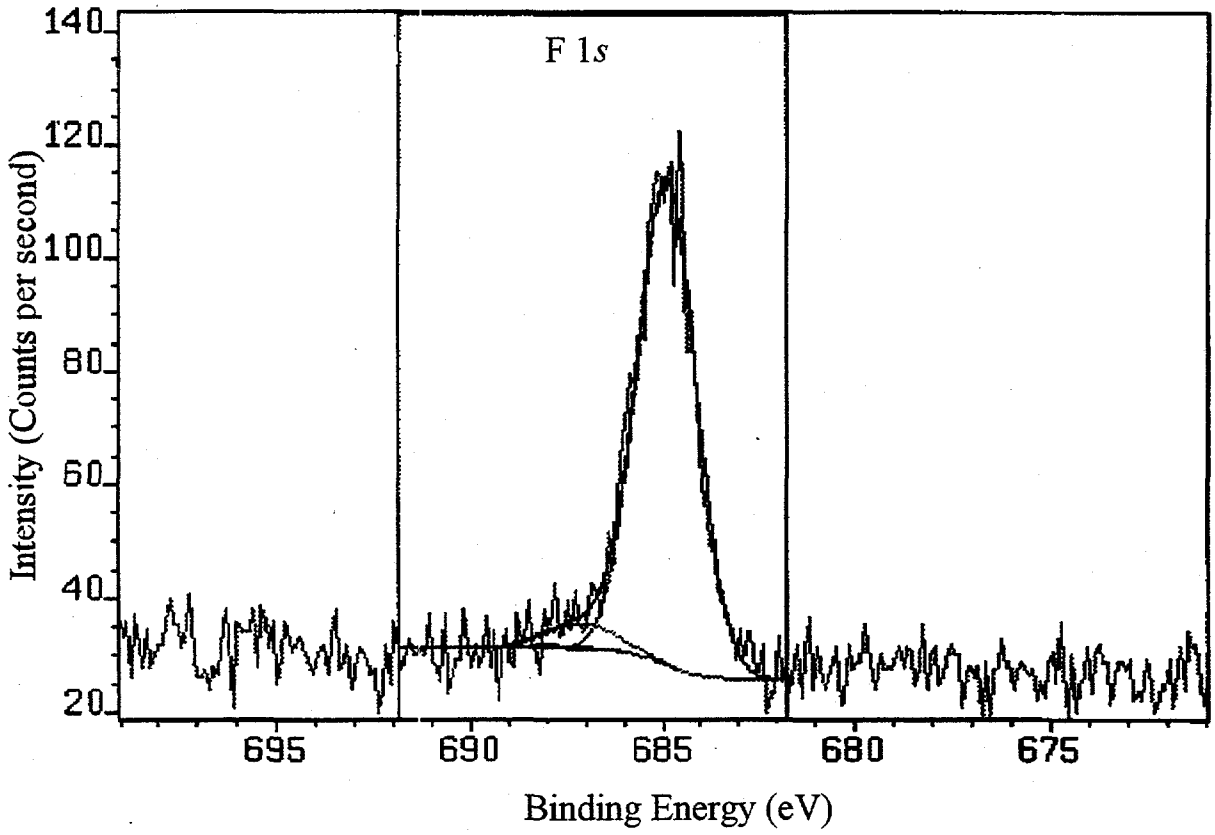

Fig. A.4 ESCA deconvoluted spectra, F 1s region, for charcoal contacted with UF_6.

Since the U 4*f* region seems to indicate UF_4 as the major species, it can be conjectured that the missing fluorine from UF_6 is consumed mainly by reactions with functional groups at the surface of the charcoal.[7] Figure A.5 displays the curve-fitted F 1*s* region for both samples and pure UF_4. As mentioned, the major peak, F_A, corresponds to UF_x (x = 4 to 6). The shape and position of the F_A peaks for pure UF_4 and the charcoal reacted with pure UF_6 are quite similar. The F_A peak for the sample contacted with F_2–UF_6 is slightly displaced toward lower binding energies. This displacement is consistent with the presence of higher uranium fluorides, in addition to UF_4.

A.1.3 ESCA Spectra, O 1*s* Region

The O 1*s* region presents two peaks, O_A and O_B, and as shown in Fig. A.6, is almost identical for both samples (UF_6 and F_2-UF_6). The O_A peak is the only one present in the untreated activated charcoal and in all the fluorinated charcoal samples, because the oxygenated functional groups are located at the surface of the charcoal crystallites. The O_B peak is consistent with uranium oxyfluorides.[3]

A.1.4 ESCA Spectra, C 1*s* Region

The C 1*s* region for the sample exposed to UF_6 (see Fig. A.7, top) displays the same peaks as the charcoal and fluorinated charcoal samples (see Sect. A.1.2). The peak at the lower energy belongs to undisturbed graphitic carbon (C-C graphite, ~284.5 eV), followed by carbon bonded to carbon influenced by neighboring fluorine (C-C, ~ 285.6 eV), and carbon bonded to one fluorine (C-F, ~287.9 eV).

The ~290-eV peaks can be attributed to isolated C-F bonds (see Sect. A.1.2) and carbon bonded to two fluorine atoms ($C\text{-}F_2$,~290 eV). The sample exposed to the mixture of F_2-UF_6 (Fig. A.7, bottom) shows, as expected, a higher concentration of C-F. There is also a small unknown peak centered at 293.5 eV that is not due to $C\text{-}F_3$ (~291.5 eV).

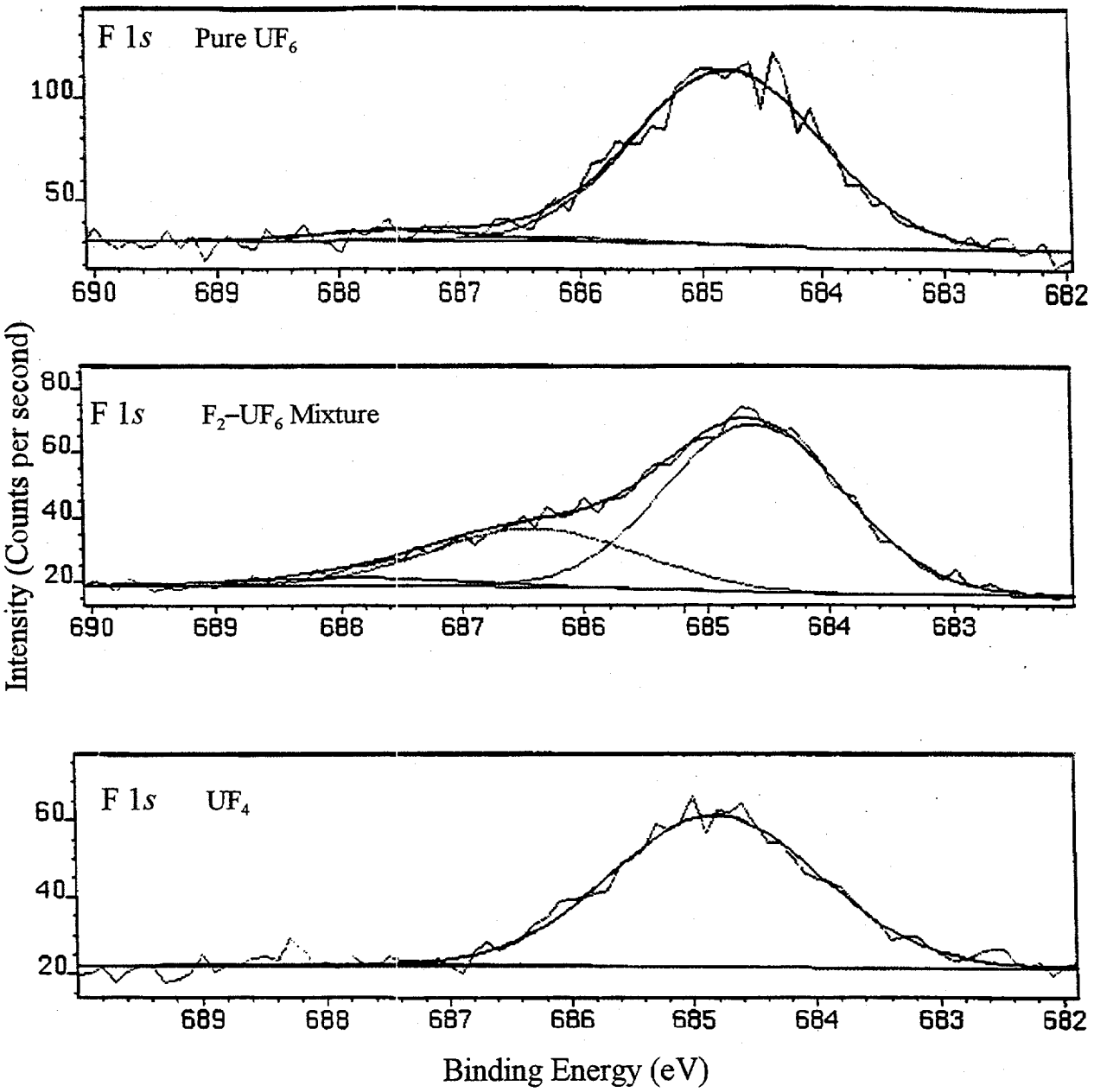

Fig. A.5. Comparison of ESCA deconvoluted spectra, F 1*s* region, for pure UF_4 and charcoal contacted with UF_6 and a UF_6-F_2 mixture.

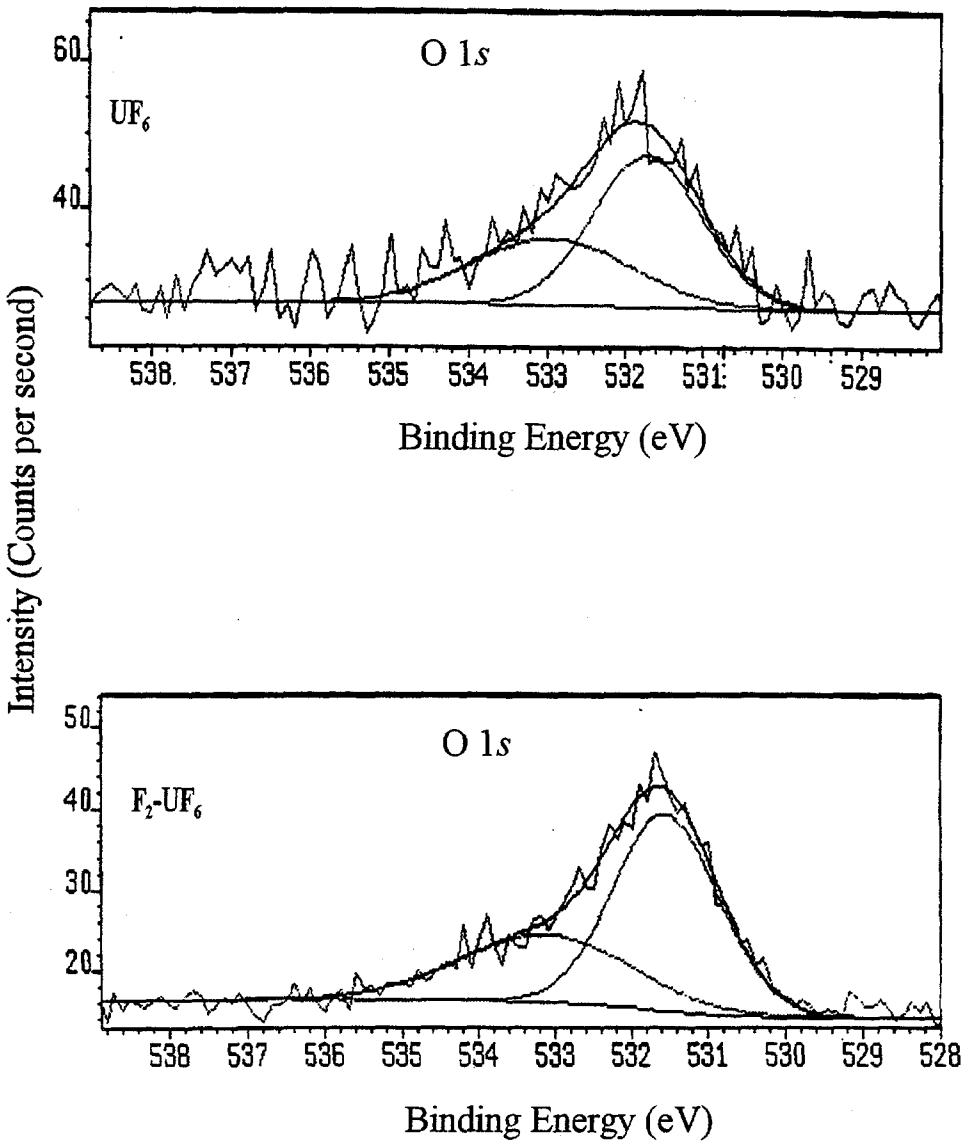

Fig. A.6. ESCA deconvoluted spectra, O 1*s* region, for charcoal contacted with UF_6 and a F_2-UF_6 mixture.

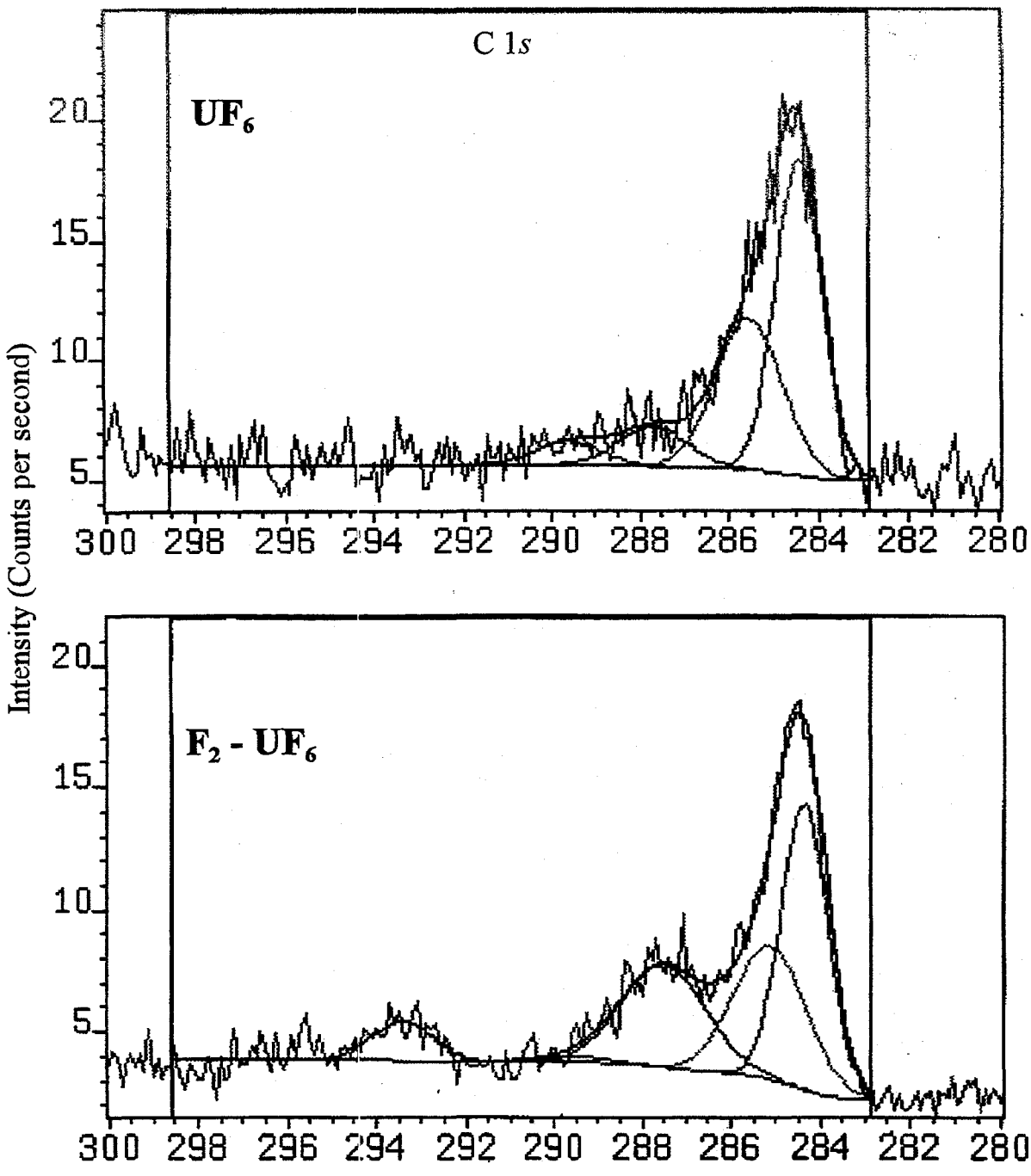

Fig. A.7. ESCA deconvoluted spectra C 1*s* region for charcoal contacted with UF_6 and a F_2-UF_6 mixture.

A.2 ESCA OF SAMPLES FROM COLUMN LOADING OF UF_6–F_2 ON CHARCOAL

Two glass columns with Teflon fittings (14.5 cm long, 1 cm ID), each filled with 4.06 g of activated charcoal, were connected in series. The MSRE 5:1 mixture of F_2-UF_6 was slowly flowed until the uranium front (visual observation) reached the top of the second column.

Samples were taken from the top (gas inlet) and bottom of the first column and from the bottom of the second column (gas exit). The samples were labeled "Top," "Mid," and "Bottom," respectively. A small portion from each sample was crushed inside a dry-helium glove box into a fine powder and mounted for ESCA.

A portion of the "Top" sample was further contacted with pure fluorine, while a second fraction of the "Top" sample was heated under vacuum to 650°C. Both tests were performed to determine the possibility of uranium removal from the charcoal by further fluorination or heating under vacuum. No significant removal of uranium was observed in either test. After treatment, a small portion from each sample was crushed inside a dry-helium glove box into a fine powder and mounted for ESCA.

A.2.1 ESCA Spectra, U 4*f* Region

The U $4f_{7/2}$ binding-energy region, as was shown previously in Fig. A.1 for the "Top" sample, can be reconstructed using three bands designated U_A, U_B, and U_C (see Sect. A.1.1). The "Mid" sample (see Fig. A.8), taken near the end of the uranium front, shows only the U_B (UF_4) and U_C components [$UF_{x>4}$ (UF_5, U_2F_9, chemisorbed UF_6)] and UO_2F_2, while the U_A (UOF_2) is missing.

Figure A.9 overlays the U $4f_{7/2}$ binding-energy region of the standard UF_4, the "Top" sample exposed to F_2-UF_6, the "Top" sample further exposed to pure F_2, and the "Top" sample after heating to 650°C. The respective curve-fitted U $4f_{7/2}$ spectra are shown in Figs. A.1, A.2, A.10 and A.11.

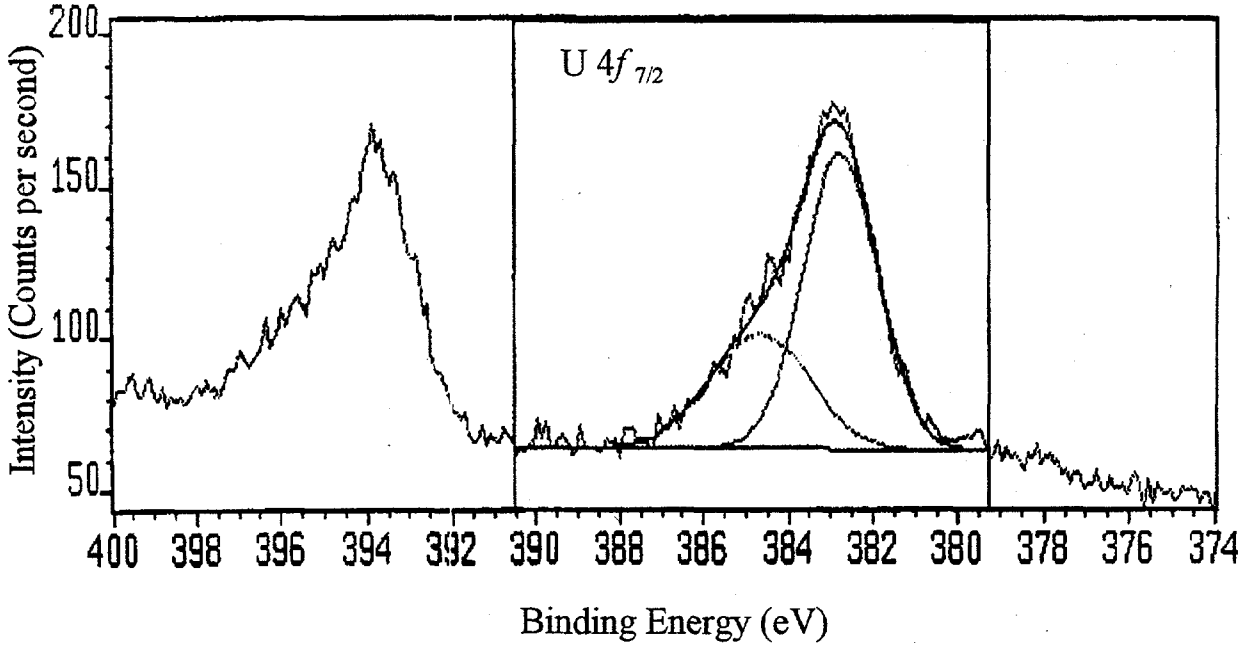

Fig. A.8. ESCA deconvoluted spectra, U4$f_{7/2}$ region, for charcoal contacted with F_2-UF_6 mixture during column loading: mid column sample.

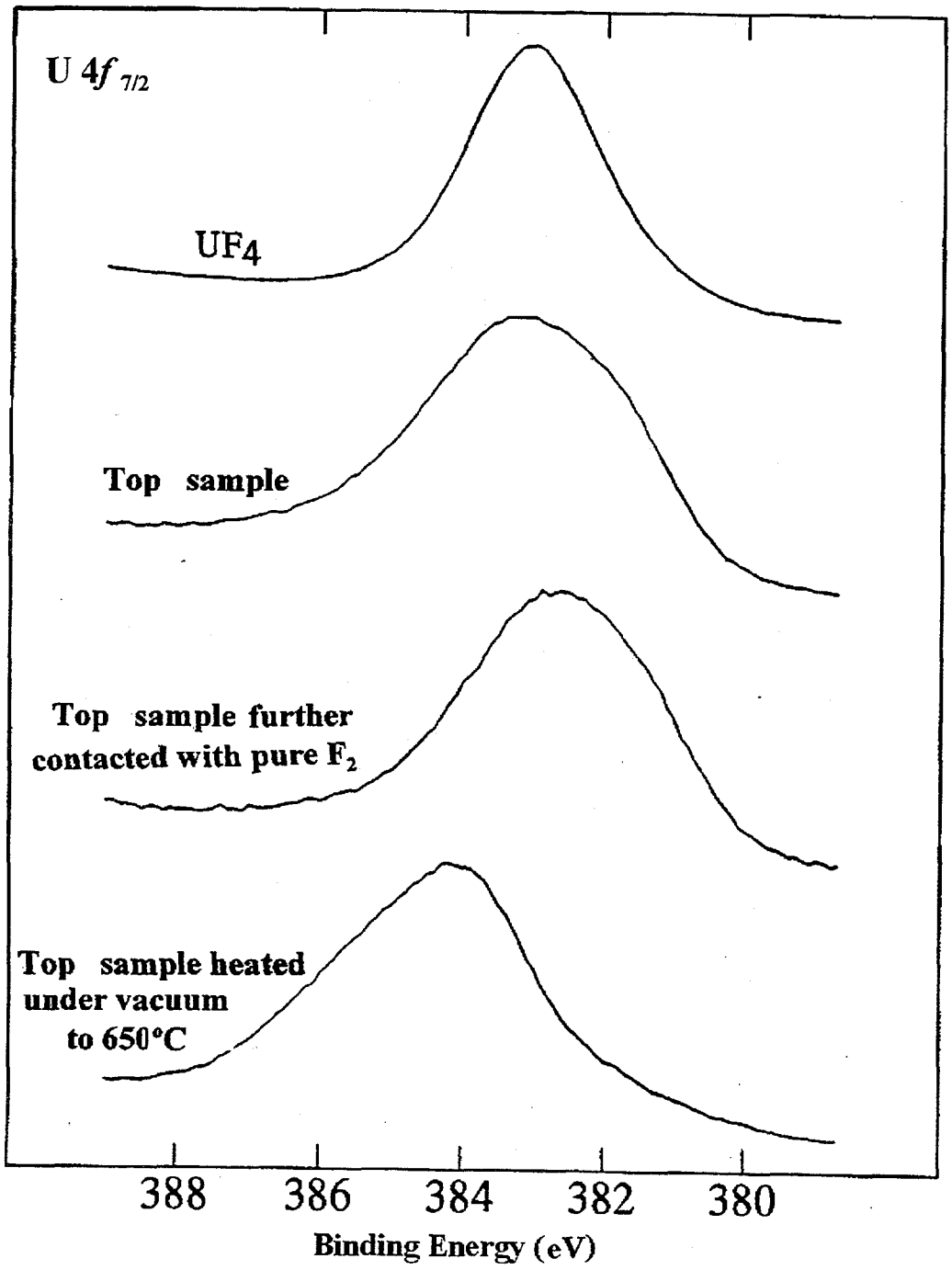

Fig. A.9. Comparison of ESCA spectra, U4$f_{7/2}$ region, for pure UF_4 and charcoal contacted with F_2-UF_6 mixture during column loading: top column sample, sample further contacted with F_2, and sample heated under vacuum to 650°C.

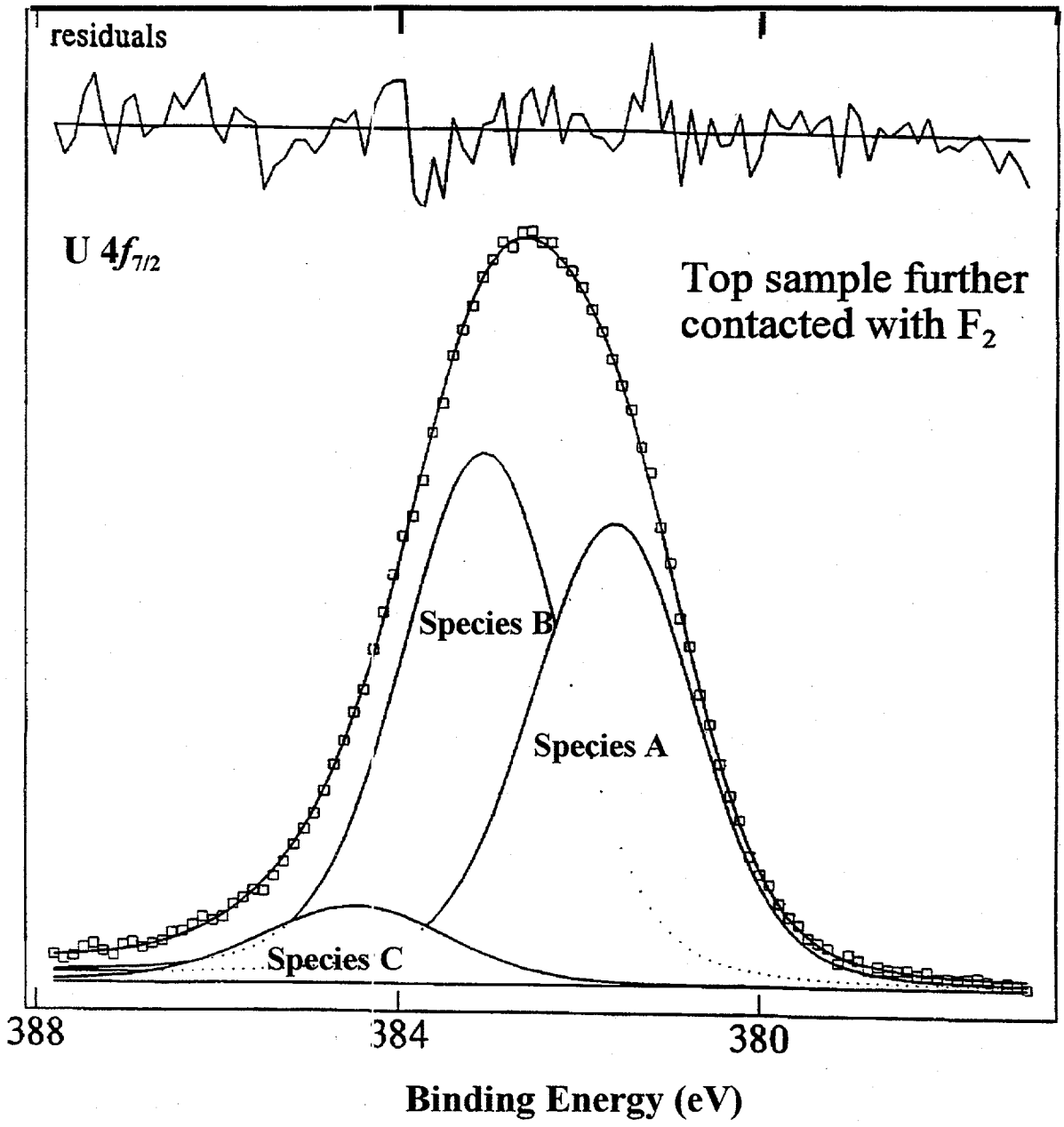

Fig. A.10. ESCA deconvoluted spectra, U4f$_{7/2}$ region, for charcoal contacted with F_2-UF_6 mixture during column loading: top sample further contacted with F_2.

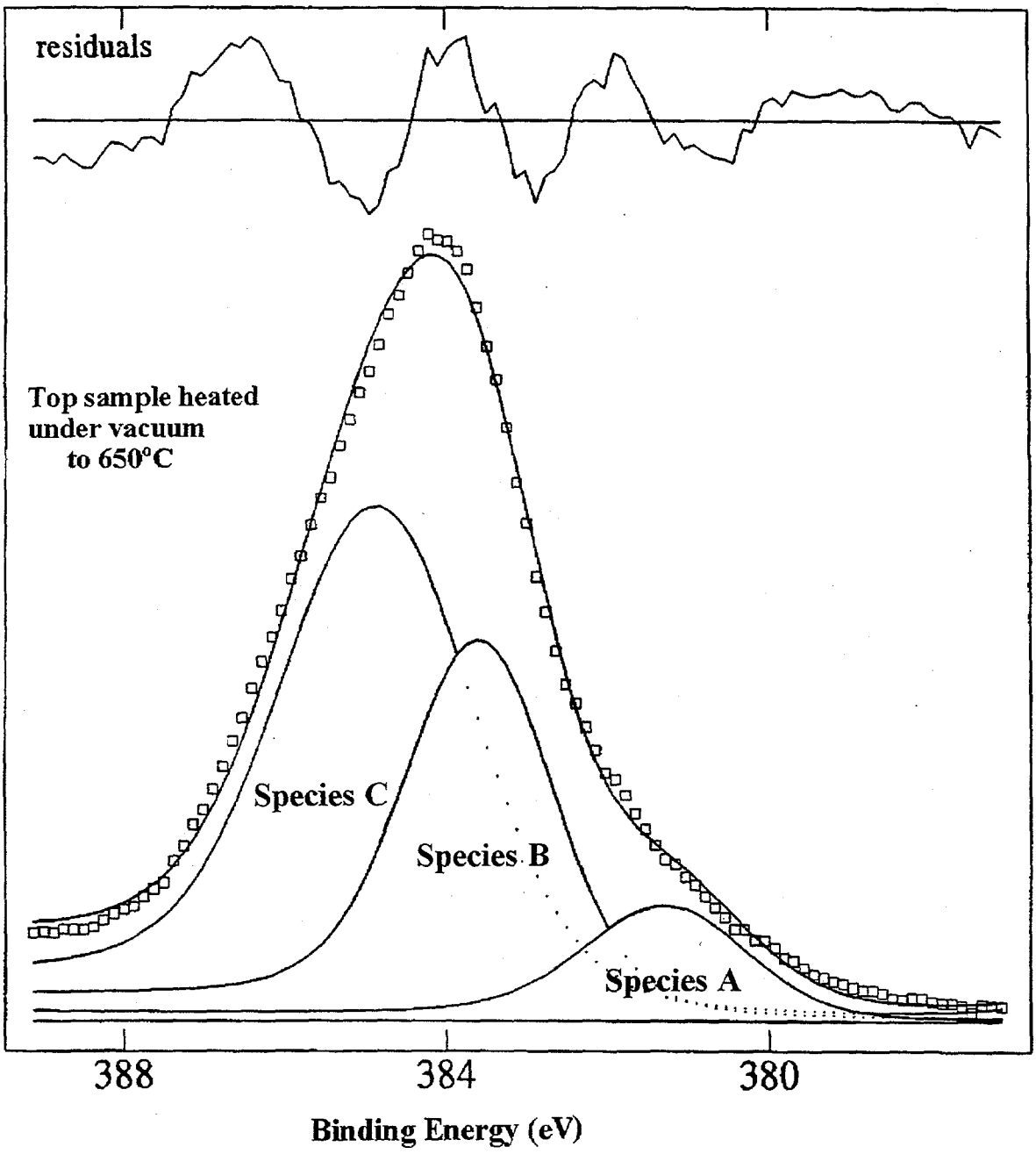

Fig. A.11. ESCA deconvoluted spectra ,U4$f_{7/2}$ region, for charcoal contacted with F_2-UF_6 mixture during column loading: top sample heated under vacuum to 650°C.

The spectra of the further-fluorinated sample, while similar to the original "Top" specimen, shows that the concentration of species U_A grew while the concentration of species U_C ($UF_{x>4}$, UO_2F_2) decreased, probably because a conversion of oxyfluoride species by fluorine ($UO_2F_2 + F_2 \rightarrow UOF_4 + 0.5\ O_2$).[8-11] The heated "Top" sample shows a significant growth of the U_C ($UF_{x>4}$, UO_2F_2) peak. This can be explained by further reaction of UF_x with oxygenated functional groups from the charcoal to form UO_2F_2.

A.2.2 ESCA Spectra, Valence Electron Region

Figure A.12 shows the valence electron spectra for pure UF_4 and UO_2F_2. The spectrum for UF_4 displays a relatively sharp peak at about 3 eV (U 5f) and a wider peak at about ~8 eV (U 7*s*, 6*d*, 5*f* and F 2*p*).

The wider peak (U 7*s*, 6*d*, and 5*f* and F 2*p*) appears also in UO_2F_2 but it is centered at about 6 eV, while the sharper peak is missing. The UO_2F_2 valence spectra shown at the bottom of Fig. A.12 actually show a minor contribution of the 3-eV peak due to impurities.

Fig. A.13 presents the the valence electron spectra for the "Top" sample. The ~8-eV peak characteristic of UF_4 is present; however, the 3-eV peak is not. The second peak at ~5.5eV could be due to UF_5 (ref.3) and UO_2F_2. The spectra for the "Mid" sample, not shown, were too weak and noisy to lead to any conclusion.

A.2.3 ESCA Spectra, F 1*s* Region

Figure A.14 displays the F 1*s* spectra for ESCA for the "Top," "Mid," and "Bottom" samples. The bottom sample had only the F_B peak because the fluorine bonded to carbon (F-C). As mentioned earlier, the loading of the column was stopped when the uranium front reached the middle of the combined column. This demonstrates that the fluorine front moves well ahead of the uranium front.

Figure A.15 overlays the ESCA F 1*s* envelopes for UF_4, the original "Top" sample, the portion further contacted with F_2, and the "Top" aliquot heated to 650°C.

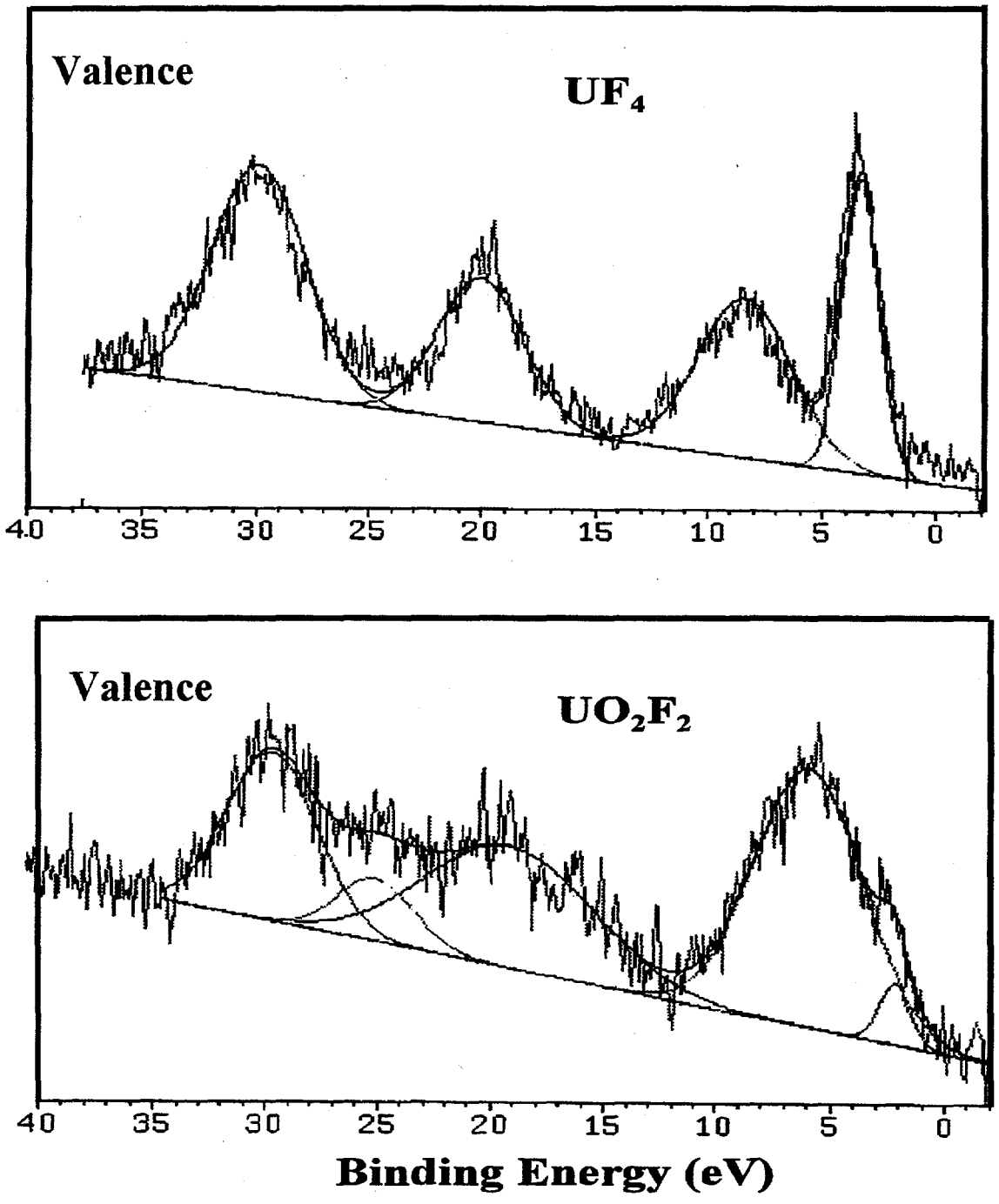

Fig. A.12. ESCA deconvoluted spectra of the valence electron region for pure UF_4 and UO_2F_2.

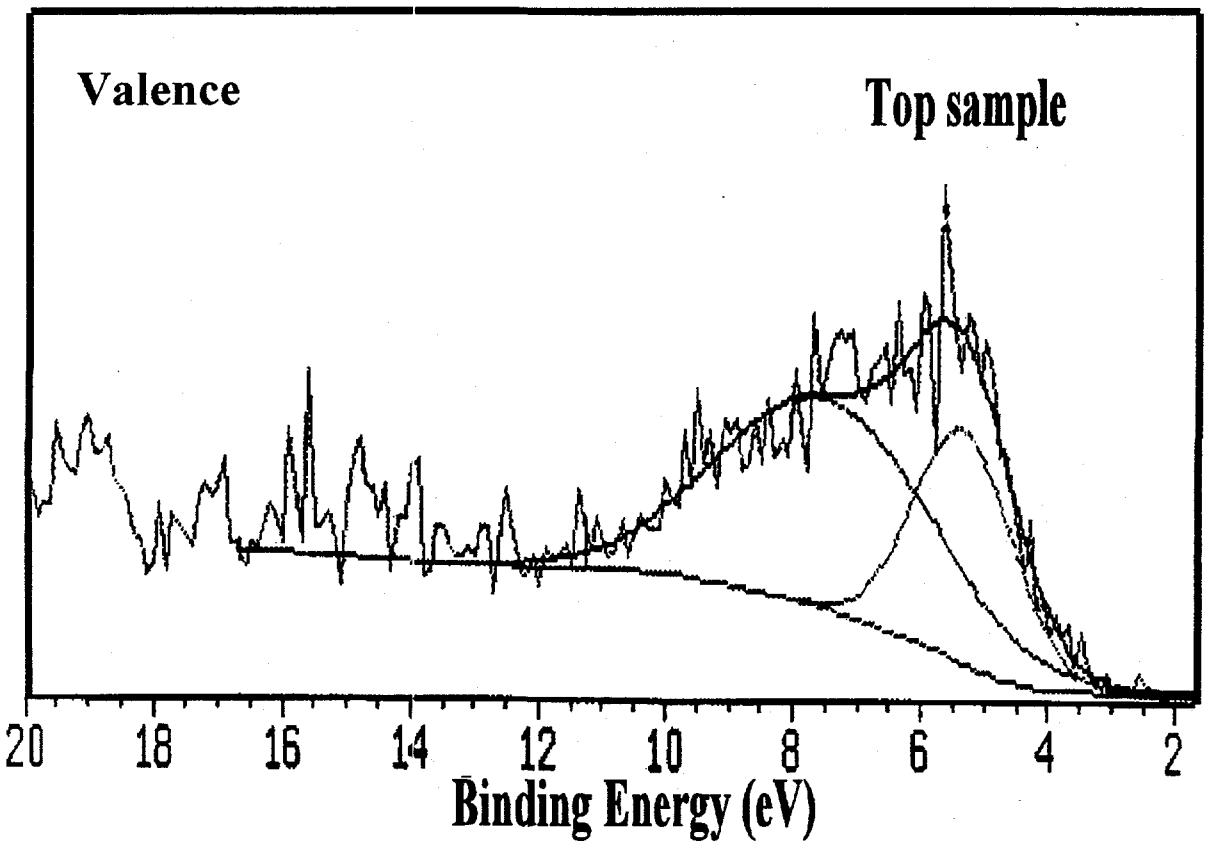

Fig. A.13. ESCA deconvoluted spectra of the valence electron region for charcoal contacted with F_2-UF_6 mixture during column loading: top sample.

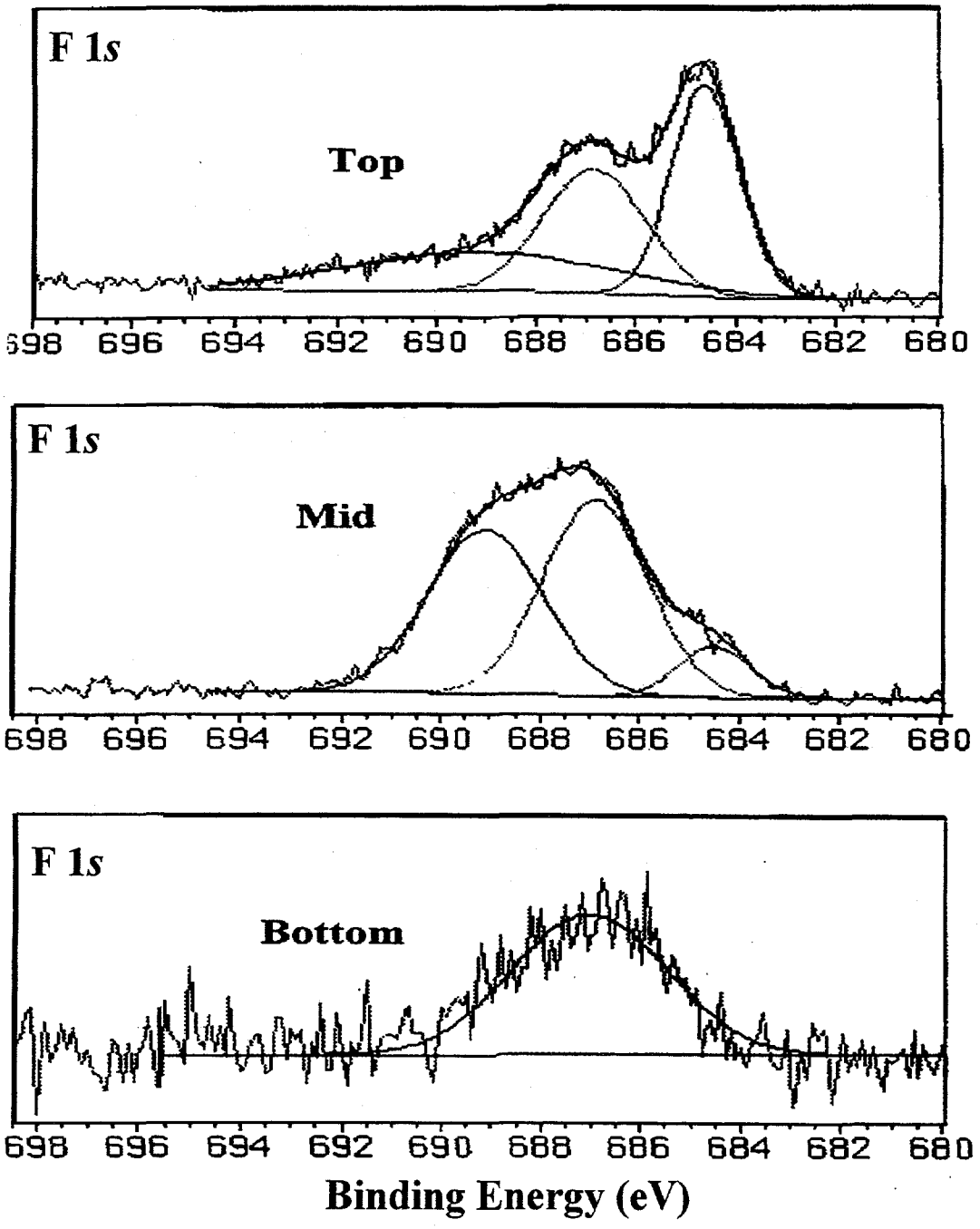

Fig. A.14. ESCA deconvoluted spectra, F 1*s* region, for charcoal contacted with F_2-UF_6 mixture during column loading: top, mid, and bottom samples.

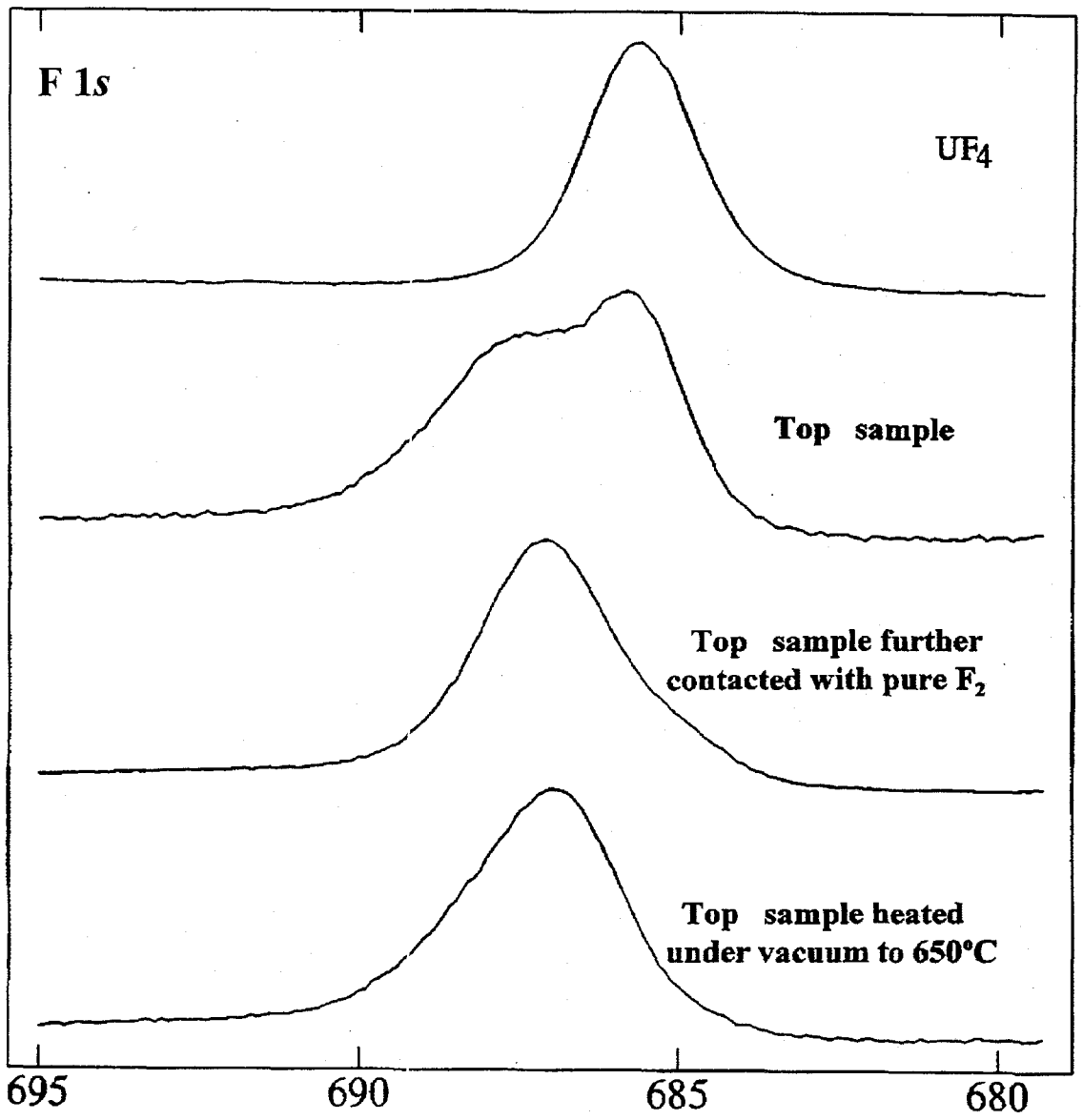

Fig. A.15. Comparison of ESCA spectra, F 1*s* region, for pure UF_4 and charcoal contacted with F_2-UF_6 mixture during column loading: top column sample, sample further contacted with F_2, and sample heated under vacuum up to 650°C.

Figures A.16 to A.18 present the curve-fitted F_A (UF_x), F_B (F-C and UO_2F_2), and F_C (U-F-C) components for the three "Top" samples (original, fluorinated, and heated). As expected, Fig. A.16 is quite similar to Fig. A.3 (Sect. A.1.2).

The "Mid" sample that corresponds to the front of the uranium in the charcoal column displays C_F (U-F-C) and B_F (F-C and UO_2F_2) as the main components along with the minor peak A_F(UF_x). A plausible explanation for the significant C_F (U-F-C) component can be drawn from the fact that the fluorine front moves faster. When the UF_6 gas reaches the charcoal particles, many sites have already become fluorinated and some of the uranium species have been chemisorbed on the fluorinated surface or intercalated between layers of fluorinated charcoal with some fluorine atoms bridging between the C and U atoms (C_F peak).

As expected, the B_F peak (F-C and UO_2F_2) is significantly larger for the portion further contacted with F_2 to carbon fluorination. The heated sample shows also a large increase of the B_F peak, which can be explained by formation of UO_2F_2 in agreement with the 4*f* ESCA since C-F is absent at this temperature (see next C 1*s* region). At the same time, there is a large increase of the C_F peak (U-F-C) with respect to the A_F peak (F-U). This finding is also in agreement with the postulated idea of the formation of tricentered binding by bridging fluoride.

A.2.4 ESCA Spectra, F 1*s* Auger Electron Region

Figure A.19 shows the fluorine Auger region for pure UF_4 and the three "Top" samples (original, fluorinated, and heated). The "top"sample is consistent with UF_4 as the major constituent. The further fluorinated sample resembles the "Teflon-like" CF_x samples (See Fig. A.9). In the heated sample, the fluorine Auger peak is displaced toward higher binding energies consistent with the suggested growth of UO_2F_2.

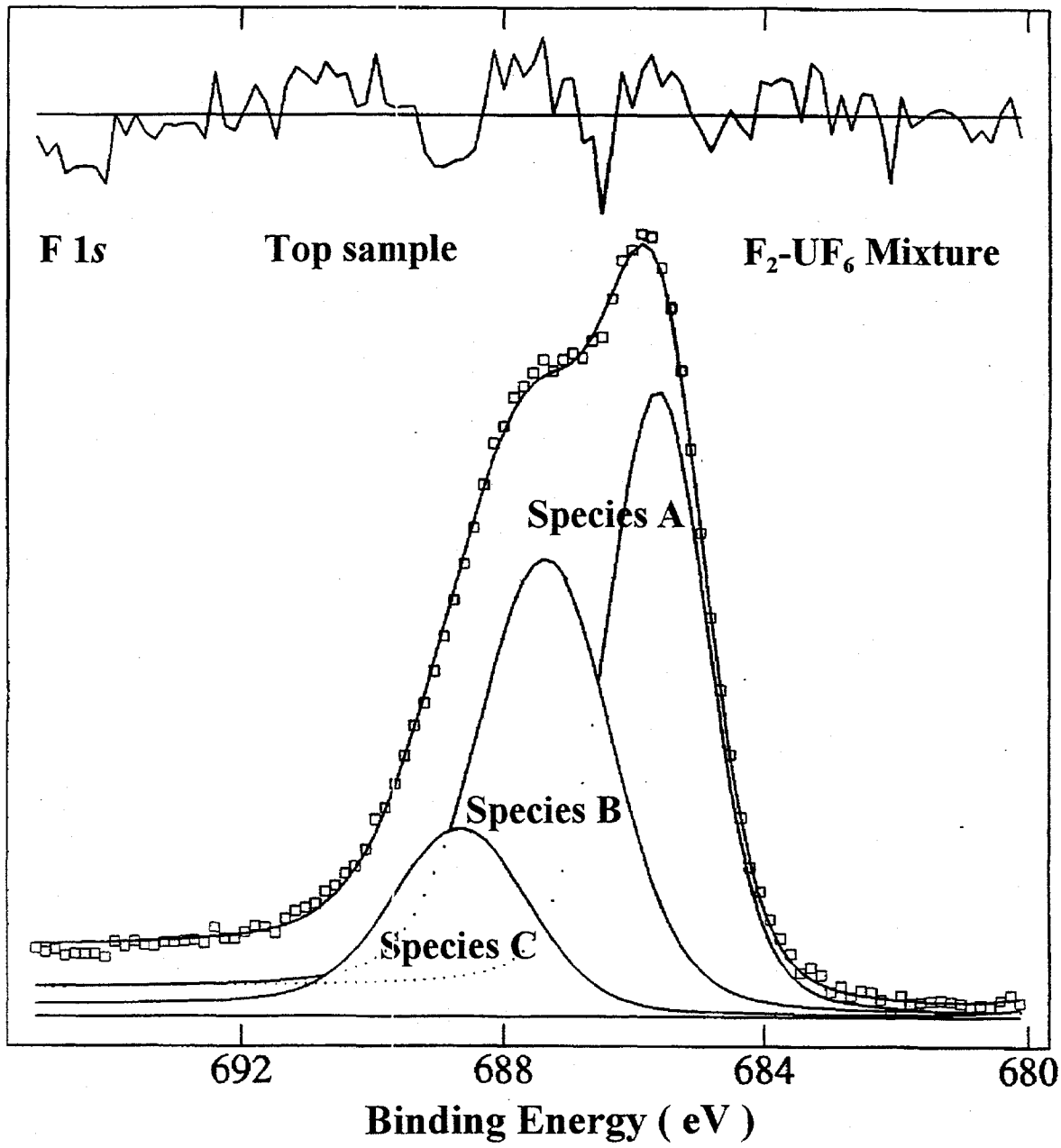

Fig. A.16. ESCA deconvoluted spectra, F 1*s* region, for charcoal contacted with F_2-UF_6 mixture during column loading: top column sample.

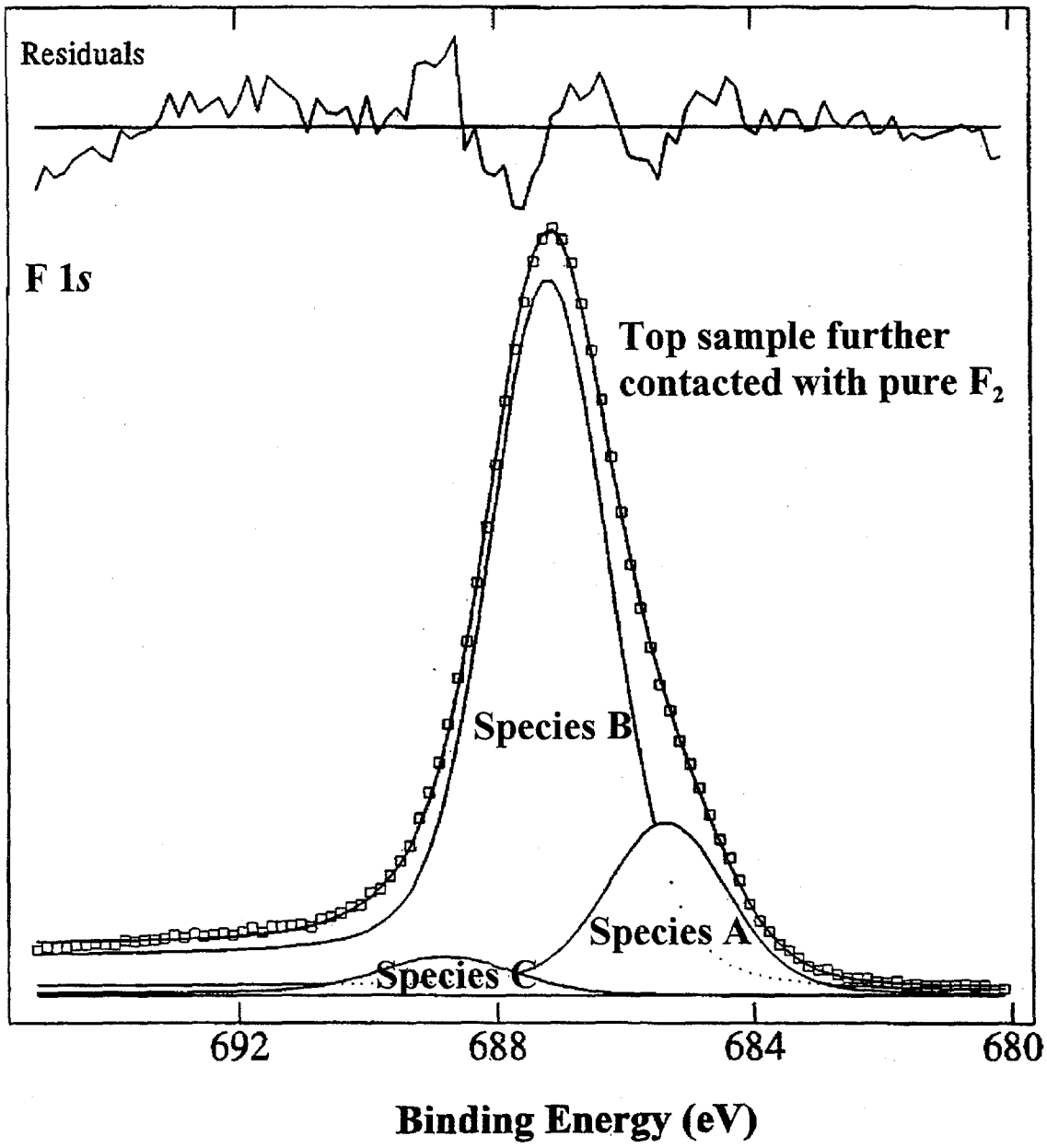

Fig A.17. ESCA deconvoluted spectra, F 1*s* region, for charcoal contacted with F_2-UF_6 mixture during column loading: top column sample further contacted with F_2.

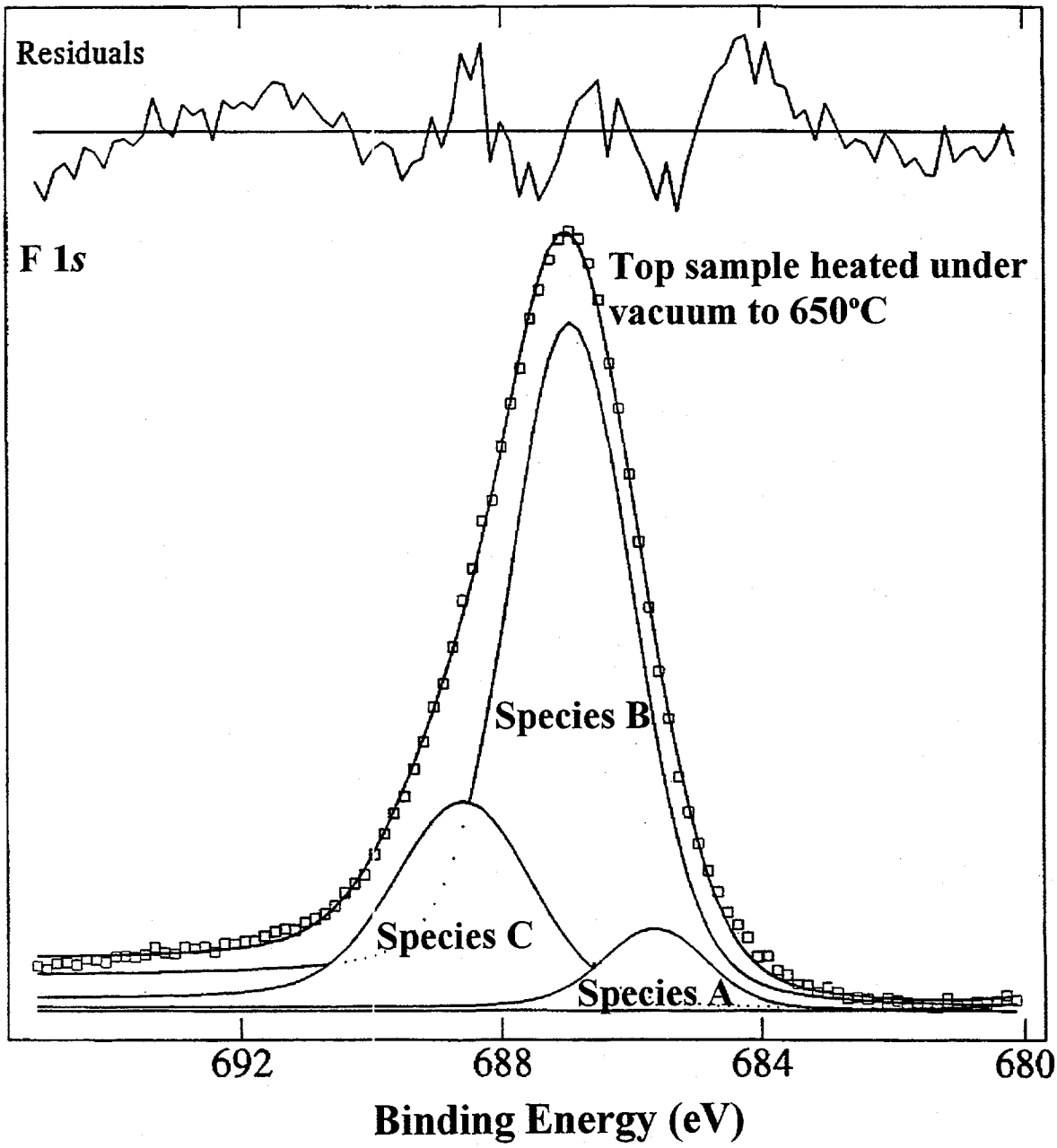

Fig A.18. ESCA deconvoluted spectra , F 1*s* region, for charcoal contacted with F_2-UF_6 mixture during column loading: top column sample heated under vacuum to 650°C.

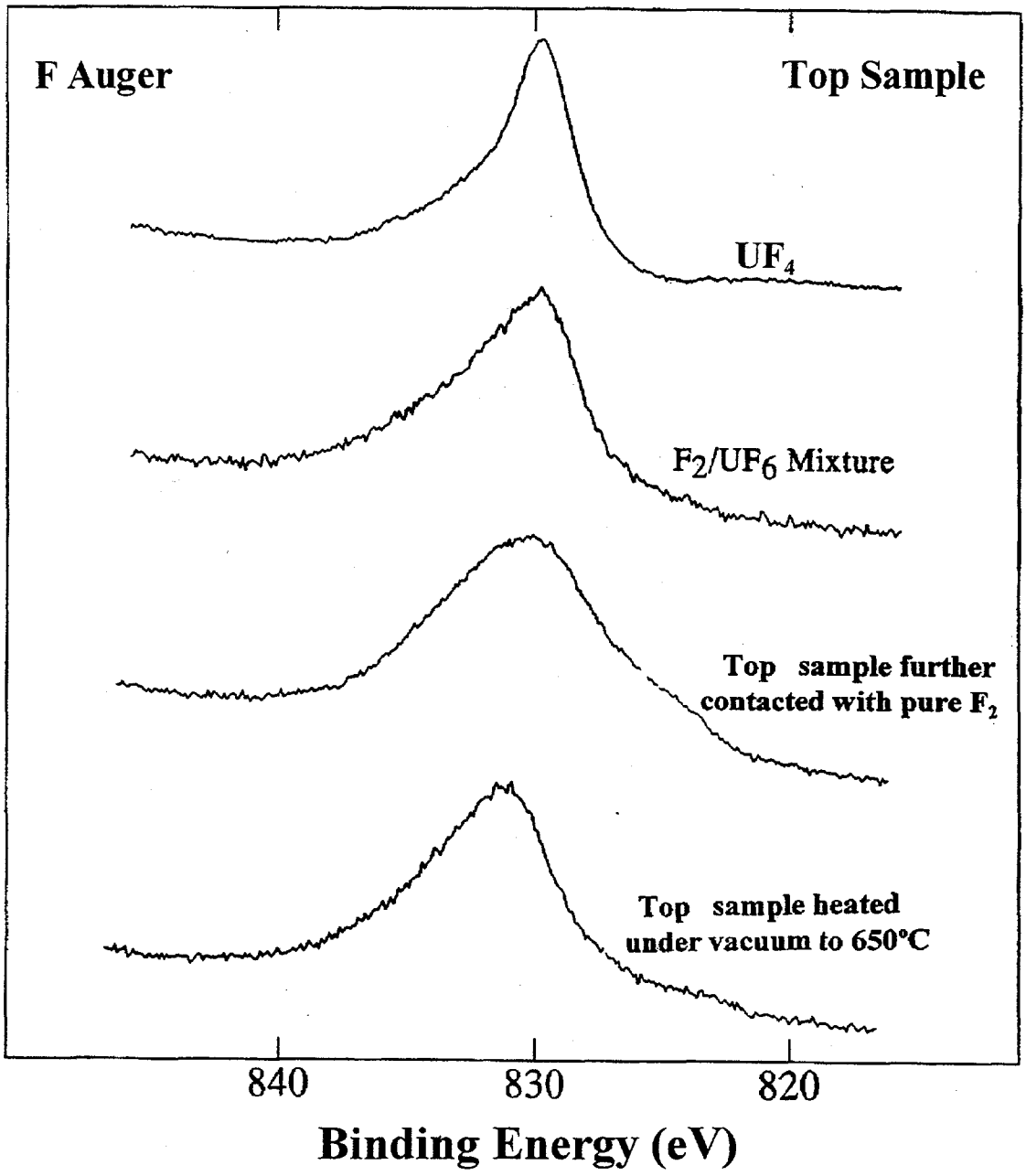

Fig A.19. Comparison of ESCA spectra, Auger region, for pure UF_6 and charcoal contacted with F_2-UF_6 mixture during column loading: top column sample, sample further contacted with F_2, and sample heated under vacuum to 650°C.

A.2.5 ESCA Spectra, O 1*s* Region

Figure A.20 displays the O 1*s* for ESCA for the "Top," "Mid," and "Bottom" samples. The A_O peak resulting from the oxygenated functional groups located at the surface of the charcoal crystallites[5] is prevalent for the "Top" sample. The B_O peak, located at higher binding energies, is larger in the "Mid" sample and is the predominant peak for the specimen taken from the bottom of the column. This behavior could be assigned to a reaction of the charcoal and oxygen (e.g., C=O), produced by fluorine displacement of oxygenated groups. The oxygenated groups are then displaced by fluorine and uranium compounds as the loading progresses.

A.2.6 ESCA Spectra, C 1*s* Region

The C 1*s* region for the "Top," "Mid," and "Bottom" samples is shown in Fig. A.21. It displays the same peaks as the fluorinated charcoal samples (see Sect. A.1.2 and Fig. A.19). The "Mid" sample has also two small unknown peaks centered at ~293.5 eV and ~297 eV. The C 1*s* ESCA for the further-fluorinated "Top" sample, as shown in Fig. A.22, is quite similar to the spectra for fluorinated charcoal prepared at room temperature (Fig. A.11). As expected, the ESCA spectra for the "Top" sample heated to 650 °C displays no C-F (see Fig. A.23 and Sect. 3.4).

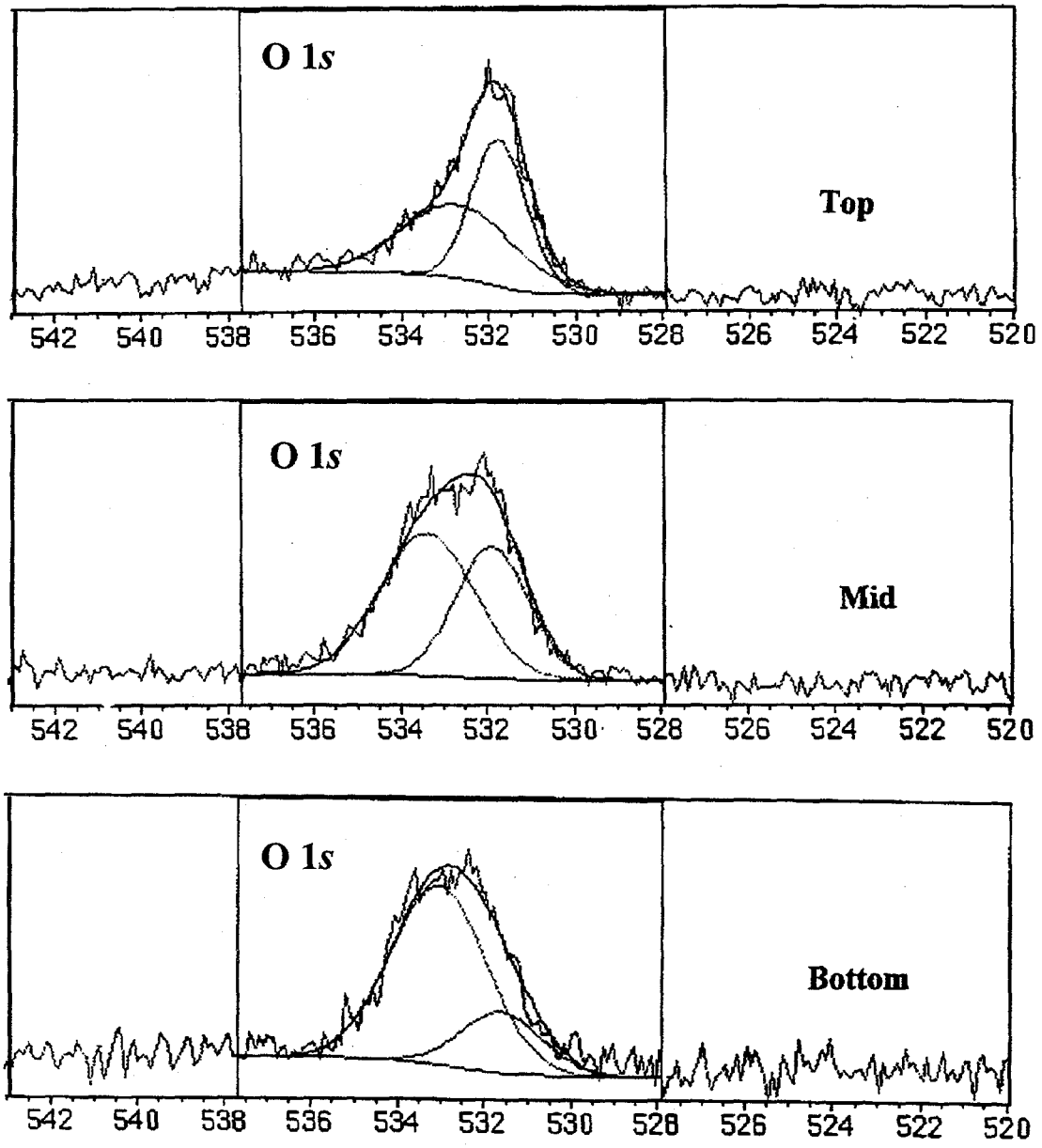

Fig. A. 20. ESCA deconvoluted spectra, O 1*s* region, for charcoal contacted with F_2-UF_6 mixture during column loading: top, mid, and bottom samples.

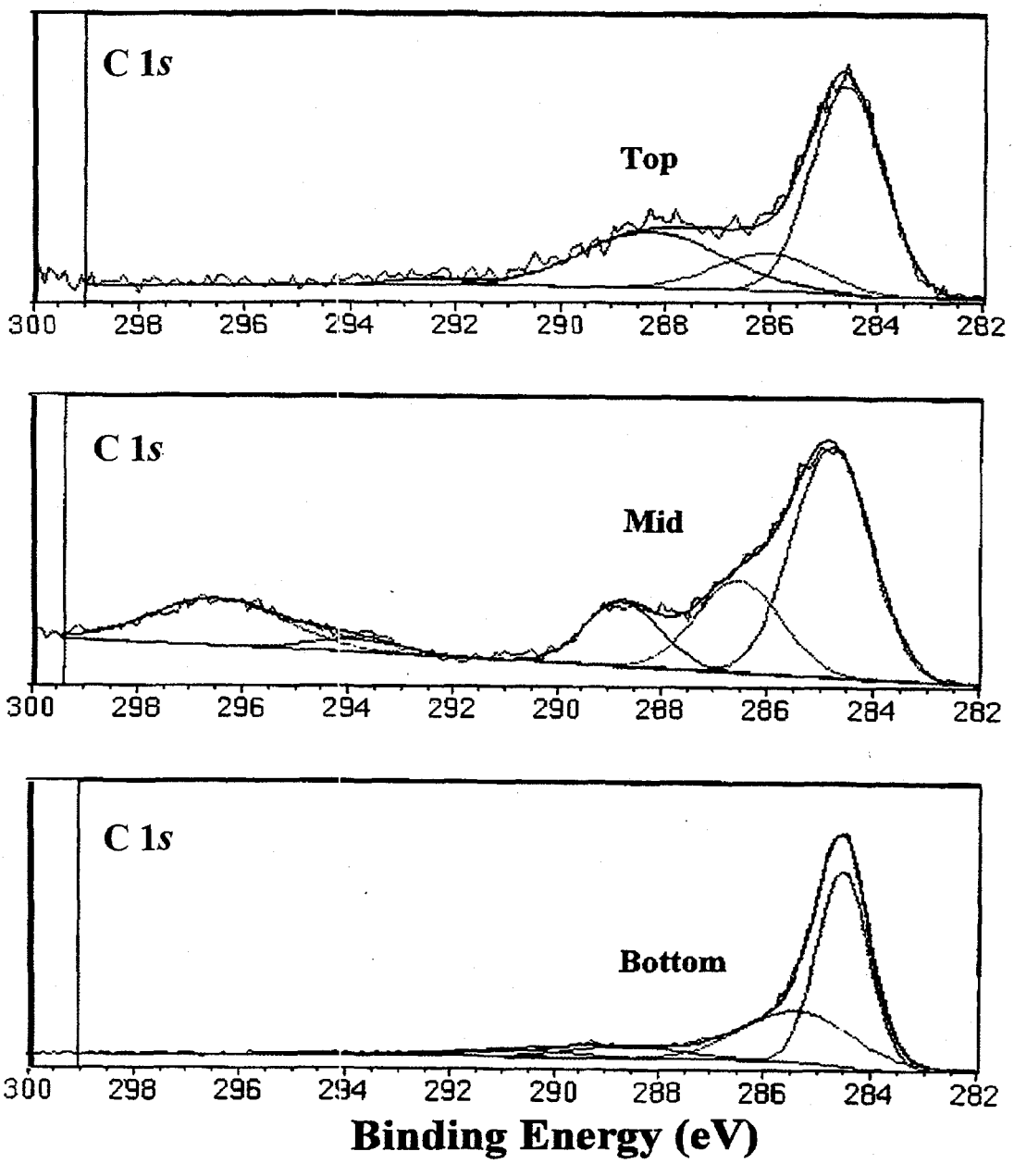

Fig. A. 21. ESCA deconvoluted spectra, C 1*s* region, for charcoal contacted with F_2-UF_6 mixture during column loading: top, mid, and bottom samples.

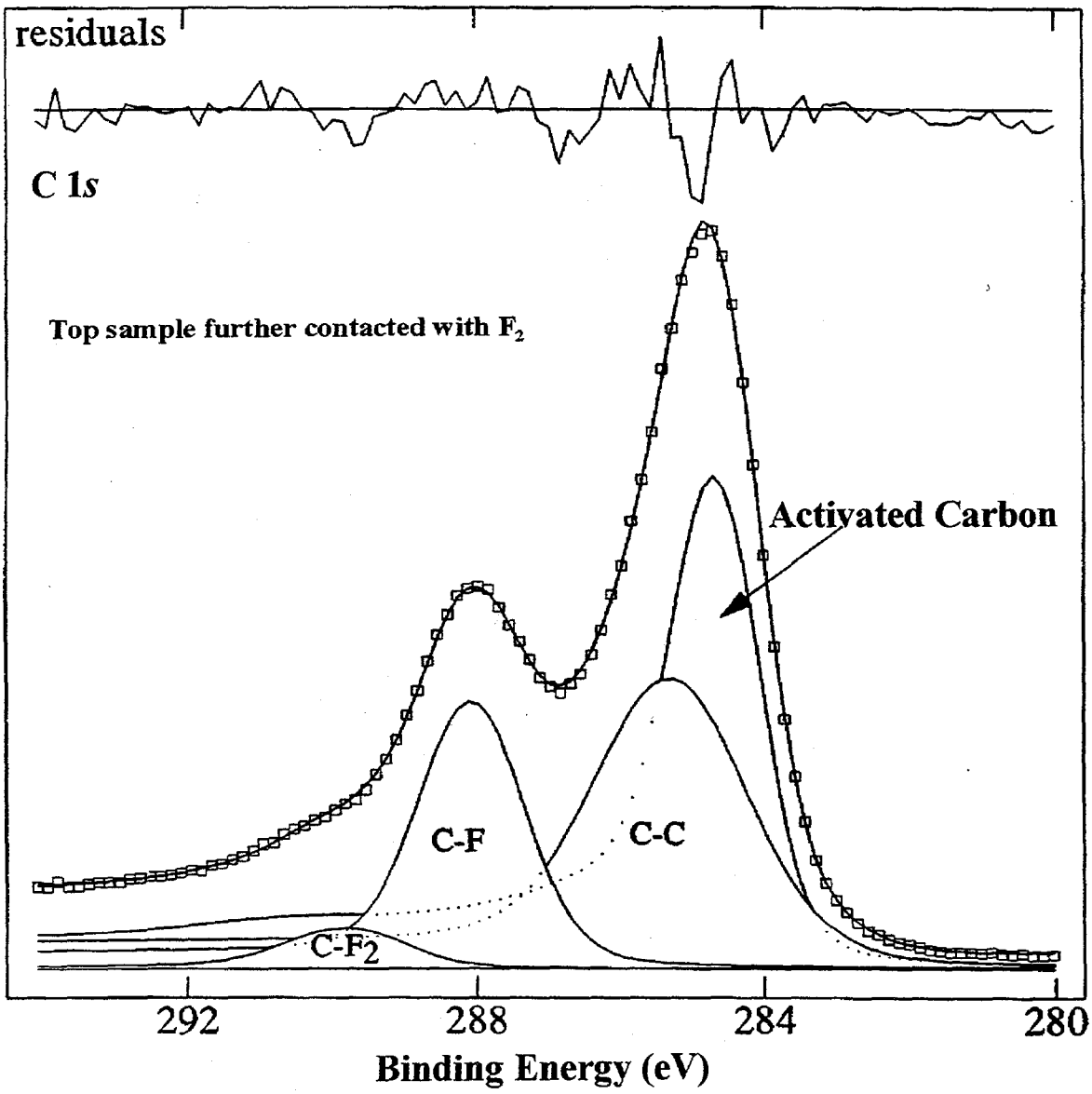

Fig. A. 22. ESCA deconvoluted spectra, C 1*s* region, for charcoal contacted with F_2-UF_6 mixture during column loading: top column further contacted with F_2.

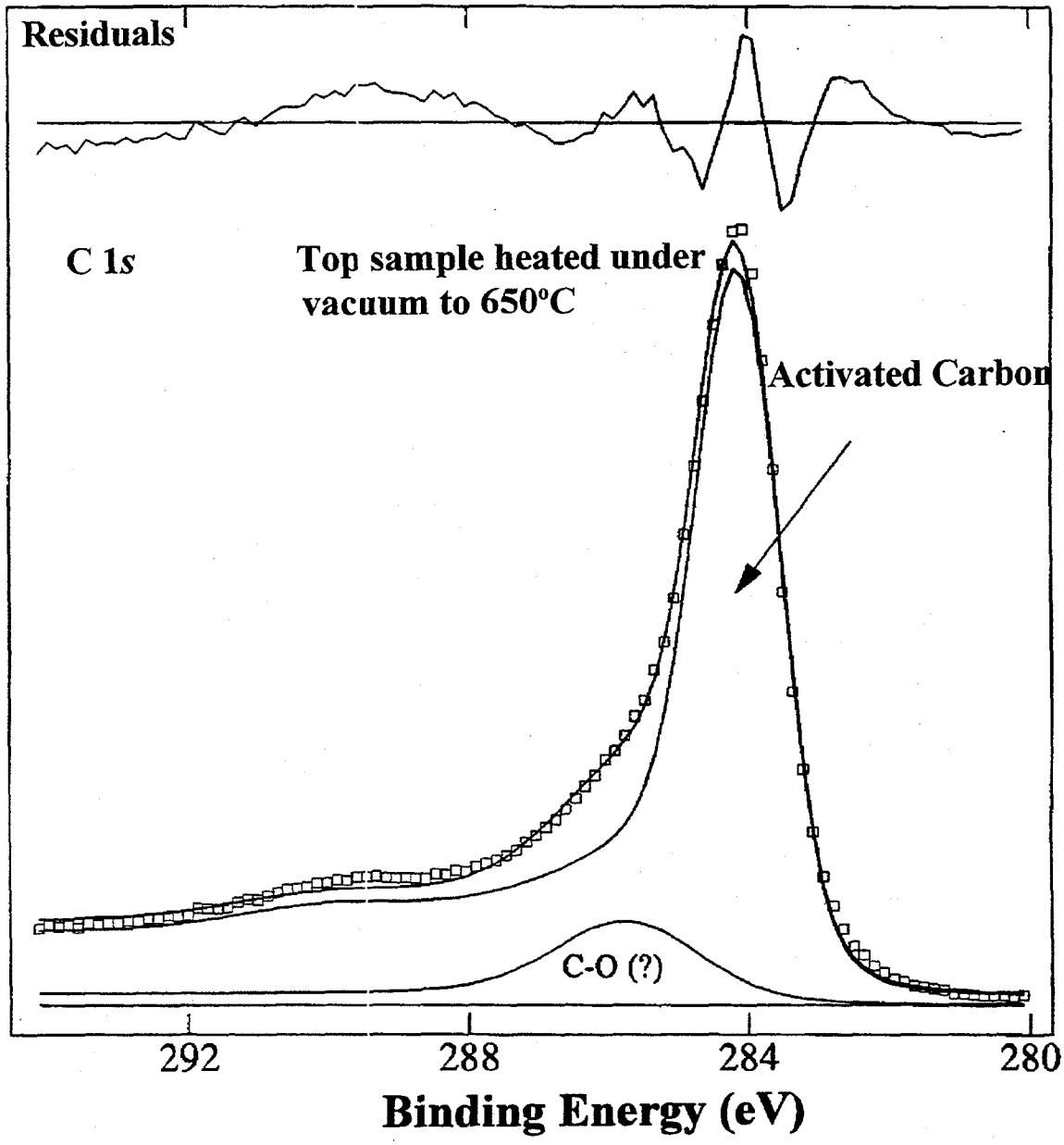

Fig. A. 23. ESCA deconvoluted spectra, C 1*s* region, for charcoal contacted with F_2-UF_6 mixture during column loading: top column sample heated under vacuum to 650°C.

REFERENCES FOR APPENDIX

1. "Compounds of Uranium and Fluorine," *Gmelin Handbuch der Anorganischen Chemie, Suplement C8*, Springer-Verlag, Berlin, 1980.

2. J. C. Bailar, *Comprehensive Inorganic Chemistry*, Vol. 5, Pergamon Press, Oxford, 1975, pp. 177.

3. E. Thibaut, J-P. Boutique, J. J. Verbist, J-C. Levet, and H. Noël, "Electronic Structure of Uranium Halides and Oxyhalides in the Solid State. An X-ray Photoelectron Spectral Study of Bonding Ionicity," *J. Am. Chem. Soc.* **104,** 5266–73 (1982).

4. L. D. Trowbridge and H. L. Richards, "X-Ray Photoelectron Spectra of the U 4*f* Levels in UF_4, UF_5, and UF_6," *Surface Interface Anal.* **4**(3), 1982.

5. D. Chadwick, "Uranium 4*f* Binding Energies Studied by X-Ray Photoelectron Spectroscopy," *Chem. Phys. Lett.* **21**, 291–94 (1973).

6. A. Tressaud, C. Guimon, V. Gupta, and F. Moguet, "Fluorine-Intercalated Carbon Fibers:II: An X-ray Photoelectron Spectroscopy Study," *Mat. Sci. Eng* **B30**, 61 (1995).

7. H. Jankowska, A. Świątkowski, and J. Choma, *Active Carbon*, Ellis Hordwood Limited, N. Y., 1991.

8. R. T. Paine, R. R. Ryan, and L. B. Asprey, "Synthesis, Characterization, and Structure of Uranium Oxide Tetrafluoride (α-UOF_4)," *Inorg. Chem.* **14**, 1113–17 (1975).

9. M. G. Otey and R. A. LeDoux, "$U_3O_5F_8$ - A New Compound in the U-O-F System," *J. Inorg. Nucl. Chem.* **29,** 2249–56 (1967).

10. K. H. Lau, R. D. Brittain, and D. L. Hildenbrand, "Complex Sublimation/Decomposition of Uranyl Fluoride: Thermodynamics of Gaseous UO_2F_2 and UOF_4," *J. Phys. Chem.* ***89***, 4369–73 (1985).

11. E. Jaco and W. Polligkeit, "Chemistry of Uranium Fluorides, I," *Z. Naturforsh. B* **28,** 120–24 (1973).